

THESIS

2

2004

56492513

This is to certify that the
dissertation entitled

DEVELOPMENT OF A BASIS FOR CONTROL OF
COMBUSTION IN AN INTERNAL COMBUSTION ENGINE

presented by

YUAN SHEN

has been accepted towards fulfillment
of the requirements for the

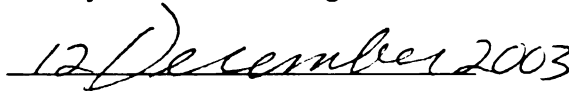
Doctoral

degree in

Mechanical Engineering



Major Professor's Signature



Date

LIBRARY
Michigan State
University

PLACE IN RETURN BOX to remove this checkout from your record.
TO AVOID FINES return on or before date due.
MAY BE RECALLED with earlier due date if requested.

DATE DUE	DATE DUE	DATE DUE

DEVELOPMENT OF A BASIS FOR CONTROL OF COMBUSTION IN AN
INTERNAL COMBUSTION ENGINE

By

Yuan Shen

A DISSERTATION

Submitted to
Michigan State University
in partial fulfillment of the requirements
for the degree of

DOCTOR OF PHILOSOPHY

Department of Mechanical Engineering

2003

DEVELO

This work
engine contr
cycles and th
variability in
could unique
probability o
the identific
pre-combus
rely on ense
necessary fo
result of th
which woul
system.

This eff
conversion
the four st
the exothe
uniquely o
basis for o
this disser
of a descr
continuous

ABSTRACT

DEVELOPMENT OF A BASIS FOR CONTROL OF COMBUSTION IN AN INTERNAL COMBUSTION ENGINE

By

Yuan Shen

This work is composed of several distinct sections however the focus is to effect engine control. The first effort represents quantification of flow during individual cycles and the development of a method which can be used to define the cycle-to-cycle variability in pre-combustion phase of a four stroke cycle. It was determined that one could uniquely describe this phase of the airflow or fuel-air mixing by evaluating the probability density function of normalized circulation. Of particular significance was the identification that cycle-resolved measurements are needed to accurately describe pre-combustion air motion and fuel-air mixing phenomena and that simulations which rely on ensemble-averaged Navier-Stokes equations cannot provide reliable indications necessary for combustion control in an internal combustion piston engine. It was the result of these experiments that inspired development of theoretically based methods which would provide insight into an algorithm for an engine control for the governor system.

This effort led to the two new concepts related to the events which occur during the conversion of reactants to products before and during the work producing segments of the four stroke cycle. We term these segments the dynamic stage of combustion and the exothermic stage of combustion. Mathematical analysis are constructed which uniquely define the bounds of these stages of combustion and provide a rational basis for developing future engine controls. The majority of the effort described in this dissertation is orientated to developing these potential control algorithms and of a description of what is termed the effectiveness of combustion. Based on these continuously differentiable algorithms, the rate of conversion of reactants to products

and the rat

Results of

engine. In

and will pro

combustion

and the rate of change of the conversion of reactants to products can be obtained. Results of this analysis have been applied to a stratified charge methanol fuelled engine. In the future, these methods can be integrated in microprocessor controls and will provide the feedback necessary to control the next generation of internal combustion engines.

To my grandma

I would

First, I v

the opportu

been able to

Second,

for his help

not make m

Third, I

Naguid, and

and though

Andy Fedev

experimenta

like to thank

company: E

Novak, Kyle

Finally, I

ACKNOWLEDGEMENT

I would like to thank the following people who make this work reality.

First, I would like to thank Dr. Harold Schock, my academic advisor, for giving me the opportunity to work in the MSU Engine Research Lab (ERL). I would not have been able to complete this dissertation without his guidance and financial support.

Second, I would like to thank Dr. Antoni K. Oppenheim, my advisory committee, for his help and patient guidance throughout my work. Without his support, I would not make much progress in my studies.

Third, I would like to extend my sincere thanks to Dr. Tom Shih, Dr. Ahmed Naguid, and Dr. Mark Dykman for being my committees and their helpful comments and thought-provoking questions; Dr. Indrek Wichman for his help on Chapter 5; Andy Fedewa, Tom Stuechen, Edward Timm for their help to make me understand experimental details; Jan Chappell for her assistance on a daily basis. I would also like to thank rest of students and research associates at MSU ERL for their wonderful company: Boon-Keat Chui, Anthony Christie, Andy Sasak, Mohmood Rahi, Mark Novak, Kyle Judd, and Bin Zhu.

Finally, I would like to thank my parents and my wife, for their love.

Cont

1 Introdu

1.1 Bac

1.2 Lito

1.2

1.2

1.2

1.3 Mo

2 Pre-con

2.1 Int

2.2 Ex

2.3 No

2.4 PP

2.5 Cy

2.5

2.5

2.6 TH

3 Dynam

3.1 In

3.2 TH

3.3 D

3.4 B

3.5 Li

3.6 D

3.6

3.6

3.7 Pr

3.8 In

3.8

3.8

4 Exothe

4.1 Int

4.2 Sta

4.2

Contents

1	Introduction	1
1.1	Background	1
1.2	Literature review	3
1.2.1	Pre-combustion analysis	3
1.2.2	Combustion analysis	12
1.2.3	Cycle-to-cycle variation reduction	16
1.3	Motivation and objectives	19
2	Pre-combustion flow analysis	21
2.1	Introduction	21
2.2	Experimental setup	22
2.3	Normalized circulation	22
2.4	PDF method	25
2.5	Cyclic variations of the flow with different port blockers	27
2.5.1	Tumble plane	27
2.5.2	Swirl plane	29
2.6	The influence of the shape of port blockers	32
3	Dynamic stage of combustion in an IC engine	37
3.1	Introduction	37
3.2	The polytropic process	38
3.3	Dynamic stage of combustion	41
3.4	Bounds	42
3.5	Life function	44
3.6	Discussion	46
3.6.1	Life function and Wiebe function	46
3.6.2	Derivatives of life function	50
3.7	Procedure	51
3.8	Implementation	52
3.8.1	Engine	52
3.8.2	Results	54
4	Exothermic stage of combustion in an IC engine	69
4.1	Introduction	69
4.2	State space	70
4.2.1	Component fractions	70

4.3

4.4

4

4

4

4

4

4.5

4

4

4.6

4.7

4.7

4.7

4.7

5 Thermo

5.1 Intr

5.2 The

5.3 Hea

5.4 Res

6 Conclusi

6.1 Cond

6.2 Rec

A Evaluatio

STANJA

A.1 Intro

A.2 Proc

A.3 Res

4.2.2	Component states	71
4.3	Combustion processes	76
4.3.1	Mixing	76
4.3.2	Exothermic center	76
4.4	Exothermic system	79
4.4.1	Balances	79
4.4.2	Coordinates	80
4.4.3	Progress parameter	81
4.4.4	Combustion in a piston engine	82
4.4.5	Correlation	84
4.5	Closed system	85
4.5.1	Thermodynamic relationship	85
4.5.2	Thermodynamic properties	87
4.6	Procedure	89
4.7	Implementation	90
4.7.1	Engine	90
4.7.2	Exothermic stage of combustion	90
4.7.3	Closed system	96
5	Thermodynamic analysis in an IC engine	105
5.1	Introduction	105
5.2	Thermodynamic analysis	106
5.3	Heat release function	110
5.4	Results	111
6	Conclusions and recommendations	115
6.1	Conclusions	115
6.2	Recommendations	117
A	Evaluation of state transformations of reactants and products with STANJAN	120
A.1	Introduction	120
A.2	Procedure	121
A.3	Results	131

List

- 3.1 Co
- 3.2 En
- 3.3 En
- 3.4 Th
- 3.5 Lif
- 4.1 Eq
- 4.2 Pa
- A.1 Th
- A.2 Th
- A.3 Th
- A.4 Th

List of Tables

3.1	Comparison of first derivatives of life function and Wiebe function . .	50
3.2	Engine specifications	52
3.3	Engine operating conditions	55
3.4	The indices of polytropic compression and expansion of four cases . .	55
3.5	Life function parameters	56
4.1	Equations of state	72
4.2	Parameters to evaluate the mass fraction of products	91
A.1	Thermodynamic properties of air, fuel, reactants, and products in case 1132	
A.2	Thermodynamic properties of air, fuel, reactants, and products in case 2133	
A.3	Thermodynamic properties of air, fuel, reactants, and products in case 3134	
A.4	Thermodynamic properties of air, fuel, reactants, and products in case 4135	

List

- 1.1 S
- 1.2 V
- 1.3 V
- 1.4 T
- 1.5 Pr
- 2.1 3.5
- 2.2 Tu
- 2.3 Sw
- 2.4 Th
- 2.5 Th
- 2.6 Infl
- 2.7 The
- 2.8 Infl
- 2.9 The
- 2.10 Infl
- 2.11 The
- 2.12 Infl
- 2.13 Tumb
- 2.14 Swirl
- 2.15 Influe
- on the

List of Figures

1.1	Schematic of MTV optical setup	5
1.2	Velocities and vorticities of the flow in the tumble plane, CAD 180, tumble port blocker (70%)	6
1.3	Velocities and vorticities of the flow in the swirl plane, CAD 270, tumble port blocker (90%)	7
1.4	The schematic of a controlled combustion engine	18
1.5	Prototype of a controlled combustion engine system: 1 - the air-blast atomizer; 2 - the flame jet generator; 3 - turbulence jet plumes; 4 - the electronic control modulator; and 5 - the pressure transducer and shaft decoder records expressed in terms of an indicator diagram.	19
2.1	3.5-liter DaimlerChrysler engine	23
2.2	Tumble port blocker	24
2.3	Swirl port blocker	24
2.4	The PDF for the circulation over a unit area on the tumble plane at CAD 180, tumble plate blocker.	26
2.5	The PDF for the circulation over a unit area on the tumble plane with different port blockers at CAD 270.	28
2.6	Influences of different port blockers on the cycle-to-cycle variations of the flow on the tumble plane at CAD 270.	29
2.7	The PDF for the circulation over a unit area on the tumble plane with different port blockers at CAD 300.	30
2.8	Influences of different port blockers on the cycle-to-cycle variations of the flow on the tumble plane at CAD 300.	30
2.9	The PDF for the circulation over a unit area on the swirl plane with different port blockers at CAD 270.	31
2.10	Influence of different port blockers on the cycle-to-cycle variations of the flow on the swirl plane at CAD 270.	31
2.11	The PDF for the circulation over a unit area on the swirl plane with different port blockers at CAD 300.	32
2.12	Influences of different port blockers on the cycle-to-cycle variations of the flow on the swirl plane at CAD 300.	33
2.13	Tumble port blocker B	34
2.14	Swirl port blocker B	34
2.15	Influences of port blockers B on the cycle-to-cycle variations of the flow on the tumble plane at CAD 270.	35

2.16	Influences of port blockers B on the cycle-to-cycle variations of the flow on the tumble plane at CAD 300.	35
2.17	Influences of port blockers B on the cycle-to-cycle variations of the flow on the swirl plane at CAD 270.	36
2.18	Influences of port blockers B on the cycle-to-cycle variations of the flow on the swirl plane at CAD 300.	36
3.1	Pressure records for ten cycles in single-cylinder spark-ignition engine operating at 1500rev/min, $\phi = 1.0$, $p_{inlet} = 0.7\text{atm}$, MBT timing 25 ° BTC. (From Heywood [1])	38
3.2	The polytropic pressure model of ideal processes in an IC engine . . .	40
3.3	The polytropic pressure model of real processes in an IC engine . . .	40
3.4	The Wiebe function and its derivatives for $\alpha = 3$ and $\chi = 0.5, 1, 2.5, 5$ and 10.	48
3.5	The life function of the dynamic stage of combustion and its derivatives for $\alpha = 3$ and $\chi = 0.5, 1, 2.5, 5$ and 10.	49
3.6	Bottom view of the engine head	53
3.7	Illustration of combustion chamber	54
3.8	Pressure trace of case 1	57
3.9	Pressure trace of case 2	57
3.10	Pressure trace of case 3	58
3.11	Pressure trace of case 4	58
3.12	Logarithmic indicator of the pressure trace of case 1	59
3.13	Logarithmic indicator of the pressure trace of case 2	59
3.14	Logarithmic indicator of the pressure trace of case 3	60
3.15	Logarithmic indicator of the pressure trace of case 4	60
3.16	Polytropic pressure model of case 1	61
3.17	Polytropic pressure model of case 2	61
3.18	Polytropic pressure model of case 3	62
3.19	Polytropic pressure model of case 4	62
3.20	Life function of DSC and its first derivative of case 1	63
3.21	Life function of DSC and its first derivative of case 2	63
3.22	Life function of DSC and its first derivative of case 3	64
3.23	Life function of DSC and its first derivative of case 4	64
3.24	Second derivative of life function of DSC of case 1	65
3.25	Second derivative of life function of DSC of case 2	65
3.26	Second derivative of life function of DSC of case 3	66
3.27	Second derivative of life function of DSC of case 4	66
3.28	Analytical and measured cylinder pressure of case 1	67
3.29	Analytical and measured cylinder pressure of case 2	67
3.30	Analytical and measured cylinder pressure of case 3	68
3.31	Analytical and measured cylinder pressure of case 4	68
4.1	Diagram of component fractions	71
4.2	3-D illustration of the state space	73

4.3

4.4

4.5

4.6

4.7

4.8

4.9

4.10

4.11

ca

4.12

ca

4.13

ca

4.14

ca

4.15

4.16

4.17

4.18

4.19

clo

4.20

clo

4.21

clo

4.22

clo

4.23

4.24

4.25

4.26

4.27

case

4.28

case

4.29

case

4.30

case

4.3	Diagram of component states with an illustration of the processes of mixing and adiabatic exothermic center, EC, and exothermic system, ES.	74
4.4	Diagram of component states for an adiabatic exothermic center in $w - e$ and $w - h$ space.	78
4.5	Diagram of component states for a non-adiabatic exothermic system in $w - e$ space.	80
4.6	Correlation between mass fractions of products.	85
4.7	State diagram of the exothermic stage of combustion for case 1	92
4.8	State diagram of the exothermic stage of combustion for case 2	92
4.9	State diagram of the exothermic stage of combustion for case 3	93
4.10	State diagram of the exothermic stage of combustion for case 4	93
4.11	Profiles of the mass fraction of products and its effective component of case 1	94
4.12	Profiles of the mass fraction of products and its effective component of case 2	94
4.13	Profiles of the mass fraction of products and its effective component of case 3	95
4.14	Profiles of the mass fraction of products and its effective component of case 4	95
4.15	State diagram of a closed system for case 1	97
4.16	State diagram of a closed system for case 2	97
4.17	State diagram of a closed system for case 3	98
4.18	State diagram of a closed system for case 4	98
4.19	Profiles of the mass fraction of products and its components in the closed system of case 1	99
4.20	Profiles of the mass fraction of products and its components in the closed system of case 2	99
4.21	Profiles of the mass fraction of products and its components in the closed system of case 3	100
4.22	Profiles of the mass fraction of products and its components in the closed system of case 4	100
4.23	Profiles of the temperature of reactants, products, and system of case 1	101
4.24	Profiles of the temperature of reactants, products, and system of case 2	101
4.25	Profiles of the temperature of reactants, products, and system of case 3	102
4.26	Profiles of the temperature of reactants, products, and system of case 4	102
4.27	Profiles of the specific volume of reactants, products, and system of case 1	103
4.28	Profiles of the specific volume of reactants, products, and system of case 2	103
4.29	Profiles of the specific volume of reactants, products, and system of case 3	104
4.30	Profiles of the specific volume of reactants, products, and system of case 4	104

- 5.1 St
- 5.2 H
- 5.3 C
- 5.4 C
- 5.5 C
- 5.6 C

- A.1 Di
- A.2 Fl
- A.3 St
- A.4 St
- A.5 St
- A.6 St
- A.7 St
- A.8 St
- A.9 St
- A.10 St
- A.11 St
- A.12 St
- A.13 St
- A.14 St
- A.15 St
- A.16 St
- A.17 St
- A.18 St
- A.19 St

5.1	Schematic of the mixture in a cylinder of a four-stroke IC engine. . .	107
5.2	Heat release function.	109
5.3	Comparison of measured cylinder pressure and analytical cylinder pressure for case 1	113
5.4	Comparison of measured cylinder pressure and analytical cylinder pressure for case 2	113
5.5	Comparison of measured cylinder pressure and analytical cylinder pressure for case 3	114
5.6	Comparison of measured cylinder pressure and analytical cylinder pressure for case 4	114
A.1	Diagram of component states with an illustration of the processes of mixing and adiabatic exothermic center, EC, and exothermic system, ES.	121
A.2	Flowchart of evaluating thermodynamic states of reactants and products during the exothermic stage of combustion.	123
A.3	Step 1a — Specify the data file	125
A.4	Step 1b — The species in the data file COMB.SUD	125
A.5	Step 2 — Specify the mole number of each species in the reactants . .	126
A.6	Step 3a — Specify the temperature and pressure of reactants at the initial state of DSC	126
A.7	Step 3b — Thermodynamic properties of reactants at the initial state of DSC	127
A.8	Step 4a — Specify the temperature and pressure of reactants at the final state of DSC	127
A.9	Step 4b — Thermodynamic properties of reactants at the final state of DSC	128
A.10	Step 5 — Specify the species of products	128
A.11	Step 6a — Specify the pressure and enthalpy of products at the initial state of DSC	129
A.12	Step 6b — Thermodynamic properties of products at the initial state of DSC	129
A.13	Step 7a — Specify the temperature and pressure of products at the final state of DSC	130
A.14	Step 7b — Thermodynamic properties of products at the final state of DSC	130
A.15	Step 8 — Quit STANJAN	131
A.16	State transformations of air, fuel, reactants, and products in case 1 .	136
A.17	State transformations of air, fuel, reactants, and products in case 2 .	136
A.18	State transformations of air, fuel, reactants, and products in case 3 .	137
A.19	State transformations of air, fuel, reactants, and products in case 4 .	137

Chap

Intro

1.1 B

With the de
are increasi
engine powe
issues. In pr
engine with

In a pre
transportati
which are in

1. During
valve in
2. During
the mix
3. During
combust
tempera
4. During
the cylin

Chapter 1

Introduction

1.1 Background

With the development of the automotive industry, energy and environment problems are increasingly concerned. For production internal combustion (IC) engines, the engine power, fuel economy, and emission have been considered as the most important issues. In principle, the aim of most engine research is to achieve a high work output engine with high efficiency and low pollution.

In a premix four-stroke internal combustion engine, which dominates personal transportation in the United States, an operating cycle is composed of four strokes, which are intake stroke, compression stroke, power stroke, and exhaust stroke.

1. During the intake stroke, the fuel and air mixture is induced through the intake valve into the cylinder;
2. During the compression stroke, both intake and exhaust valves are closed and the mixture inside the cylinder is compressed by the piston;
3. During the power stroke, the mixture inside the cylinder is ignited and the combustion propagates throughout the charge, raising the mixture pressure and temperature and forcing the piston to do mechanical work;
4. During the exhaust stroke, the exhaust valve is open and the burned gases exit the cylinder.

To inc
pollution
that each
the intake
factors inc
shape. Fo
the spark
timing, etc
manifold p
recirculatio

Since an
and some c
on the pres
inevitably a

In natur
process on a
process in a
chamber geo
turbulence, c
effects exist,
but they can

Reducing
performance a
of the cycle-to
fuel consumpt
would help co
of the fuel-air

To increase the work output of a four-stroke IC engine with high efficiency and low pollution, each stroke should be well understood and optimized. It has been studied that each stroke in a engine operation cycle is affected by several factors [1][2]. For the intake and compression stroke, the flow in the cylinder is turbulent, subjective to factors including compression ratio, engine speed, intake valve timing, and intake port shape. For the power stroke, the combustion is mainly affected by the flow around the spark plug, the location of the spark plug, the air-to-fuel (A/F) ratio, ignition timing, etc. For the exhaust stroke, the A/F ratio, exhaust valve timing, and exhaust manifold pressure strongly affect the residual mass fraction (RMF) and exhaust gas recirculation (EGR), which further affect the next engine operation cycle.

Since an operating cycle of a four-stroke SI engine is affected by numerous factors and some of them are different from each cycle, there exist cycle-to-cycle variations on the pressure and emission output. The existence of cycle-to-cycle variations will inevitably affect the performance of an IC engine.

In nature, cycle-to-cycle variations are superposition of a non-chaotic deterministic process on a stochastic process [3][4]. The deterministic effects on the combustion process in an IC engine are from intake system geometry, A/F ratio, combustion chamber geometry, etc. The randomly changed parameters would be the in-cylinder turbulence, exhaust gas recirculation (EGR), valve leakage, etc. Since these stochastic effects exist, cycle-to-cycle variations in a four-stroke SI engine cannot be eliminated, but they can be minimized.

Reducing the cycle-to-cycle variations in an IC engine would improve the engine performance and increase the engine power. Studies have shown that the reduction of the cycle-to-cycle variations would increase the engine power output at the same fuel consumption [5]. It is also believed that the reduction of cycle-to-cycle variations would help control the emission. Specifically, a reduction of cycle-to-cycle variability of the fuel-air mixture motion in the cylinder allows knock-limit timing to be more

advanced

1.2

Cycle-to-cycle
engine. To
should be
on the cycle
analysis (in
exhaust and
to-cycle vari-
analysis.

1.2.1 P

For the pre-
was used to
engine in the
advanced opti-
measurement
(in the MSU
UV laser light
cylinder, and
camera. This
a reference in
is recorded at
molecules. The
distance each
for each inter-

advanced, thus improving the engine efficiency.

1.2 Literature review

Cycle-to-cycle variations exist in every stroke of an operating cycle of a four-stroke IC engine. To minimize the cycle-to-cycle variations, each stroke of an operating cycle should be studied. Based on the time sequence of a four-stroke cycle, the analysis on the cycle-to-cycle variations in an IC engine can be classified into pre-combustion analysis (intake and compression strokes), combustion analysis (power stroke), and exhaust analysis (exhaust stroke). So far, most of the efforts to minimize the cycle-to-cycle variations have been focused on the pre-combustion analysis and combustion analysis.

1.2.1 Pre-combustion analysis

For the pre-combustion flow in the cylinder, Molecular Tagging Velocimetry (MTV) was used to examine the flow pattern in a motored four-stroke spark-ignition (SI) engine in the Engine Research Lab at Michigan State University. MTV [6][7][8] is an advanced optical diagnostic technique for making non-intrusive instantaneous velocity measurements at multiple locations over a plane simultaneously. A tracer chemical (in the MSU case biacetyl) combined with nitrogen gas is "tagged" by a pulse of UV laser light ($\lambda=308$). Two sets of intersecting lines form a grid inside the engine cylinder, and an image is taken of the fluorescing biacetyl with an intensified CCD camera. This is done approximately 200 times and the images are averaged to obtain a reference image. Next, the excitation process is repeated. This time the image is recorded after the laser pulse, but still within the phosphorescence lifetime of the molecules. The time between these images and the reference image is known and the distance each line intersection has traveled can be measured giving a velocity vector for each intersection point. Traditional scattering methods require the flow to be

seeded with
advantage
the flow and
in Figure 1

The ens
Figures 1.2
(tumble and
ures, vector
The results
et. al. [9].
geometries

The ens
flow. Howev
to-cycle vari
field is an ar
It represents
strong. The
the cycle-to-

Trigui, K
four-stroke IC
examining flo
of very well o
and their ax

Zhang, U
combustion ef
injection (DI)
between two a

seeded with light-scattering particles that may have difficulty following the flow. The advantage of this measurement technique is that the tracer is molecularly mixed with the flow and follows it perfectly. The schematic of the MTV optical setup is shown in Figure 1.1.

The ensemble-averaged flow patterns in the cylinder recorded MTV are present in Figures 1.2 and Figure 1.3, which show typical ensemble averaged rotational motions (tumble and swirl) of the flow on the tumble and swirl planes, respectively. In figures, vectors represent flow velocities, and the shading represents the flow vorticity. The results are generally consistent with the visualization results obtained by Trigui, et. al. [9], Choi and Guezennec [10], Reuss [11] and Khalighi [12], though intake geometries were different.

The ensemble-averaged flow pattern in the cylinder is of help to characterize the flow. However, it neglects detailed features in the real individual flow field and cycle-to-cycle variations on the flow pattern. In other words, the ensemble-averaged flow field is an artificial field containing common features of the real individual flow fields. It represents none of the real individual flow fields if cycle-to-cycle variations are strong. Therefore, the individual flow field has to be studied in order to understand the cycle-to-cycle variations on the pre-combustion flowpattern in the cylinder.

Trigui, Kent, et. al. [9] implemented a visualization of the pre-combustion flow in a four-stroke IC engine by 3-D particle tracking velocimetry (3-D PTV). After carefully examining flow patterns for several consecutive cycles, they found that even in the case of very well organized swirl or tumble, the vortices are rarely centered in the volume and their axes are usually inclined in some complex way inside the 3D volume.

Zhang, Ueda, et. al. [13] visualized the two-dimensional bulk flow fields inside the combustion chamber around top dead center (TDC) in a motored four-stroke direct injection (DI) diesel engine. By comparing the continuous cycle-resolved flow fields between two arbitrary cycles from BTDC 3° to TDC on the swirl plane, they found

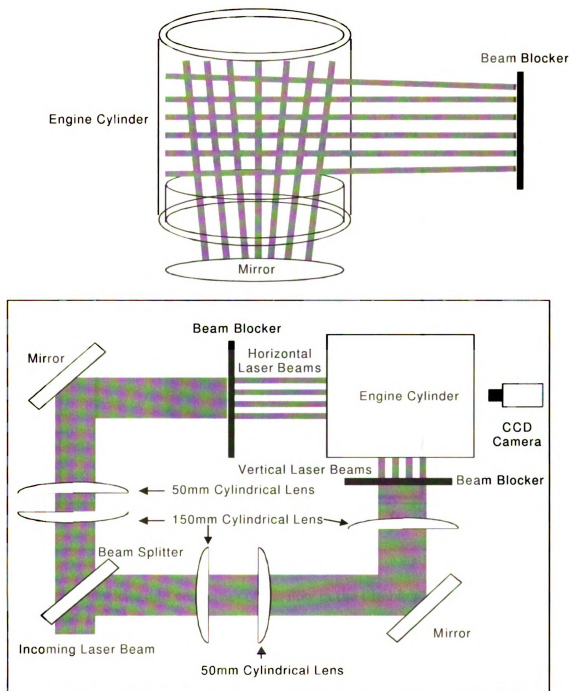


Figure 1.1: Schematic of MTV optical setup

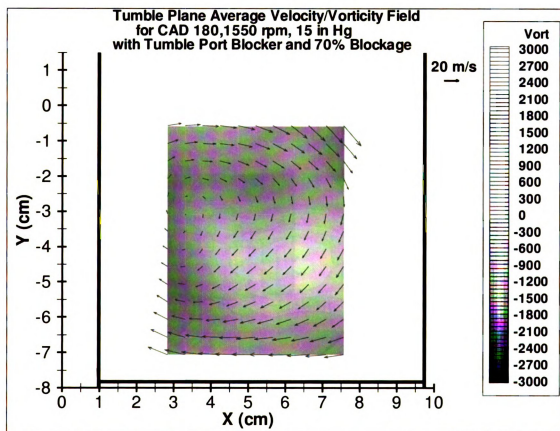


Figure 1.2: Velocities and vorticities of the flow in the tumble plane, CAD 180, tumble port blocker (70%)

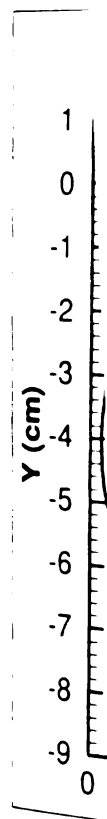


Figure 1.3: y
port blocker

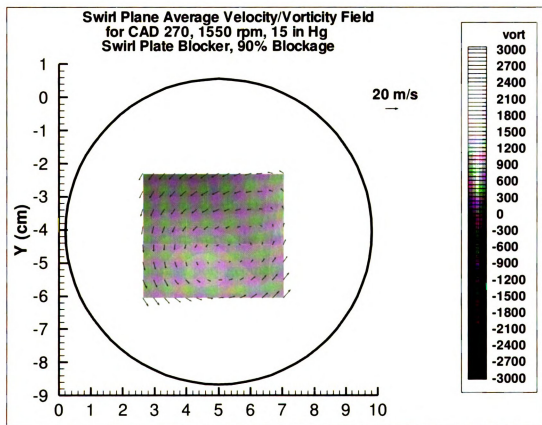


Figure 1.3: Velocities and vorticities of the flow in the swirl plane, CAD 270, tumble port blocker (90%)

that for the

the swirl of

The cy

ous factors

leading to

sient in sp

geometry of

Hasche

four-stroke

and load.

intensities

different en

motions be

at idle condi

pattern at t

Lee and

played a sig

stages of the

Khalighi

180-degree s

configuration

during early

dead center

dominates the

shrouded inte

Urushihar

at the upstre

that for the in-cylinder flow during the intake and compression strokes, the center of the swirl changed its location from one cycle to the next.

The cycle-to-cycle variations on the pre-combustion flow are introduced by numerous factors. These include fluctuations of pressure in the intake and exhaust system, leading to boundary conditions variations at the intake and exhaust valves and transient in speed and throttle position. It is believed that the engine speed and the geometry of the intake system are the most important factors.

Hascher, Novak, et. al. [14] measured the in-cylinder pre-combustion flow in a four-stroke SI engine with the same intake port geometry but variable stroke, speed, and load. They found that the maximum mean flow velocities and the turbulent intensities inside the cylinder scaled with the engine speed, but the flow patterns at different engine speeds exhibit strong similarities. They also found that the tumbling motions break down into two equally strong downward flows along the cylinder liner at idle conditions. In another word, the throttle condition affects the in-cylinder flow pattern at the specific intake port geometry.

Lee and Yoo's studies [15] showed that the different intake port configurations played a significant role in the generation of the initial tumbling motion in the early stages of the intake stroke.

Khalighi [12] generated a well-defined tumble motion in the cylinder by using 180-degree shrouds on both intake valves in a four-valve engine. With this inlet configuration, a small (less than half-cylinder-diameter in size) vortex is generated during early induction and it becomes larger as the piston moves down. At bottom dead center (BDC), the vortex becomes as large as the cylinder bore diameter and dominates the in-cylinder flow. This suggests that the tumbling motion generated by shrouded intake valves would continue into the compression stroke.

Urushihara, Murayama, et. al. [16] used 13 types of swirl control valves installed at the upstream of the intake port to generate different combinations of swirl flow

and tumbl
that tum
swirl flow
mean velo
it.

Based
eral chara
variations

Since re
cross-tumb
were freque
20]. The d
the integra
and normal
body rotati

For a flo
velocity \vec{v} .

Then, the t
is calculated

Or

$$\tilde{H} = \int \tilde{h}$$

and tumble flow in the cylinder. Their studies on these combinations of flow showed that tumble flow generates turbulence in combustion chamber more effectively than swirl flow does. In addition, swirling motion reduces the cycle-to-cycle variation of mean velocity in the combustion chamber, while tumbling motion tends to increase it.

Based on the qualitative understanding on the in-cylinder flow is important, several characteristic quantitative parameters were introduced to reduce cycle-to-cycle variations of the flow in the cylinder.

Since rotational motion is a significant characteristic of the cold flow, tumble ratio, cross-tumble (perpendicular to both tumble and swirl planes) ratio, and swirl ratio were frequently used to quantify the pre-combustion flow in the cylinder [9, 17, 18, 19, 20]. The definition of the tumble, cross-tumble and swirl ratios involves computing the integral of the angular momentum about a specific axis over the entire volume and normalizing it with the angular momentum of a similar volume of fluid in solid body rotation at crankshaft speed.

For a flow particle at \vec{r} (with respect to the origin) having velocity \vec{v} and angular velocity $\vec{\omega}$, the angular momentum of the particle is

$$\vec{h} = \vec{r} \times \vec{v} = \vec{r} \times (\vec{\omega} \times \vec{v}) = h_x \hat{i} + h_y \hat{j} + h_z \hat{k} \quad (1.1)$$

Then, the total angular momentum of mass in the cylinder with respect to the origin is calculated by the integral,

$$\vec{H} = \int \vec{h} \, dm = \int (\vec{r} \times \vec{v}) \, dm = \int (\vec{r} \times (\vec{\omega} \times \vec{v})) \, dm \quad (1.2)$$

Or

$$\vec{H} = \int \vec{h} \, dm = \int h_x \hat{i} \, dm + \int h_y \hat{j} \, dm + \int h_z \hat{k} \, dm = H_x \hat{i} + H_y \hat{j} + H_z \hat{k} \quad (1.3)$$

where H ,

angular m

with resp

If the

momentum

H ,

Similarly,

where I_{xx} ,

particle with

crankshaft

Therefore

the cross-tu

and the swin

Since the

they affect e

tumbling mo

where H_x is the total angular momentum with respect to the x-axis, H_y is the total angular momentum with respect to the y-axis, and H_z the total angular momentum with respect to the z-axis.

If the flow is imagined to rotate as a solid at crankshaft speed, the total angular momentum with respect to x-axis is

$$H_{Sx} = \int h_x dm = \int (\vec{r} \times \vec{v})_x dm = \omega_0 \int (\vec{r} \times \vec{r})_x dm = \omega_0 \int I_{xx} dm \quad (1.4)$$

Similarly,

$$H_{Sy} = \omega_0 \int I_{yy} dm \quad (1.5)$$

$$H_{Sz} = \omega_0 \int I_{zz} dm \quad (1.6)$$

where I_{xx} , I_{yy} , and I_{zz} are three components of the momentum inertia of a flow particle with respect to the x-axis, y-axis, and z-axis, respectively. And ω_0 is the crankshaft angular velocity.

Therefore, according to the definition, the tumble ratio is

$$TR = \frac{H_x}{H_{Sx}} = \frac{\int h_x dm}{\omega_0 \int I_{xx} dm} \quad (1.7)$$

the cross-tumble ratio is

$$CR = \frac{H_z}{H_{Sz}} = \frac{\int h_z dm}{\omega_0 \int I_{zz} dm} \quad (1.8)$$

and the swirl ratio is

$$SR = \frac{H_y}{H_{Sy}} = \frac{\int h_y dm}{\omega_0 \int I_{yy} dm} \quad (1.9)$$

Since the tumbling, cross-tumbling and swirling motions coexist in the cylinder, they affect each other. At the end of compression, the tumbling motion and cross-tumbling motion break. The break of tumbling/cross-tumbling motion not only dis-

turbs t

correlat

introdu

E

where E

the tumbl

In Eq

turbulenc

kinetic en

of these tw

Althou

pre-combu

ratio. Acco

tumble or s

located acco

(including t

Circulat

the velocity

Accordin

turbs the swirl motion but also strengthens and stabilizes the swirl motion. To correlate such complicated interactions, a model based on the heuristic reasoning was introduced by Trigui, Kent, et. al. [9], which is

$$E = (TR^2 + CR^2 + SR^2) - \alpha(|TR||CR| + |TR||SR| + |SR||CR|) \quad (1.10)$$

where E is a quantitative parameter characterizing the flow in the cylinder, TR is the tumble ratio, CR is the cross-tumble ratio, and SR the swirl ratio.

In Equation (1.10), the first three quadratic terms have a favorable influence of the turbulence, while the mixed terms represent an unfavorable influence (destruction of kinetic energy through interaction). The constant α represents the relative influence of these two effects.

Although the tumble ratio and swirl ratio were often used to characterize the pre-combustion flow in the cylinder, it is hard to obtain the accurate tumble or swirl ratio. According to the definition of the tumble and swirl ratio, the calculation of the tumble or swirl ratio depends on the flow rotation center, which is very difficult to be located accurately. To overcome this disadvantage, Jaffri, et. al. [19] used circulations (including total, average, and root-mean-square) to describe the flow in a cylinder.

Circulation Γ [21] is defined as the line integral of the tangential component of the velocity taken around a closed curve C in the flow field, i.e.,

$$\Gamma = \oint_C \vec{v} \cdot d\vec{s} \quad (1.11)$$

According to the definition, vorticity $\vec{\zeta}$ is

$$\vec{\zeta} = \vec{\nabla} \times \vec{v} \quad (1.12)$$

Then

where A

Since

process of

Reuss [1]

at some of

the in-cyl

averaged of

the standa

1.2.2 C

Combustion

Principal co

air. They a

an exotherm

is conventio

observed as

combustion

characterize

Daw and

variable of in

applied chaos

stroke SI eng

variations of

Therefore,

$$\Gamma = \oint_C \vec{v} \cdot d\vec{s} = \iint_A (\vec{\nabla} \times \vec{v}) \cdot \hat{n} dA = \iint_A \vec{\zeta} \cdot \hat{n} dA \quad (1.13)$$

where A is the area enclosed by the curve C and \hat{n} is the normal of A .

Since the cycle-to-cycle variation is superposition of a non-chaotic deterministic process on a stochastic process, a statistical method is preferred to characterize it. Reuss [11] introduced the probability density function (PDF) of the flow velocity at some characteristic points in the cylinder to characterize the cyclic variations of the in-cylinder flow. By using the PDF method, Reuss obtained both ensemble-averaged (represented by the mean of velocities) and cycle-resolved (represented by the standard deviation of velocities) quantities of the flow at characteristic points.

1.2.2 Combustion analysis

Combustion is a necessary process for an internal combustion engine to generate work. Principal components of an engine combustion system are the hydrocarbon fuel and air. They are first combined into a molecular aggregate, and then transformed by an exothermic reaction to form products. The process of the exothermic reaction is conventionally referred to as heat release. In an IC engine, the transformation is observed as a measurable cylinder pressure rise manifesting the essential outcome of combustion. Thus, cylinder pressure is frequently utilized as a direct parameter to characterize the combustion and cycle-to-cycle variations in IC engines.

Daw and Kahl [22] employed the peak cylinder pressure in each power stroke as a variable of interest to study cycle-to-cycle variations in a four-stroke SI engine. They applied chaotic time series analysis (CTSA) method to the cylinder pressure in a four-stroke SI engine fueled with methanol and iso-octane and found that cycle-to-cycle variations of peak pressure exhibit some of the characteristic features of deterministic

chaos.

Ludw

sure curv

their stud

obtained

tor case.

the cycle-

Based

istic proce

established

ries to cha

a four-stro

The pr

characteris

as rate of

record.

The mil

the percent

pressure ch

motion and

the cylinder

established.

the value of

percent pres

of this result

instant durin

chaos.

Ludwig, Leonhardt, et. al. [23] selected the gravity center of the difference pressure curve as a characteristic parameter to study combustion in a diesel engine. In their studies, a difference pressure curve containing information of the combustion is obtained by subtracting the pressure samples of a firing motor from the non-firing motor case. The gravity center of the difference pressure curve was used to characterize the cycle-to-cycle variations of the combustion in the engine.

Based on the fact that cycle-to-cycle variations are superposition of a deterministic process on a stochastic process, Roberts, Peyton Jones, and Landsborough [24] established a stochastic process model for the entire ensemble of pressure-time histories to characterize the cycle-to-cycle variation throughout the combustion period in a four-stroke SI engine.

The pressure in the cylinder is important not only for itself as a quantitative characteristic parameter, but also because some combustion related parameters, such as rate of heat release and rate of mass burned, can be derived from the pressure record.

The milestone was set by Rassweiler and Withrow [25]. After failing to correlate the percent mass burned with the measured pressure data, they divided the measured pressure change in a specific interval into two parts: pressure change due to piston motion and pressure change due to combustion. In this way, a relationship between the cylinder pressure rise during the combustion and the fraction of mass burned was established. They concluded that throughout the entire period of the combustion, the value of percent mass burned at any given crank angle is very nearly equal to the percent pressure rise due to combustion at the same crank angle. The significance of this result is that information about the fraction of mass of charge burned at any instant during the combustion may be obtained by finding the percent of the pressure

rise due to

where M

total mass

reduced pressure

combustion

With the

thermodynamic

to the cycle

The final

from inlet

for an increase

where dQ_{int}

done by the

internal energy

If the gas

pressure, cycle

rise due to combustion using measured pressure data, i.e.,

$$\frac{M_b}{M} = \frac{P - P_i}{P_f - P_i} \quad (1.14)$$

where M_b is the mass of inflamed section of the charge at the given time, M is the total mass of charge, P_i is the measured pressure at the time of ignition, P is the reduced pressure at the given time, and P_f the reduced pressure at the end of the combustion.

With the cylinder pressure data, a heat release model based on the first law of thermodynamics was proposed by Homsy and Atreya [26] for the study of heat transfer to the cylinder wall during the combustion.

The first law equation for the in-cylinder mass in a closed system, which starts from inlet valve close (IVC) and ends at exhaust valve open (EVC), can be written for an incremental crank angle interval as

$$dQ_{hr} = dW + dU_S + dQ_w \quad (1.15)$$

where dQ_{hr} is the gross heat energy released during the combustion, dW is the work done by the piston and expressed as $dW = p \cdot dV$, dU_S is the change in sensible internal energy, and dQ_w the heat transfer to cylinder wall.

If the gas in the cylinder is assumed the ideal gas, three equations relating cylinder pressure, cylinder volume, and gas temperature are obtained.

$$m \cdot c_v \cdot dT = dU_S \quad (1.16)$$

$$\frac{d(p \cdot V)}{m \cdot R} = dT \quad (1.17)$$

$$\frac{R}{c_v} = \gamma - 1 \quad (1.18)$$

where m

at constant

By ap

heat trans

There

from the p

gas and th

Similar

for direct-i

For mo

acterizing

with with

However, t

sure is not

i.e., ignitic

burn rate

flame burn

to describe

combustion

The cyl

independen

cycle variat

Urushih

developed fi

in the cylind

where m is the mass in the cylinder, T is the gas temperature, c_v is the specific heat at constant volume, R is the gas constant, and γ the ratio of specific heats.

By applying the above ideal gas relationships to the first law equation (1.15), the heat transfer model is reduced to

$$dQ_w = dQ_{hr} - \frac{\gamma}{\gamma - 1} \cdot p \cdot dV - \frac{1}{\gamma - 1} \cdot V \cdot dp \quad (1.19)$$

Therefore, the heat transfer to the wall during the combustion can be calculated from the pressure data based on the assumptions that gas in the cylinder is the ideal gas and that there is no blow-by or valve leakage.

Similar heat transfer models were described by Heywood [1] and Brunt, et. al. [27] for direct-injection engines.

For most cases, the cylinder pressure is a preferable quantitative parameter characterizing the combustion process, since it is easily measured and when combined with piston position is the macroscopic manifestation of the four stroke cycle. However, the combustion in an IC engine is such a complex process that cylinder pressure is not able to characterize it completely. The combustion-related parameters, i.e., ignition delay, crank angle location at 50% mass fraction burned (MFB), early burn rate (crank angle duration corresponding to 0-10% MFB), and fully developed flame burn rate (crank angle duration corresponding to 10-90% MFB), are of help to describe and have been implemented to provide more detailed information about combustion process in an IC engine.

The cylinder pressure and the above combustion-related parameters could be used independently or simultaneously to characterize the combustion process and cycle-to-cycle variations on the combustion in an IC engine.

Urushihara, Murayama, et. al. [28] used early burn rate (0-10% MFB) and fully developed flame burn rate (10-90% MFB) to determine the influence of the turbulence in the cylinder on the combustion process. They found that the fully developed flame

burn rate

that incr

Johan

on the co

burn rate

combusti

combusti

Steve

effective

study the

They fou

work out

reduce cy

Dai, 7

of cycle-t

ratio, in-

rate, and

up a com

ignition c

Despi

adapted

next sect

burn rate is directly proportional to the early burn rate. In addition, they observed that increasing turbulence intensity would shorten the combustion duration.

Johansson and Olsson [29] studied the effects of the shape of combustion chamber on the combustion process by early burn rate (0-10% MFB) and fully developed flame burn rate (10-90% MFB). They also found that fully developed flame burn rate of the combustion has a strong correlation to the average turbulence in the cylinder during combustion.

Stevens, Shayler and Ma [30] calculated cross-correlation of gross indicated mean effective pressure (IMEP) and crank angle location at 50% mass fraction burned to study the effect of the spark timing and fuelling level on the cycle-to-cycle variations. They found that modifying A/F ratio or spark timing has a significant effect on the work output of that cycle, and thereby can be used as an effective control variable to reduce cycle-to-cycle variations.

Dai, Trigui, and Lu [3] identified seven physical parameters to represent the sources of cycle-to-cycle variations in a SI engine, which are engine speed, engine load, A/F ratio, in-cylinder residual mass fraction, early burn rate, fully developed flame burn rate, and crank angle location at 50% MFB. By correlating these parameters, they set up a complex nonlinear model to characterize the cycle-to-cycle variations in spark ignition engines.

Despite efforts of nearly 100 years, no satisfactory method have been universally adapted to quantify and control cycle-to-cycle variabilities in piston engines. In the next section, we begin to outline a strategy with this problem.

1.2.3 Cycle-to-cycle variation reduction

Upon the understanding of the pre-combustion flow and combustion in an IC engine, many methods have been presented to reduce cycle-to-cycle variation.

It is believed that the main source of cycle-to-cycle variation is the turbulent

nature

was to

at the e

The

der has

35], shro

how to s

motion c

kernel co

and prod

Ohsug

uniform A

optimizati

wall is uni

obtain a u

Combu

ratio in the

that when

lence gener

the charge

The abo

ing the cyc

systems no

the engine.

information

be introduce

Two rese

nature of charge motion at the time of ignition [31, 32, 33, 34]. Therefore, most effort was to obtain the consistent flow pattern and stable A/F ratio around the spark plug at the end of compression.

The rotational motion (tumble, cross-tumble and swirl) of the charge in the cylinder has been investigated widely. Swirl control valves [28], port blockers [19, 20, 17, 35], shrouded intake valves [12] and masked cylinder head [9] were used to investigate how to stabilize the flow at the end of the compression. And it was found that swirling motion can generate a more stabilized flow field at the time of ignition, cause flame kernel convection in the tangential direction, especially with an off-center spark plug, and produce high levels of small-scale turbulence in the cylinder.

Ohsuga, Yamguchi, et. al. [36] studied three fuel-supply systems and achieved a uniform A/F ratio in the cylinder by optimizing the fuel supply system. With the optimization of the fuel-supply system, fuel vapor distribution around the cylinder wall is uniform and this uniform fuel vapor is transported by the tumbling motion to obtain a uniform A/F ratio around the spark plug at the time of ignition.

Combustion chamber geometry, which has strong influences on the flow and A/F ratio in the cylinder, was extensively studied by Johansson, et. al. [29, 37]. It is found that when the standard disc-shaped combustion chamber was replaced with a turbulence generating geometry, such as cross combustion chamber, the inhomogeneity of the charge in the cylinder became very low.

The above flow control techniques have been successful in a limited manner reducing the cycle-to-cycle variation in work in a SI engine. However, they are open-loop systems not able to implement the real-time control on the combustion process in the engine. Other techniques, having the ability to extract real-time characteristic information for each cycle and effectively reduce the cycle-to-cycle variations, have to be introduced.

Two researches suggested that the fundamental source of cycle-to-cycle variations

is the n
on this v
actively
the fuel s
introduce

In a c
are the sa
a governo
strategies
actuators
reacting jo
is a micro
to modula
The schem

A prot
In this pro
from cylin
informatio
the combu

is the non-linear nature of the chemical reactions in combustion [33, 38]. Based on this viewpoint and the experimental evidence that combustion instability can be actively controlled by coupling pressure variation in the combustion chamber with the fuel supply system [45], the concept of controlled combustion engines (CCE) was introduced [39, 42, 43, 44].

In a controlled combustion engine, principal elements of the engine control system are the same as those in general feedback control systems, i.e., sensors, actuators, and a governor. In this application, the sensor measures cylinder pressure. In other control strategies [39], the emission sensors (e.g. oxygen concentration sensor) are used. The actuators for the CCE could be fuel jet injectors and jet igniters producing turbulent reacting jet plumes where combustion takes place away from the walls. The governor is a micro-electronic processor incorporating a sufficiently fast data reduction facility to modulate the execution of the exothermic process in real time of the engine cycle. The schematic of a controlled combustion engine is shown in Figure 1.4.

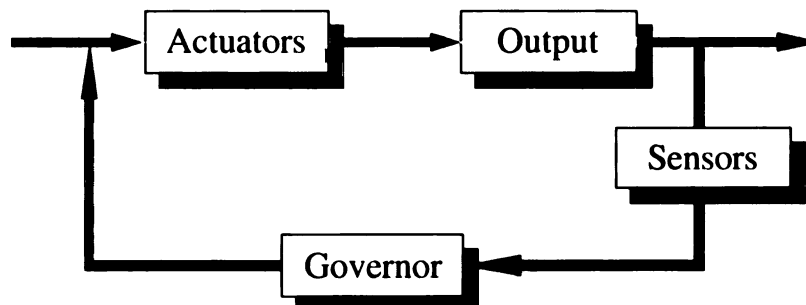


Figure 1.4: The schematic of a controlled combustion engine

A prototype [43, 44] of a controlled combustion engine is shown in Figure 1.5. In this prototype, the electronic control modulator generates the control information from cylinder pressure, which is measured by pressure sensors. The feedback control information is then sent to the air-blast atomizer and flame jet generator to control the combustion in the cylinder.

Figure 1.5
omizer: 2
modulator
terms of a

1.3 M

There cur
which are
control m
to have an
not able t
In this dis
variations
blockers on
Combu
alters some
event. The
close-loop s

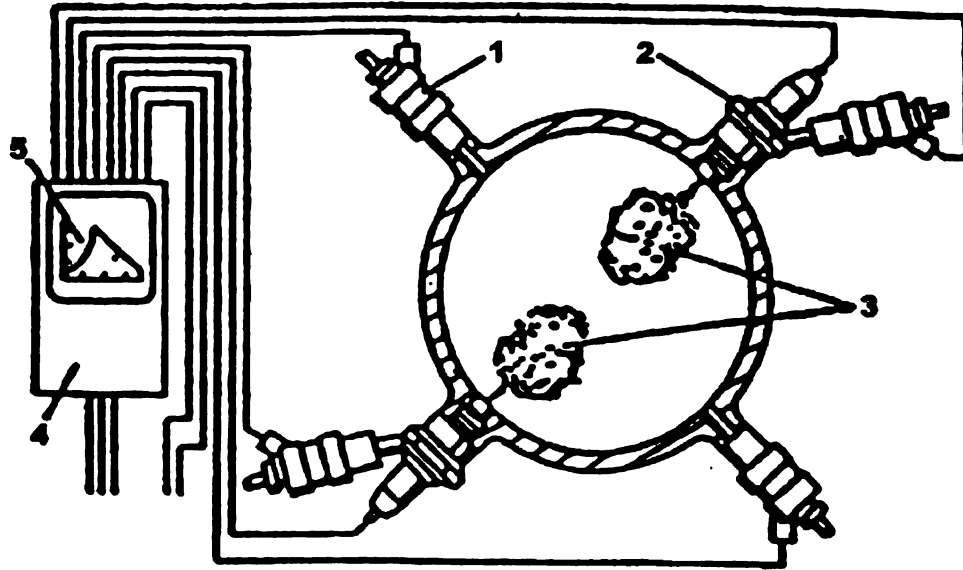


Figure 1.5: Prototype of a controlled combustion engine system: 1 - the air-blast atomizer; 2 - the flame jet generator; 3 - turbulence jet plumes; 4 - the electronic control modulator; and 5 - the pressure transducer and shaft decoder records expressed in terms of an indicator diagram.

1.3 Motivation and objectives

There currently exist two ways to reduce cycle-to-cycle variations in an IC engine, which are pre-combustion flow control and combustion control. Pre-combustion flow control means that one changes the flow field characteristics in such a manner so as to have an influence on the subsequent combustion events. It is an open-loop system not able to implement real-time control on cycle-to-cycle variations in the cylinder. In this dissertation, a statistical method is improved to quantify the cycle-to-cycle variations of the pre-combustion flow field and the influence of 3 different port plate blockers on the flow field is investigated.

Combustion control means that based on analysis of the combustion process one alters some type of input actuator to change the nature of the subsequent combustion event. The combustion control, realized by controlled combustion engines (CCE), is a close-loop system having a perspective to reduce cycle-to-cycle variations effectively.

The con

cycle-to-

the natu

charge c

controlle

tant [40

the cycl

In a

a key to

in an IC

the inpu

cycle.

nature

sensors.

the con

control

in a cor

informa

In t

introdu

cycle va

evaluati

Upon p

quantif

tained.

dynam

the cyc

The combustion control has the advantage over pre-combustion flow control to reduce cycle-to-cycle variations in an IC engine as this method can provide an input based on the nature of the previous event. In addition, with the emerging of the homogeneous charge compression ignition (HCCI) engine in which the combustion process can be controlled by adjusting the initial temperature and species concentrations of reactant [40][41], combustion control becomes a practical technique to effectively reduce the cycle-to-cycle variations in the engine.

In a controlled combustion engine, the data reduction algorithm in the governor is a key to implementing the correct and accurate real-time control on the combustion in an IC engine. There are two requirements for the data reduction algorithm. First, the input data should be measured conveniently and accurately for each operating cycle. The cylinder pressure is an ideal choice as input because of its descriptive nature with respect to the desired output and the availability of reliable pressure sensors. Second, the algorithm for data reduction should not be complicated so that the control information can be quickly generated by a micro-electronic combustion control unit (CCU). Current data reduction algorithms are not readily implemented in a control algorithm [42]. Little effort has been expended to date to obtain control information from the cylinder pressure.

In this dissertation, a new data-reduction method based on the cylinder pressure is introduced to pave the way for controlling the combustion and reducing the cycle-to-cycle variation in an IC engine. The pressure diagnostics is an inverse process, which evaluates the mechanism of the combustion in the cylinder from its measured output. Upon pressure diagnostics, the development of the dynamic stage of combustion is quantified and the effectiveness of combustion during the exothermic process is obtained. Therefore, a concept for the controlled combustion engine, which controls the dynamic stage of combustion to improve the effectiveness of combustion and reduce the cycle-to-cycle variations on combustion, is present.

Cha

Pre

2.1

The pre-

engine ge

have diff

The cycl

to be res

estimate

the same

decade,

variabili

function

character

In th

the turn

of choos

instanta

samples

the avera

is calcula

Chapter 2

Pre-combustion flow analysis

2.1 Introduction

The pre-combustion flow in the engine cylinder is affected by many factors including engine geometry, speed, valve timing, and valve lift. From cycle to cycle, these factors have different influences on the in-cylinder flow, and thus a cyclic variation is created. The cycle-to-cycle variation of the pre-combustion flow inside the cylinder is known to be responsible for various aspects of the combustion characteristics. It has been estimated that there would be a 10% increase in power output of premix engines for the same fuel consumption if cyclic variability could be eliminated [5] . In the last decade, various methods were developed to characterize in-cylinder flow and the cyclic variability of this flow. Specifically, Reuss [11] introduced the probability density function (PDF) of the flow velocity at some characteristic points in the cylinder to characterize the cyclic variations of the in-cylinder flow.

In this chapter, an improved PDF method is introduced to quantify the effects of the tumble and swirl port blockers on cyclic variability of in-cylinder flow. In stead of choosing the velocities at a local point as samples, the author employ normalized instantaneous circulation of the flow on a tumble or swirl plane. The PDFs of such samples are generated to characterize the cycle-to-cycle variations. Besides PDFs, the averaged turbulent kinetic energy (TKE) of the flow on the tumble or swirl plane is calculated and compared to the PDF results.

2.2

Molecul

ine passi

Figure 2

re-stroke

as well as

and the l

insert. B

inside of

intake run

to accept

Three

no port b

and a sw

three cas

The two

on the flo

which the

was run a

2.3

Shown in

the flow o

flow is rota

Equation (

When t

2.2 Experimental setup

Molecular Tagging Velocimetry (MTV), described in Section 1.2.1, was used to examine passive control of the flow to a 3.5-liter DaimlerChrysler engine, which is shown in Figure 2.1. The head is mounted on top of a single cylinder Hatz engine that has been re-stroked to 81 mm to match the crankshaft geometry of the DaimlerChrysler engine as well as use the original connecting rod. Located between the DaimlerChrysler head and the Hatz reciprocating assembly are the quartz cylinder and piston with a quartz insert. Both the cylinder and piston are designed to provide optical access to the inside of the engine cylinder while retaining the original engine bore of 96 mm. The intake runner of the standard DaimlerChrysler intake manifold is used and modified to accept the port blockers for studying passive flow control.

Three different intake port configurations were considered for these experiments: no port blocker or open port, a tumble port blocker with 70% blockage (Figure 2.2) and a swirl port blocker with 90% blockage (Figure 2.3). Data was acquired for all three cases at the tumble plane and a swirl plane for crank angles 270° and 300° . The two specific crank angles are chosen for studies on the influence of port blockers on the flow field near the end of compression. The latter crank angle is the limit at which there is still optical access to the tumble plane flow. In all cases, the engine was run at 1550 rpm and throttled to 15 inches Hg.

2.3 Normalized circulation

Shown in Figure 1.2 and 1.3 are typical rotational motions (tumble and swirl) of the flow on the tumble and swirl planes inside the cylinder, respectively. Since the flow is rotational, the circulation of the flow on the tumble or swirl plane, defined by Equation (1.11) and (1.13), is used to characterize the motion of the flow.

When the flow on the tumble or swirl plane was studied at different CADs, the

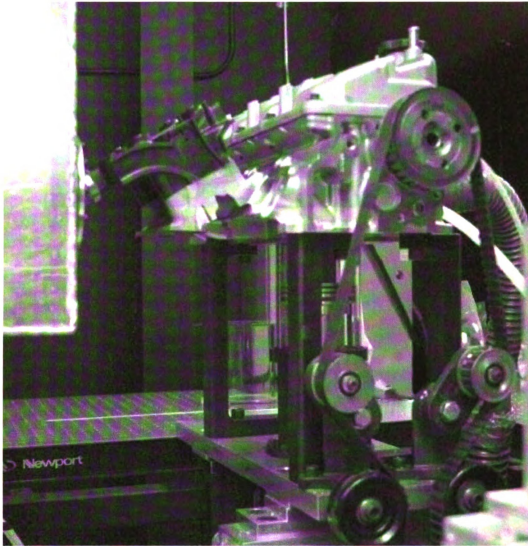


Figure 2.1: 3.5-liter DaimlerChrysler engine

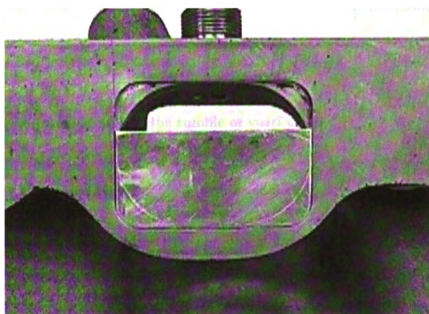


Figure 2.2: Tumble port blocker

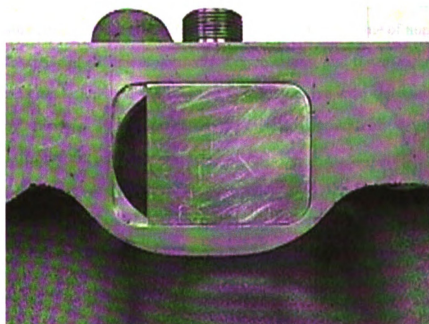


Figure 2.3: Swirl port blocker

area of
of flow

where A

2.4

The pro
acterize
dissert
the cyl
circula
veloci

Fi

impo
cular
of no
stand
and

S
over
nor

area of each plane is not the same. To make the results comparable, the circulations of flow on different planes have to be normalized by the area of the plane, which is

$$\Gamma_N = \frac{1}{A_T} \oint_C \vec{v} \cdot d\vec{s} = \frac{1}{A_T} \iint_A \vec{\zeta} \cdot \hat{n} dA \quad (2.1)$$

where A_T is the studied area of the tumble or swirl plane.

2.4 PDF method

The probability density function (PDF) of a local flow velocity is introduced to characterize the cyclic variations of the flow inside the cylinder by Reuss [11]. In this dissertation, the PDFs of the normalized circulation over a tumble or swirl plane in the cylinder are generated. This method has an advantage over Reuss's method, since circulation over a plane is a better parameter characterizing the flow field than local velocities [17].

Figure 2.4 shows a PDF of the normalized circulation on the tumble plane. Three important quantities are calculated based on the PDF: mean value of normalized circulations, the range of change of normalized circulations, and the standard deviation of normalized circulations. In this work, a Gaussian curve with the same mean and standard deviation was superimposed on the measured probability density function and used to display the experimental results.

Suppose there are M sample cycles. For each cycle, the normalized circulation over a tumble or swirl plane Γ_{Ni} is computed by Equation (1.13). The mean of the normalized circulation is the ensemble-averaged NC defined by Equation (2.2).

$$\bar{\Gamma} = \frac{\sum_{i=1}^M \Gamma_{Ni}}{M} \quad (2.2)$$

The range of change of normalized circulations, which represents the range of

0
0
0
0
0
0
0
0

Probability

Figure
180.

cycli

15
17

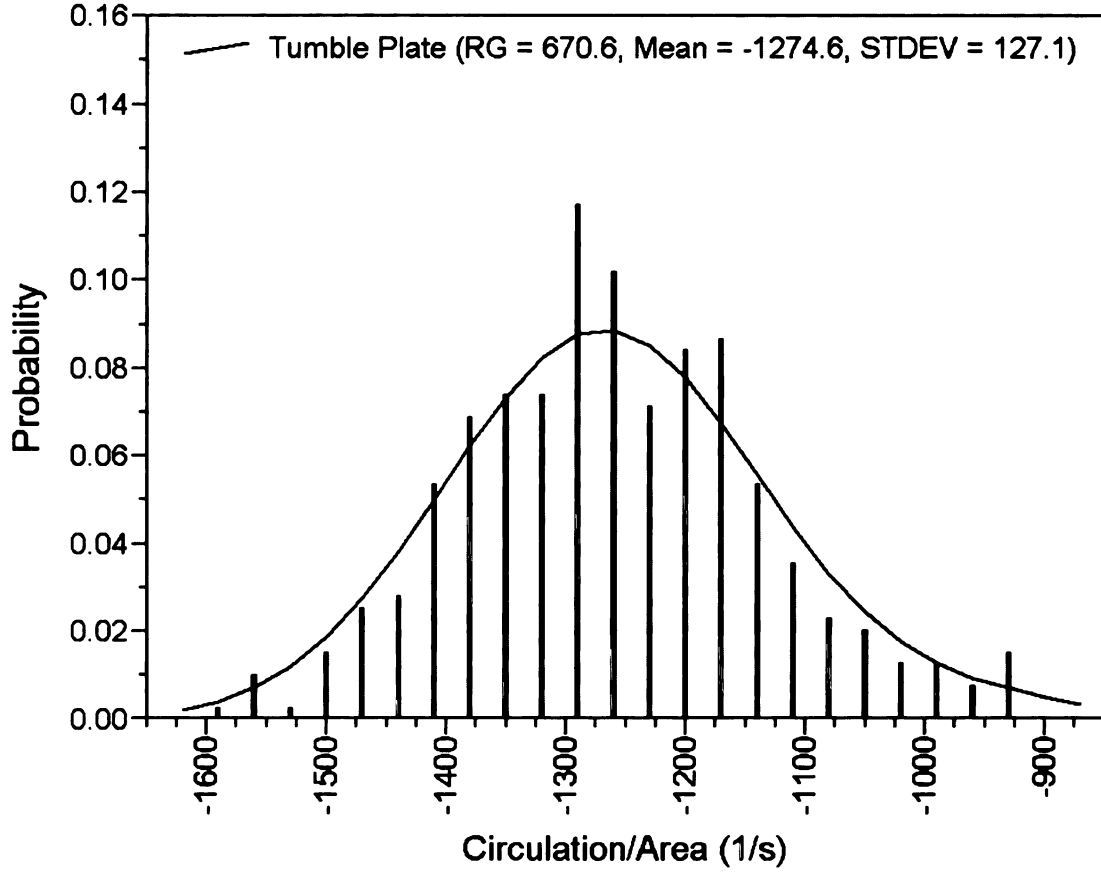


Figure 2.4: The PDF for the circulation over a unit area on the tumble plane at CAD 180, tumble plate blocker.

cyclic variation of the flow inside the cylinder, is formulated as

$$RG = \max\{\Gamma_{Ni}\} - \min\{\Gamma_{Ni}\} \quad (2.3)$$

The standard deviation of normalized circulations is

$$STDEV = \sqrt{\frac{M \sum \Gamma_{Ni}^2 - (\sum \Gamma_{Ni})^2}{M(M-1)}} \quad (2.4)$$

The mean value of normalized circulations gives the ensemble-averaged information of the flow inside the cylinder, generally characterizing the rotational motion inside the cylinder. The range of change of normalized circulations could quantify

the cyc
range in
cant pa
data ca
cyclic v
circula
mately
circula
shown

2.5

2.5.

The
mali
that
shov
(ST
the
tion
(M

cat
ax
to
to

the cycle-to-cycle variability of the flow inside the cylinder. A higher value of the range indicates more cyclic variations. However, the range is not statistically significant parameter to quantify the cyclic variations because extraordinary experimental data can contaminate the results. A more representative quantity characterizing the cyclic variation of the flow inside the cylinder is the standard deviation of normalized circulations. In general, the range of change of the normalized circulation is approximately 6 times equal to the standard deviation, which indicates that the normalized circulation of the flow on a tumble or swirl plane is normally distributed. This is shown clearly by the shape of the PDF in Figure 2.4.

2.5 Cyclic variations of the flow with different port blockers

2.5.1 Tumble plane

The results shown in Figure 2.5 show that the standard deviations (STDEV) of normalized circulation (NC) increases when port blockers are applied, which indicates that cycle-to-cycle variations of the flow are strengthened by port blockers. It is also shown that the tumble port blocker ($\text{STDEV} = 112.12s^{-1}$) and swirl port blocker ($\text{STDEV} = 117.0s^{-1}$) have the same effect on strengthening the cyclic variations of the flow, though tumble port blocker has stronger effect on strengthening the rotational motion of the flow ($|\text{MEAN}| = 1354.2s^{-1}$ for the tumble port blocker, while $|\text{MEAN}| = 609.7s^{-1}$ for the swirl port blocker).

To further evaluate this conclusion, the turbulent kinetic energy (TKE) [81][82] is calculated for the same flow field. The flow in the cylinder is known to be turbulent and thus the turbulent kinetic energy is a eligible parameter characterizing cycle-to-cycle variations of the flow. Higher turbulent kinetic energy indicates stronger turbulence and more cyclic variations.

Similar to normalizing the circulation, the averaged TKE over the studied plane

Figure
differ

is cal

are P

TKE

where

F

STD

obtai

to-cy

block

tumb

Si

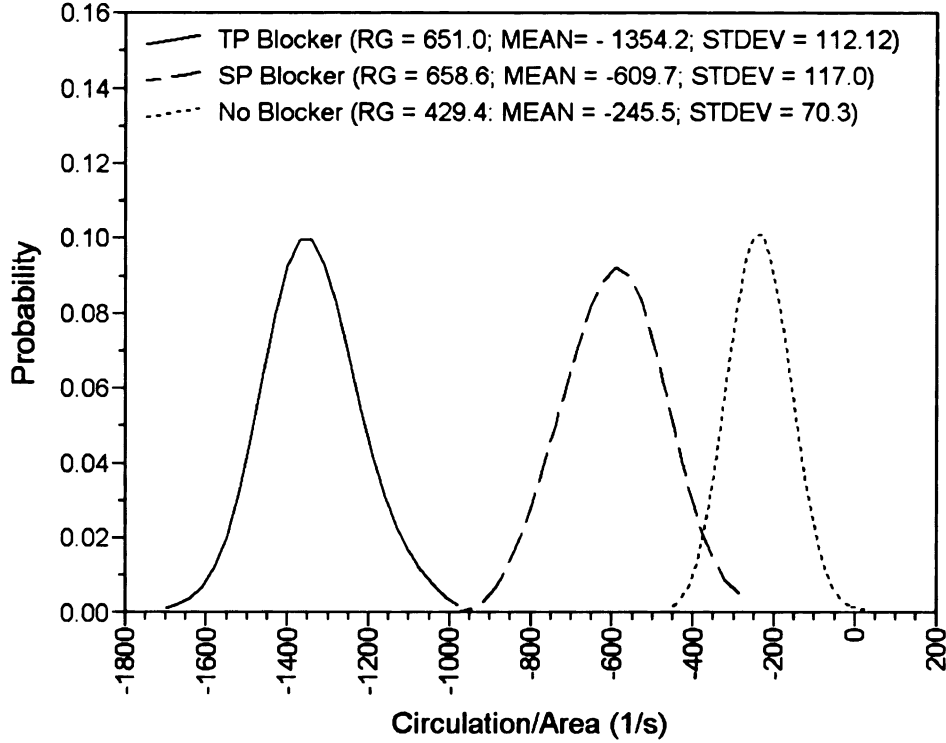


Figure 2.5: The PDF for the circulation over a unit area on the tumble plane with different port blockers at CAD 270.

is calculated by normalizing the TKE by the area of the studied plane. Suppose there are P vectors on the plane, and the local TKE at point i is E_i , then the averaged TKE is

$$E_N = \frac{1}{A_T} \sum_{i=1}^N E_i A_i \quad (2.5)$$

where A_T is the total area of the studied plane and A_i the area containing point i .

Figure 2.6 shows the comparison of the cyclic variability characterized by the STDEV of normalized circulation and by the averaged TKE. It is shown that results obtained with both methods are consistent, i.e., port blockers strengthen the cycle-to-cycle variations of the flow. However, the averaged TKE of flow with tumble port blocker is about 1.5 times greater than that with swirl port blocker, indicating the tumble port blocker has stronger influence on the cyclic variations of the flow.

Similar results and conclusions are found for the tumble plane at 300° , as shown

Figure
flow on

in Fig

2.5.1

Show

plan

the n

bloo

cha

It y

str

tw

th

ch

in

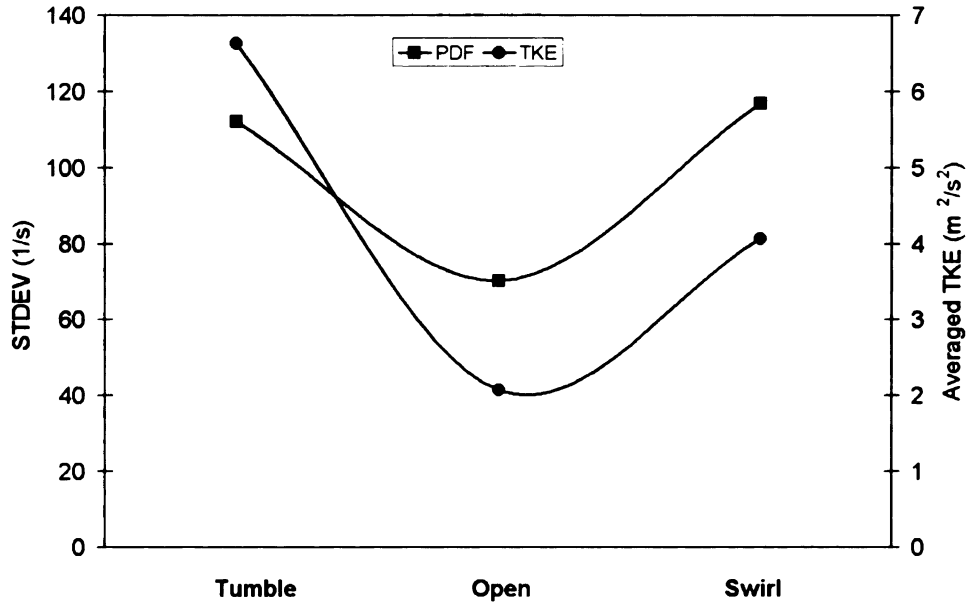


Figure 2.6: Influences of different port blockers on the cycle-to-cycle variations of the flow on the tumble plane at CAD 270.

in Figure 2.7 and 2.8.

2.5.2 Swirl plane

Shown in Figure 2.9 are the PDFs of normalized circulation of the flow on the swirl plane with different port blockers. It is shown that the swirl plate blocker strengthens the rotational motion on the swirl plane ($|\text{MEAN}| = 865.7s^{-1}$), while the tumble plate blocker slightly weakens it ($|\text{MEAN}| = 18.5s^{-1}$). In addition, both port blockers change the rotational direction of the flow from the clockwise to counter-clockwise. It is also indicated by the STDEV that both port blockers has the same effects on strengthening cycle-to-cycle variations of the flow ($\text{STDEV} = 116.8s^{-1}$ for the tumble port blocker and $\text{STDEV} = 113.4s^{-1}$ for the swirl port blocker). Figure 2.10 shown the comparison of the cyclic variability characterized by the STDEV of normalized circulation and by the averaged TKE. It is shown that results obtained by both methods are consistent.

Similar results and conclusions are found for the flow on the swirl plane at 300°

Figure
differ

Figure
flow of

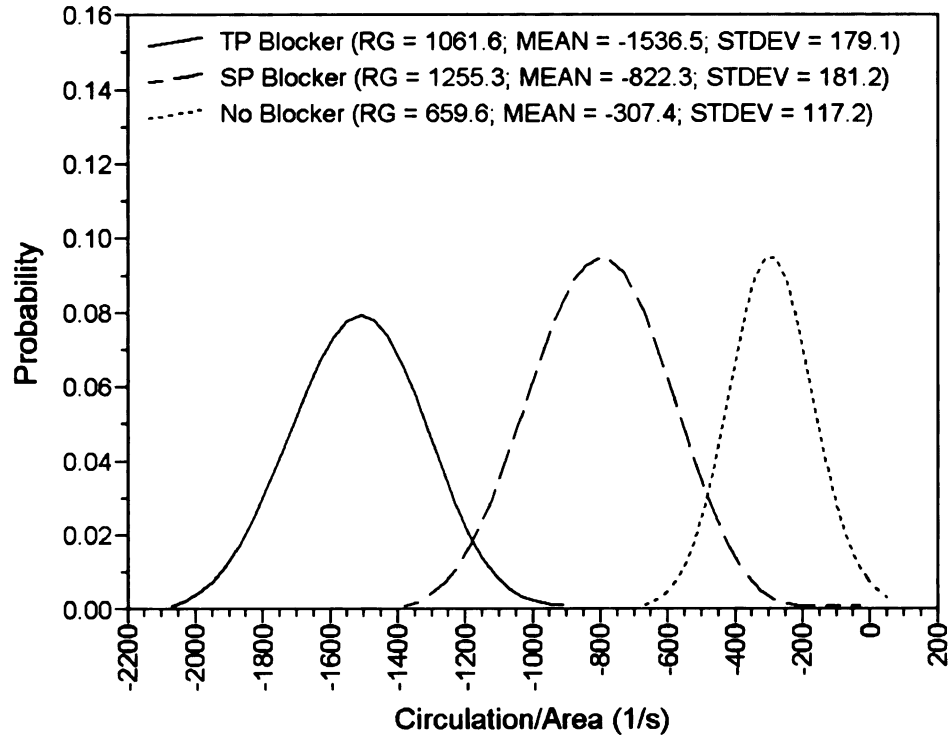


Figure 2.7: The PDF for the circulation over a unit area on the tumble plane with different port blockers at CAD 300.

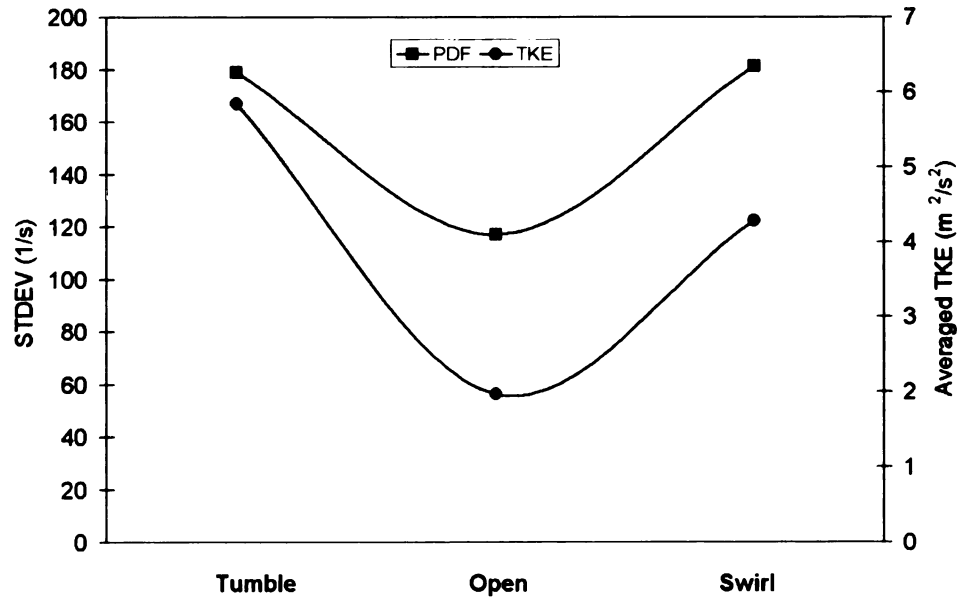


Figure 2.8: Influences of different port blockers on the cycle-to-cycle variations of the flow on the tumble plane at CAD 300.

Figure
differ

Figure
flow

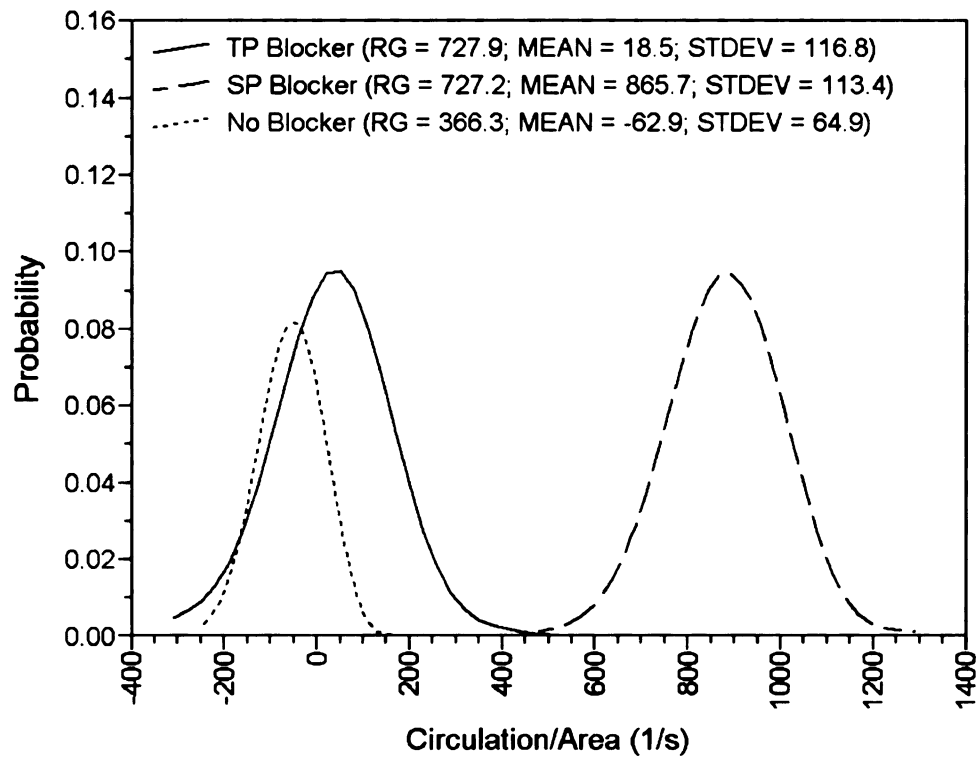


Figure 2.9: The PDF for the circulation over a unit area on the swirl plane with different port blockers at CAD 270.

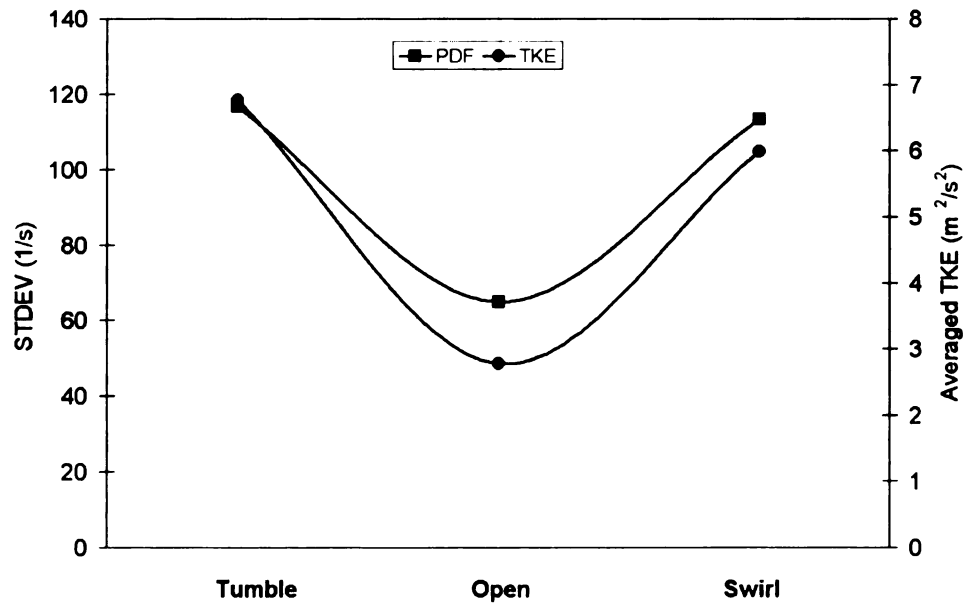


Figure 2.10: Influence of different port blockers on the cycle-to-cycle variations of the flow on the swirl plane at CAD 270.

Figure
differ

except
ation

2.6

The

Figure

show

2.3

blo,

the

inf

A

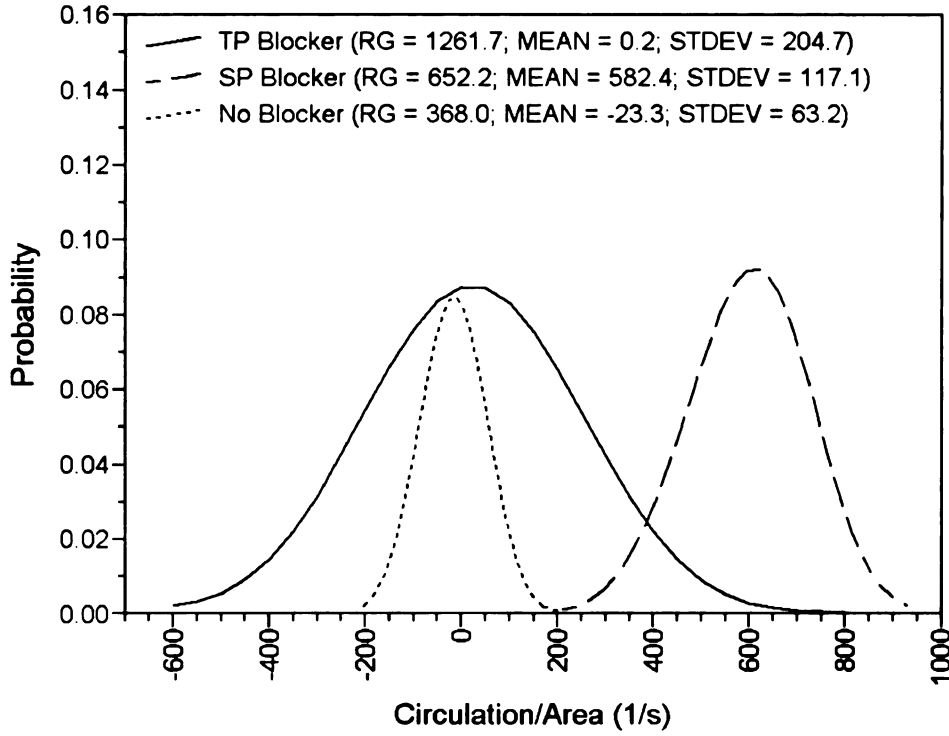


Figure 2.11: The PDF for the circulation over a unit area on the swirl plane with different port blockers at CAD 300.

except that the tumble port blocker has stronger influence on the cycle-to-cycle variations of the flow than swirl port blocker, which are shown in Figure 2.11 and 2.12.

2.6 The influence of the shape of port blockers

The influence of the shape of port blocker is also studied in the dissertation. Shown in Figure 2.13 and 2.14 are tumble and swirl port blockers with different shape from those shown in Figure 2.2 and 2.3. In the context, port blockers shown in Figure 2.2 and 2.3 are called blockers A, while port blockers shown in Figure 2.13 and 2.14 are called blockers B. It is shown in Figure 2.15 -- 2.18 that the shape of the port blocker has the strong influence on the flow. Both tumble and swirl port blockers B have weaker influence on the rotational motion of the flow on the tumble plane than blockers A. However, blockers B and blockers A have a similar influence on cyclic variations

Figure
the fl

of th

block

block

in-cy

block

the i

effici

7

of it

of c

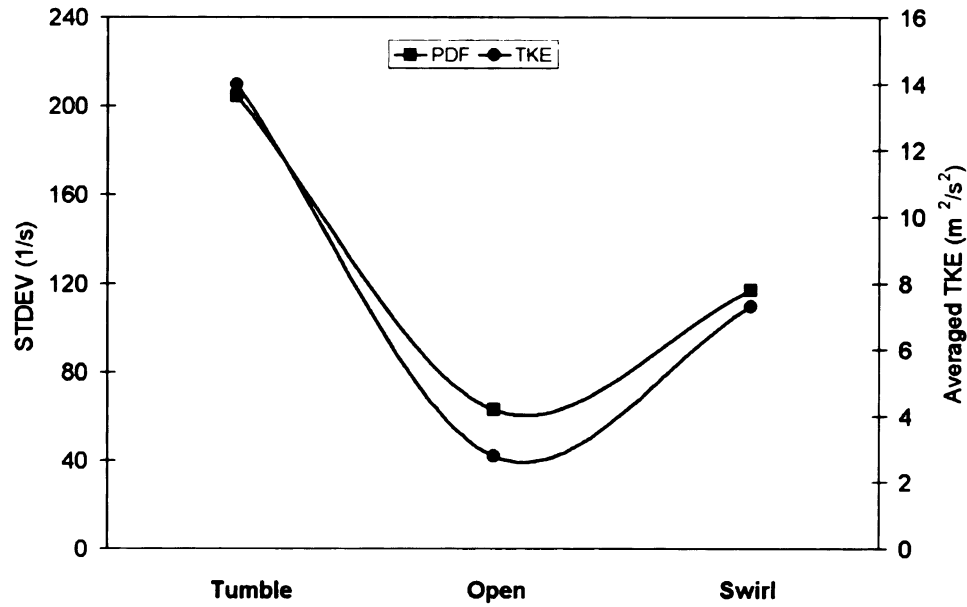


Figure 2.12: Influences of different port blockers on the cycle-to-cycle variations of the flow on the swirl plane at CAD 300.

of the flow on the tumble plane. For the flow on the swirl plane, the influences of blockers A and blockers B are similar. It is apparent that geometric nature of port blockers have a significant influence on the rotational motion and cyclic variations of in-cylinder flow. Experiment has shown that the level of variation produced by port blockers A had a strong influence on the combustion rate and engine efficiency, while the influence of blockers B was ineffective in changing the combustion rate or engine efficiency.

This leads us to believe that in order to further evaluate the nature of the influence of in-cylinder flow motion on combustion, we must develop a realistic measure of rate of conversion of reactants to products. This development is discussed in next chapters.

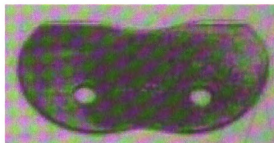


Figure 2.13: Tumble port blocker B

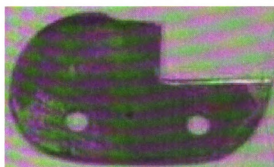


Figure 2.14: Swirl port blocker B

Figure
on the

Fi
on

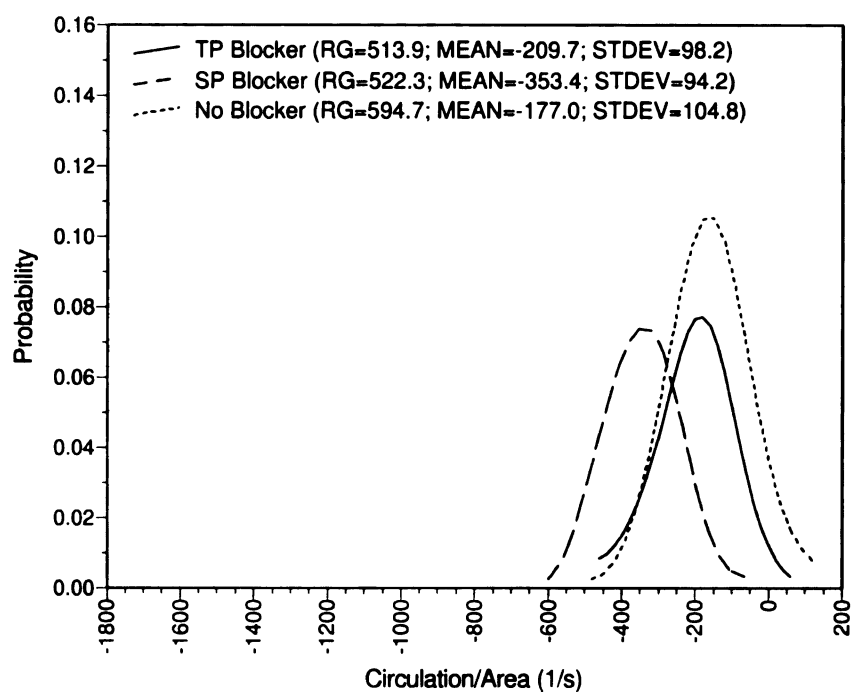


Figure 2.15: Influences of port blockers B on the cycle-to-cycle variations of the flow on the tumble plane at CAD 270.

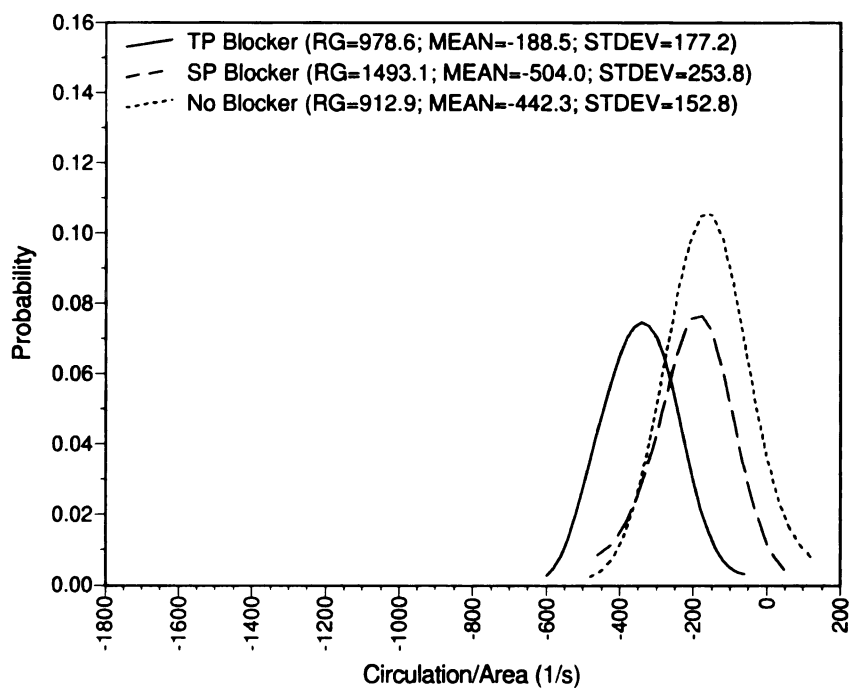


Figure 2.16: Influences of port blockers B on the cycle-to-cycle variations of the flow on the tumble plane at CAD 300.

Figure
on the

Figure
on the

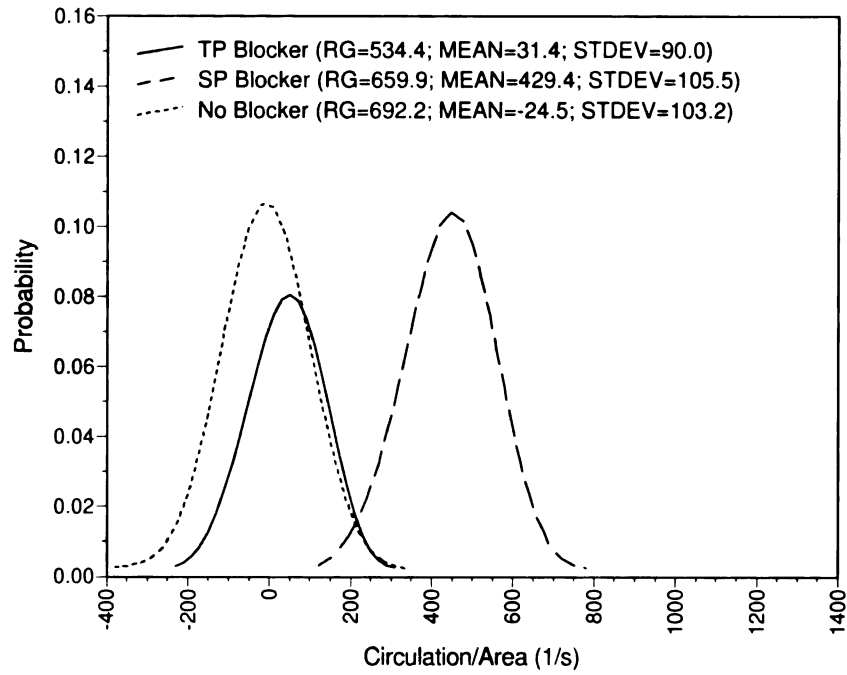


Figure 2.17: Influences of port blockers B on the cycle-to-cycle variations of the flow on the swirl plane at CAD 270.

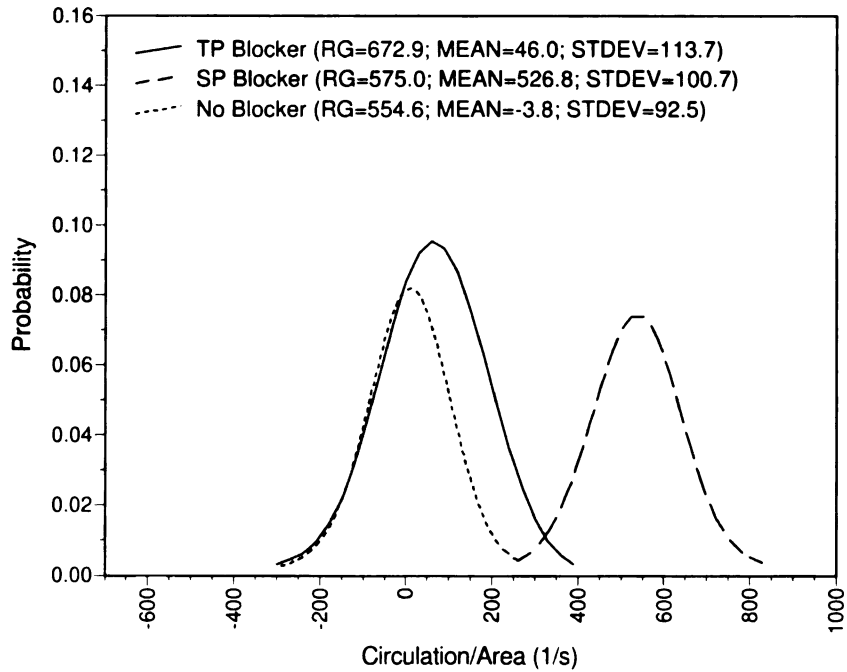


Figure 2.18: Influences of port blockers B on the cycle-to-cycle variations of the flow on the swirl plane at CAD 300.

Chapter 3

Dynamic stage of combustion in an IC engine

3.1 Introduction

The sole purpose of combustion in a piston engine is to generate pressure in order to push the piston and produce work. In a work-production cycle, the air/fuel mixture is first induced into the cylinder, then experiences the polytropic compression from the piston. The compression increases the pressure and temperature in the cylinder, and a heat-release chemical reaction is activated by a spark or other means. Finally, gases in the cylinder experience an expansion process and push the piston to produce work.

The cylinder pressure is the most significant parameter characterizing the engine operation. The processes of compression, chemical reaction, and expansion during an engine operation cycle are all recorded by the cylinder pressure.

Because of the existence of cycle-to-cycle variations in chemical reaction rates, the cylinder pressure records are different from cycle to cycle. The pressure records for ten cycles in a single-cylinder spark-ignition engine are shown in Figure 3.1. It is shown in the figure that cycle-to-cycle variations of the pressure records are macroscopic manifestation of the exothermic chemical reaction process. Therefore, studies on the pressure records during the chemical reaction process in a piston engine are of help to reduce the cycle-to-cycle variations in the engine. In this chapter, the dynamic stage

of co
cycle

Figure
opera
Heyv

3.2

In p
gine
mod
plot

wh
vol

of combustion in a SI engine is defined and analyzed to characterize and control the cycle-to-cycle variations in the combustion.

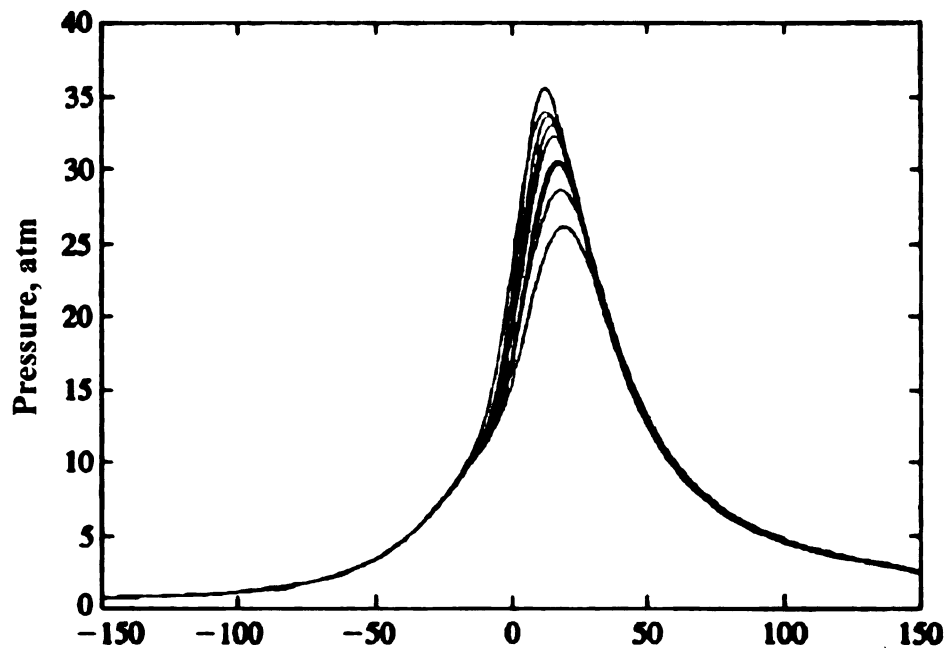


Figure 3.1: Pressure records for ten cycles in single-cylinder spark-ignition engine operating at 1500rev/min, $\phi = 1.0$, $p_{\text{inlet}} = 0.7\text{atm}$, MBT timing 25° BTC . (From Heywood [1])

3.2 The polytropic process

In principle, the compression and expansion processes in an internal combustion engine are considered to be polytropic processes. By introducing the polytropic pressure model π_k , the two polytropic processes are represented by two horizontal lines in the plot of the polytropic model. The polytropic pressure model is defined as

$$\pi_k \equiv p v_S^{n_k} \quad (3.1)$$

where v_S denotes the volume of the system normalized with respect to the clearance volume, and n_k , the polytropic index of expansion for $k = e$, or of compression when

$k =$

I

press

the r

of st

In th

where

crank

rewri

Sh

an int

gas le

polyt

in Fig

Ex

appro

proxin

and g

that t

end of

busic

$k = c$.

It has been proposed that the exponent n in the polytropic relationship of the pressure and the volume during the combustion varies approximately n_c to n_e with the mass fraction burned, x_b . Since the evaluation of x_b requires the priori knowledge of start and end of combustion, a simple evaluation of the exponent n is proposed. In the simple evaluation, the exponent n varies linearly from n_c to n_e with time, i.e.,

$$n_k = n_c + (n_e - n_c) \times \frac{\Theta - \Theta_i}{\Theta_f - \Theta_i} \quad (3.2)$$

where Θ_i is the crank angle at which the polytropic compression ends and Θ_f is the crank angle at which the polytropic expansion starts. Therefore, Equation 3.1 can be rewritten as

$$\pi_k \equiv p v_S^{n_k} \quad \text{where} \quad n_k = \begin{cases} n_k = n_c & \text{for compression} \\ n_k = n & \text{for combustion} \\ n_k = n_e & \text{for expansion} \end{cases} \quad (3.3)$$

Shown in Figure 3.2 is a plot of polytropic pressure model of ideal processes in an internal combustion engine. However, because of the heat transfer to the wall and gas leakage during and after the exothermic process of combustion, the plot of the polytropic model of real processes in a direct-injection spark-ignition engine is shown in Figure 3.3.

Examination of Figure 3.3 reveals that the compression process can be reasonably approximated by a polytropic process, while the expansion process can only be approximated by a polytropic process in a short range since the heat transfer to the wall and gas leakage decreases the polytropic pressure model. It is also shown in the figure that the polytropic pressure model increases during the combustion process. At the end of the compression, the polytrope increases due to the exothermic process of combustion. Before the engine piston reaches the top dead center (TDC), the heat release

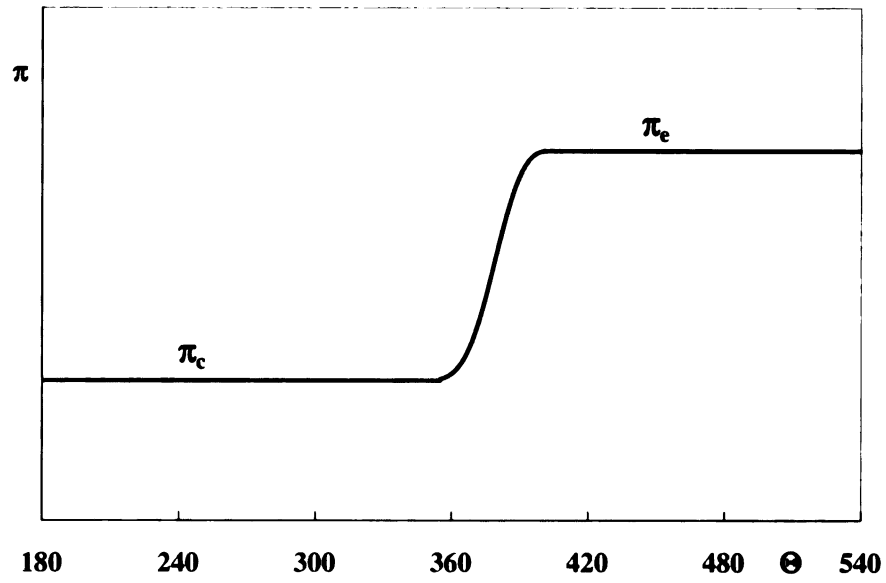


Figure 3.2: The polytropic pressure model of ideal processes in an IC engine

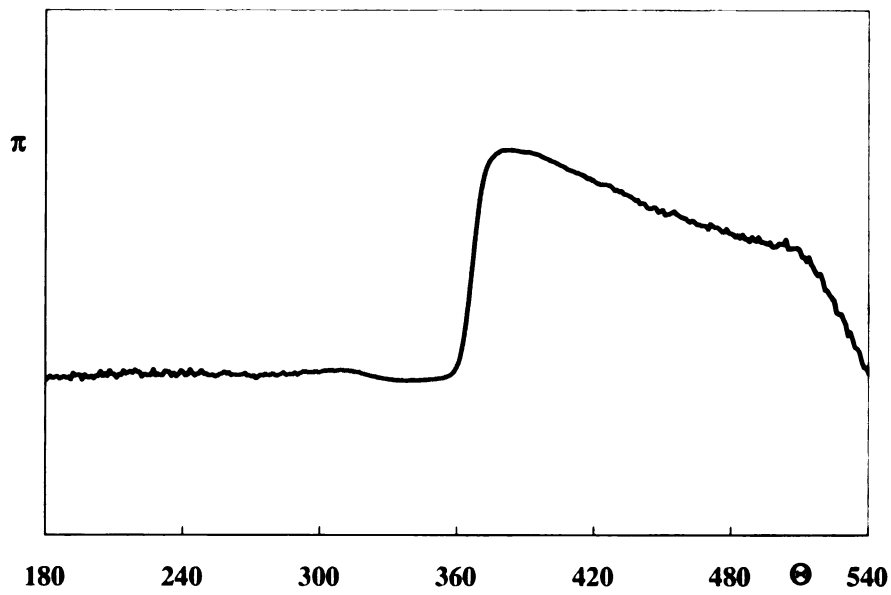


Figure 3.3: The polytropic pressure model of real processes in an IC engine

from c
bigger
model
the po
heat tr
maxim
heat tr

3.3

The dy
shifts th
producti
bustion
is record

The
the proc
diffusion
point of t
process c
the energ
dynamic
a discont
reached a
a vessel c
polytropi

The e

from combustion slows down the piston movement, making the combustion chamber bigger than that without the combustion process, therefore the polytropic pressure model increases. After the TDC, the heat release accelerates the piston and increases the polytropic model. When the heat release from the combustion is balanced by the heat transfer to the wall near the end of the combustion, the polytrope reaches the maximum point, after which the polytrope decreases because of the domination of heat transfer to the wall.

3.3 Dynamic stage of combustion

The dynamic stage of combustion constitutes a part of the exothermic process that shifts the expansion polytrope away from the compression polytrope to create a work-producing cycle. It expresses the essential function of the exothermic process of combustion and provides the sole reason for the use of fuel. Its evolution, or management, is recorded by the measured pressure profile.

The initial state of the dynamic stage of combustion, **i**, takes place at the end of the process of polytropic compression, following ignition dominated by the effects of diffusion associated with heat and mass transfer. Its final state, **f**, occurs at a balance point of the system when the positive effect of pressure generation by the exothermic process of combustion reaches its maximum imposed by the negative influence of the energy lost by heat transfer to the walls of the cylinder-piston enclosure. The dynamic stage of combustion is identified by its bounds with their singular nature: a discontinuity in the rate of pressure signal at the initial state, **i**, and its maximum reached at the final state, **f**. The signal is provided by the measured pressure, p , in a vessel of constant volume, or by its equivalent in a cylinder-piston enclosure, the polytropic pressure model π_k .

The evolution of pressure, or its model, is expressed in terms of a progress param-

eter

In E
and

when
crank
3.4 t
exter

$\bar{\pi}_i =$

In
forme
comp
solv
For a
The a
is pre

3.4

The se
by two
len.

Th
At the

eter, which is the normalized polytropic pressure model.

$$x_{\pi}(\tau_{\pi}) \equiv \frac{\pi - \pi_i}{\pi_f - \pi_i} \quad (3.4)$$

In Equation 3.4, τ_{π} is the normalized life time of the dynamic stage of combustion and it is defined as

$$\tau_{\pi} \equiv \frac{\Theta - \Theta_i}{\Theta_f - \Theta_i} \quad (3.5)$$

where Θ_i is the crank angle of the start of dynamic stage of combustion and Θ_f the crank angle of the end of dynamic stage of combustion. It is shown in Equation 3.4 that the evolution of dynamic stage of combustion is depicted as a time profile extending from the intersection of the polytropic pressure model with the baseline of $\pi_i = \text{const}$ to the maximum point of the polytropic pressure model.

In the course of the dynamic stage of combustion, most of the reactants are transformed into products, which is a process associated with changes of state of all the components of the system. The essential features of this process are revealed by solving an inverse problem: deduction of information on an action from its outcome. For an internal combustion engine, this task is accomplished by pressure diagnostics. The analytical technique for it has been developed over the last decade [41–56] and is presented here in a refined version.

3.4 Bounds

The solution of the inverse problem, $x_{\pi}(\tau_{\pi})$, is expressed by an integral curve bounded by two singularities. Thus, it is actually a solution of a double-boundary-value problem.

The initial state, \mathbf{i} , is an essential singularity of the dynamic stage of combustion. At the initial state, specific volume of products is $v_i = V_i/M_i = 0/0(!)$. Thus,

depending on the round-off error, calculations of the initial state of products tend to approach either infinity or that of reactants.

The final state, \mathbf{f} , is also a singularity because of the balance reached then between the positive effects of the pressure generated in the course of the exothermic process of combustion and the negative influence of heat transfer to the walls and exhaustion of reactants. Thus, in contrast to the intrinsically discontinuous nature of initiation, the final state of the dynamic stage is approached smoothly at the maximum of polytropic pressure model, π .

The trajectory of the dynamic stage of combustion in an IC engine is, then, an integral curve bounded by two singularities. It starts at a saddle point singularity of the initial point, \mathbf{i} , specified by the intersection between the profile of polytropic pressure model with that of the preceding process of compression with $\pi_c = \text{const.}$ In order to determine the coordinates of point \mathbf{f} , a nodal singularity of the polytropic pressure model is identified by its maximum.

The initial point, \mathbf{i} , is obviated by experimental data. However, this state is pivotal for expressing the dynamic features of the exothermic process. Its identification has to be treated, therefore, with special care — a task that implies disregarding a certain number of experimental data (quite small in practice) in its immediate vicinity, associated with ignition. The analysis is, thus, focused on the dynamics of the exothermic process, irrespective of the mechanism by which it is initiated, or of the particular form in which it takes place. In particular, it is independent of the type of ignition or of the kind of flame by which it is executed, and is thus applicable to turbulent, as well as flameless combustion.

It is thus evident that, in order to obtain a solution accommodating the requirements of the two singularities within which it is bounded, $x_\pi(\tau_\pi)$ has to be expressed in terms of a sufficiently smooth analytic function. This is accomplished by means of the life function introduced in the next section.

3.5 Life function

The life function of the dynamic stage of combustion is an analytical function $x_\pi(\tau_\pi)$ fitting the discrete value calculated by Equation (3.4). According to the nature of the dynamic stage of combustion, the analytic function has to comply with the requirements of the singularities at its two bounds. Their particular features can be expressed succinctly as follows. To simplify the expression, all subscripts π are omitted in the derivation.

1. At $\tau = 0$ and $x_i = 0$,

$$(dx/d\tau)_i > 0, \text{ marking the start of initiation (or birth);}$$

2. At $0 < \tau < 1$ and $0 < x < 1$,

$$dx/d\tau > 0, \text{ commensurate with propagation (or life);}$$

3. At $\tau_f = 1$,

$$(dx/d\tau)_f = 0, \text{ identifying the termination (or death).}$$

The above conditions are satisfied by an ordinary differential equation

$$\frac{dx}{d\tau} = \alpha(\xi + x)(1 - \tau)^\chi \quad (\chi > 0) \quad (3.6)$$

with all its parameters positive, so that at initial state **i**, where $\tau = 0$ and $x = 0$,

$$\left(\frac{dx}{d\tau}\right)_i = \alpha\xi > 0 \quad (3.7)$$

while at final state **f**,

$$\left(\frac{dx}{d\tau}\right)_f = 0 \quad (3.8)$$

For convenience, Equation (3.6) is split into two parts by the introduction of an explicit function of time, ζ , so that

$$\frac{dx}{d\zeta} = \xi + x \quad (3.9)$$

and

$$\frac{d\zeta}{d\tau} = \alpha(1 - \tau)^\chi \quad (3.10)$$

By quadrature, Equation (3.9) yields

$$\ln\left(\frac{\xi + x}{\xi}\right) = \zeta \quad (3.11)$$

or

$$x = \xi(e^\zeta - 1) \quad (3.12)$$

Solving Equation (3.10), one gets

$$\zeta = \frac{\alpha}{\chi + 1} [1 - (1 - \tau)^{\chi+1}] \quad (3.13)$$

at the final state of dynamic stage of combustion, $\tau = 1$, $x = 1$, and $\zeta = \zeta_f$, then

$$\zeta_f = \frac{\alpha}{\chi + 1} \quad (3.14)$$

and according to Equation (3.12)

$$\xi = \frac{1}{e^{\zeta_f} - 1} \quad (3.15)$$

Therefore, with the final conditions of the dynamic stage of combustion specified, Equation (3.12) yields the integral expression for the life function

$$x = \frac{e^\zeta - 1}{e^{\zeta_f} - 1} \quad (3.16)$$

where ζ and ζ_f are specified by Equation (3.13) and (3.14), respectively.

3.6 Discussion

3.6.1 Life function and Wiebe function

In studies of combustion in an internal combustion engine, several heat-release functions have been introduced. A famous function is the Wiebe function [1, 62, 63, 64].

$$x_W = 1 - \exp\left[-\frac{\alpha}{\chi + 1} \left(\frac{\Theta - \Theta_s}{\Theta_e - \Theta_s}\right)^{\chi+1}\right] \quad (3.17)$$

where Θ is the crank angle, Θ_e is the crank angle at which the combustion starts, Θ_s is the crank angle at which the combustion ends, α and χ are adjustable parameters.

The life function of the dynamic stage of combustion is a power function of time. By combining Equation (3.6), (3.13) and (3.14), the life function of the dynamic stage of combustion is reformatted as

$$x = \frac{e^{\frac{\alpha}{\chi+1}[1-(1-\tau)^{\chi+1}]} - 1}{e^{\frac{\alpha}{\chi+1}} - 1} \quad (3.18)$$

Comparing the Wiebe function and life function, it is found that these two functions have a relationship if $\Theta_s = \Theta_i$ and $\Theta_e = \Theta_f$. The life function is in effect a reverse of the Wiebe function, i.e., the start of the Wiebe function is the end of the life function and the end of the Wiebe function is the start of the life function.

For $\Theta_s = \Theta_i$ and $\Theta_e = \Theta_f$, the Wiebe function is reduced to

$$x_W(\tau) = 1 - \exp\left[-\frac{\alpha}{\chi + 1}\tau^{\chi+1}\right] \quad (3.19)$$

and the reverse of the Wiebe function is

$$x_W^R(\tau) = 1 - x_W(1 - \tau) = e^{-\frac{\alpha}{\chi+1}(1-\tau)^{\chi+1}} \quad (3.20)$$

From Equation (3.18),

$$x = \frac{e^{\frac{\alpha}{\chi+1}}[e^{-\frac{\alpha}{\chi+1}(1-\tau)^{\chi+1}} - e^{-\frac{\alpha}{\chi+1}}]}{e^{\frac{\alpha}{\chi+1}} - 1} \quad (3.21)$$

usually, $\frac{\alpha}{\chi+1} > 5$, then $e^{\frac{\alpha}{\chi+1}} \approx (e^{\frac{\alpha}{\chi+1}} - 1)$ and $e^{-\frac{\alpha}{\chi+1}} \approx 0$. Therefore, the life function of the dynamic stage of combustion is reduced to

$$x = e^{-\frac{\alpha}{\chi+1}(1-\tau)^{\chi+1}} \quad (3.22)$$

which is the same as the reverse of the Wiebe function.

The reverse relationship between these two functions is illustrated by Figure 3.4 and Figure 3.5. In figures, the Wiebe function and life function, together with their derivatives expressing the “rate of burn,” are illustrated for the same parameters of $\alpha = 3$ and $\chi = 0.5, 1, 2.5, 5$ and 10 .

A comparison of first derivatives of the life function and Wiebe function is shown in Table 3.1. It is shown that the first derivative of the Wiebe function is greater than zero at the final state, indicating that the combustion is continuing. According to the definition of heat-release functions, the combustion is ended at the final state, therefore Wiebe function loses the physical meaning at the final state.

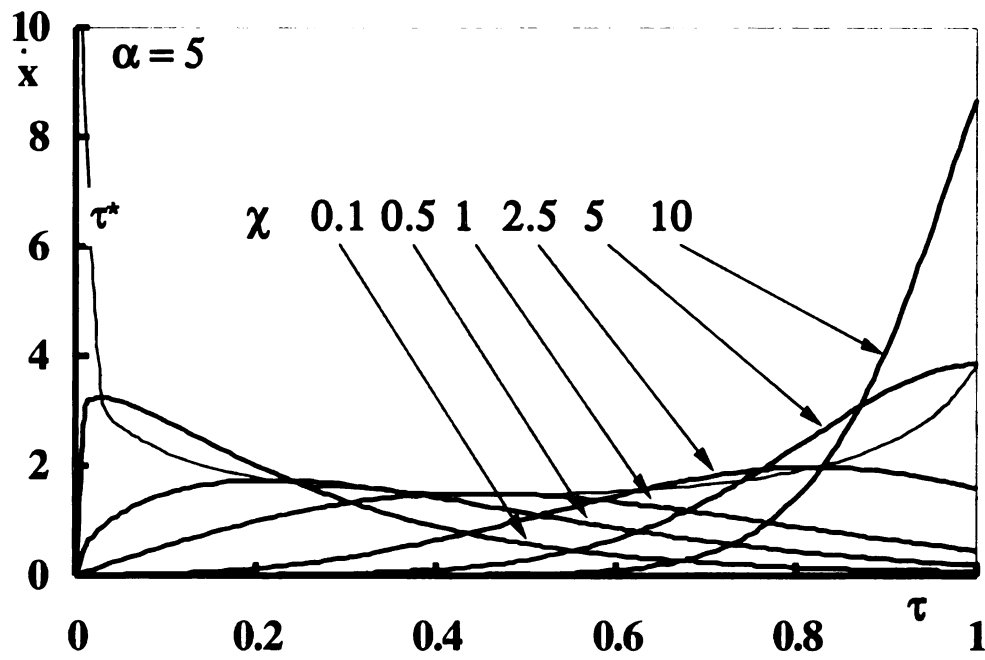
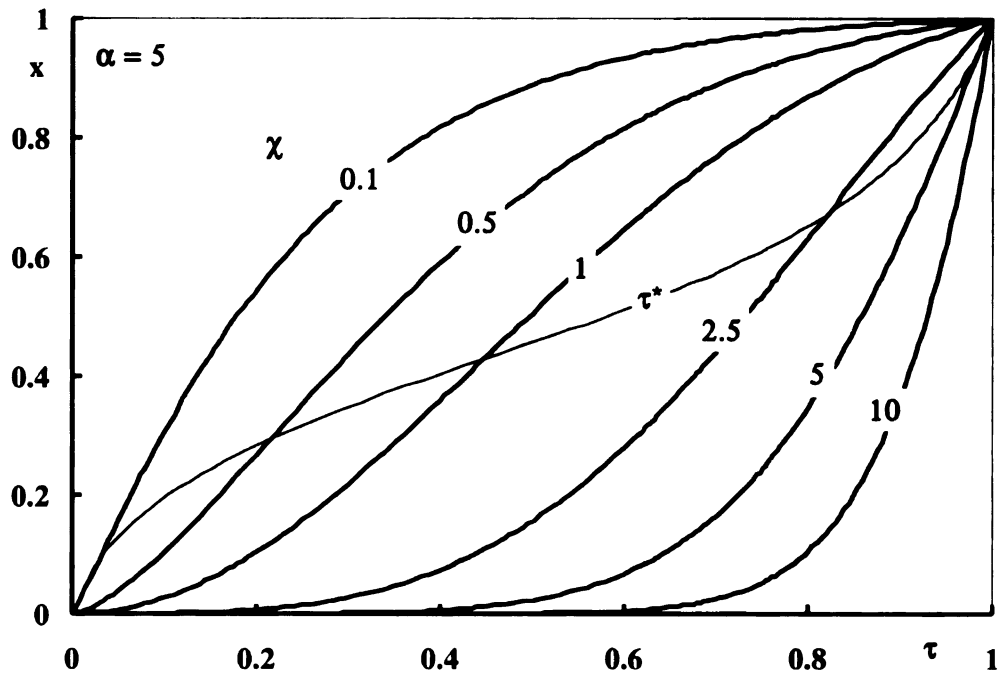


Figure 3.4: The Wiebe function and its derivatives for $\alpha = 3$ and $\chi = 0.5, 1, 2.5, 5$ and 10.

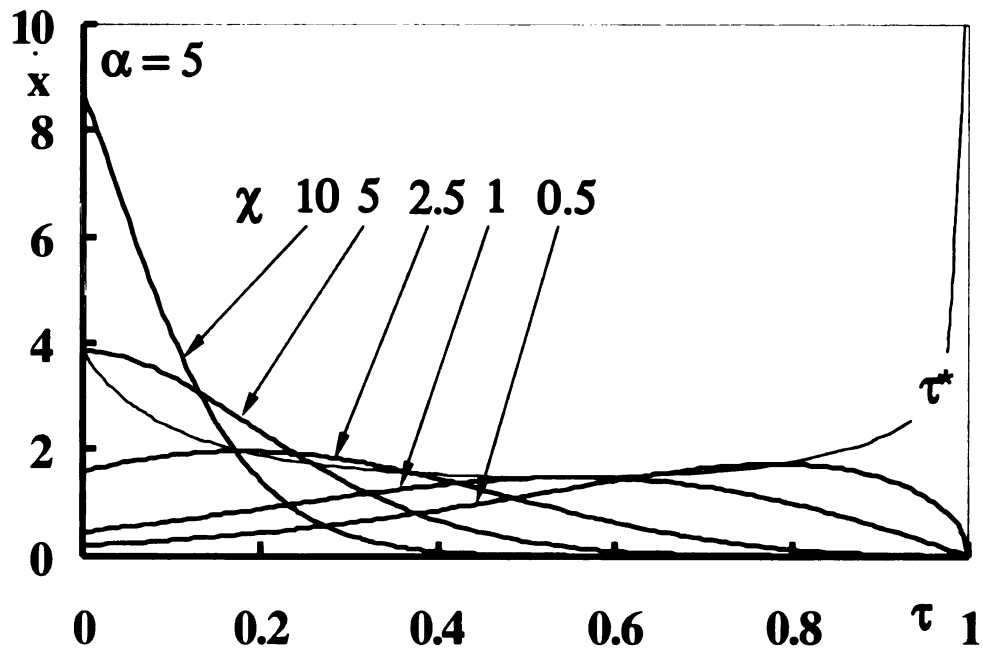
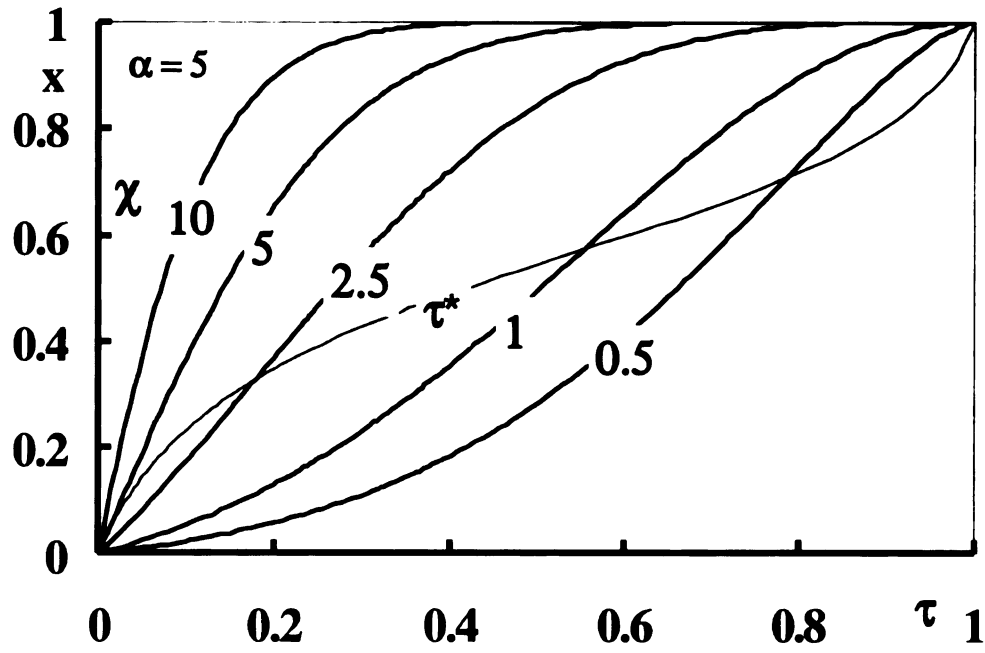


Figure 3.5: The life function of the dynamic stage of combustion and its derivatives for $\alpha = 3$ and $\chi = 0.5, 1, 2.5, 5$ and 10 .

3

E

b

e

S

at

w

oh

by

can

Table 3.1: Comparison of first derivatives of life function and Wiebe function

	life function	Weibe function
$\Theta = \Theta_i$	$dx/d\Theta > 0$	$dx/d\Theta = 0$
$\Theta_i < \Theta < \Theta_f$	$dx/d\Theta > 0$	$dx/d\Theta > 0$
$\Theta = \Theta_f$	$dx/d\Theta = 0$	$dx/d\Theta > 0$

3.6.2 Derivatives of life function

By setting three conditions at the initial and final states of the dynamic stage of combustion as well as during the stage, an continuous analytical function describing the evolution of the dynamic stage of combustion is obtained, which is the life function. Since life function is continuous, its derivatives are available.

From Equation (3.6) and (3.15), the first derivative of life function is

$$\dot{x} = \frac{dx}{d\tau} = \alpha \left(x + \frac{1}{e^{\frac{\alpha}{\lambda+1}} - 1} \right) (1 - \tau)^\chi \quad (3.23)$$

and the second derivative of life function is

$$\ddot{x} = \frac{d^2x}{d\tau^2} = (\xi + x)(\dot{\zeta}^2 + \ddot{\zeta}) \quad (3.24)$$

where ξ is obtained from Equation (3.15), ζ is obtained from Equation (3.13), $\dot{\zeta}$ is obtained from Equation (3.10), and

$$\ddot{\zeta} = -\alpha\chi(1 - \tau)^{\chi-1} = -\frac{\chi}{1 - \tau}\dot{\zeta} \quad (3.25)$$

Similar to the principle that the distance of a vehicle approaches can be controlled by its speed and acceleration, the evolution of the dynamic stage of combustion can be controlled by the first and second derivatives of the life function. In this

control mechanism, the life function of the dynamic stage of combustion is akin to the distance, its first derivative is akin to the velocity, and its second derivative to the acceleration.

3.7 Procedure

The procedure for identifying the dynamic stage of combustion and obtaining its life function is as follows.

1. The measured pressure profile with respect to time, $p(\Theta)$, is used together with the profile of the volume of the cylinder-piston enclosure normalized with respect to the clearance volume, $v_S(\Theta)$, to obtain the indicator diagram, expressing the functional relationship $p(v_S)$.
2. From the indicator diagram in logarithmic scales, the slopes of the compression polytrope, n_c , the expansion polytrope, n_e , are obtained by linear regression.
3. The profile of the polytropic pressure model, $\pi_k(\Theta)$, to determine the dynamic stage of the combustion, is then obtained on the basis of step 2, according to Equation (3.1), together with the base line of $\pi_c(\Theta) = \text{const.}$
4. The initial state **i** and the final state **f** of the dynamic stage are identified on the basis of step 3: the initial state is the first point deviating from the compression polytrope, while the final state is the maximum of the expansion polytrope.
5. Based on the identification of initial state and final state, the discrete values of life function and life time of dynamic stage of combustion are obtained by Equation (3.4) and (3.5), respectively.
6. The profile of the polytropic pressure model expressed in terms of the analytical life function is obtained by Equation (3.16), (3.13) and (3.14), whereby its parameters, α and χ , are established by regression.

7. The first and second derivatives of life function of the dynamic stage of combustion are evaluated by Equation (3.23) and (3.24).

3.8 Implementation

3.8.1 Engine

The technique of pressure diagnostics to evaluate the performance of a dynamic stage of combustion was carried out for a single cylinder, dual overhead-cam, four-valve, direct injection, spark ignition, AVL model 503 engine connected to a 200 hp General Electric DC dynamometer [65]. The engine specifications are listed in Table 3.2.

Table 3.2: Engine specifications

Bore	7.95 cm
Stroke	9.99 cm
Connecting Rod Length	19.8 cm
Compression Ratio	19.3:1
Intake Valve Open	12 ° BTDC
Intake Valve Close	8 ° ABDC
Exhaust Valve Open	38 ° BBDC
Exhaust Valve Close	20 ° ATDC

The front of the engine block was modified to allow access to shafts operating at half-crank-angle speed for the overhead cams and the fuel pump. The engine contained a Mahle piston with a hemispherical bowl machined into the center of its face. The cylinder head and the camshaft were, in effect, separate units, allowing changes in combustion chamber geometry to be made without any modification of the engine head. Towards this end, the top of the cylinder was fitted with a removable

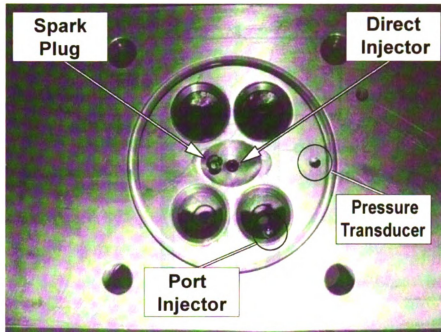


Figure 3.6: Bottom view of the engine head

block accommodating the direct injector, a 10mm spark plug, and an optical pressure transducer. A facility for changing the location of these units was furnished, as well as means to modify the shape and volume of the cylinder-piston enclosure without affecting the compression ratio. The block was connected to the cylinder head by six cap screws, and sealed by a CNC machined copper crush washer. A set of removable blocks was machined with hemispherical bowls of different shapes.

A photograph of the cylinder head, viewed from the bottom, is presented in Figure 3.6, showing the bowl with the spark plug and the direct injector located close to the center between the valve seats, as well as the tapped hole for the pressure transducer. The geometrical configuration of the combustion bowl in the piston and in the block, forming the cylinder head, is depicted in Figure 3.7. The hemispherical bowl in the piston is 2.258 cm (1.125 inch) in diameter, accommodating 23.25% of total compression volume. The bowl in the head is 3.28 cm³ (0.2 inch³) in volume, providing 12.45% of total compression volume. The squish volume takes up the rest.

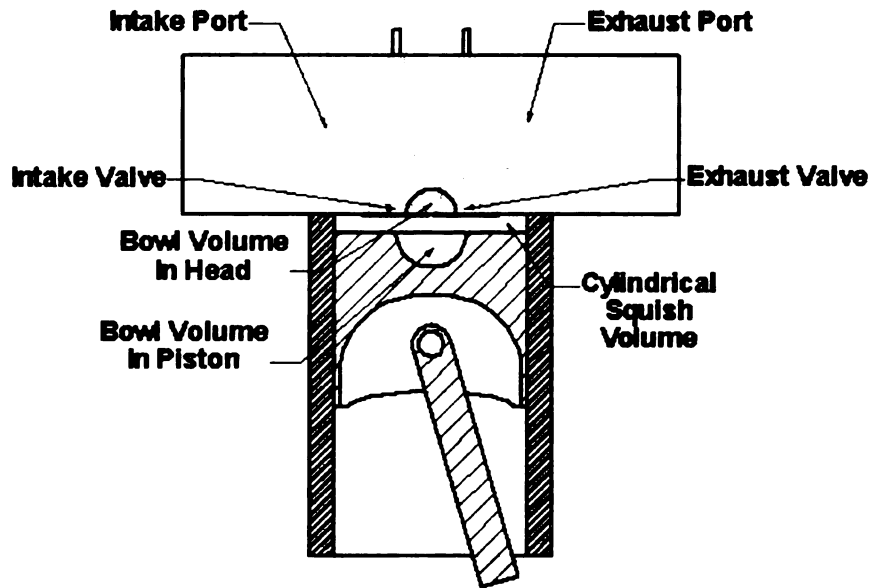


Figure 3.7: Illustration of combustion chamber

All engine tests were run at an operating speed of 1500 rpm. The experiments conducted in this engine assembly examined several hundred operating conditions. The objective of the experiments was to evaluate the mechanical integrity and performance of a stratified charge engine assembly which can accommodate the variable geometry inserts described earlier in this section. For the current work, the operating conditions for a sample of four, selected for pressure diagnostics, are listed in Table 3.3. The air/fuel ratios are expressed by the relative air/fuel ratio, λ (with respect to the stoichiometric ratio of 6.435 for methanol). The selection was made to cover a full scope of measured indicated mean effective pressure (IMEP), represented by the maximum and the minimum of two relative air/fuel ratios, $\lambda = 1.5$ and $\lambda = 1.75$.

3.8.2 Results

Measured pressure data for the four selected cases are displayed in Figures 3.8–3.11 (step 1). The corresponding indicator diagrams in logarithmic scales are displayed in Figures 3.12–3.15. In the logarithmic scales, the slopes of the compression polytrope,

Table 3.3: Engine operating conditions

Case	λ	IMEP	Injection (° BTDC)	Ignition (° BTDC)
1	1.5	max	60	10
2	1.5	min	50	20
3	1.75	max	50	10
4	1.75	min	70	12.5

n_c , and the expansion polytrope, n_e , are evaluated by linear regression (step 2). The values of n_c and n_e for four cases are shown in Table 3.4. Figures 3.16—3.19 display the polytropic pressure models; the solid horizontal lines in the figures represent the polytropic compressions (step 3).

Table 3.4: The indices of polytropic compression and expansion of four cases

	1	2	3	4
n_c	1.2451	1.2672	1.2679	1.2348
n_e	1.2864	1.2842	1.299	1.2502

The initial state of the dynamic stage of combustion, **i**, is then determined by the first point of the polytrope deviating from the base line of $\pi_c = \text{const}$. Its final state, **f**, is established at the maximum of the polytrope (step 4). Then, profiles of the polytropic pressure models, specified by Equation (3.1) and (3.4), are expressed by regression in terms of life functions, yielding their parameters, α and χ (steps 5 and 6). The parameters of the life functions are listed in Table 3.5

In Figures 3.8—3.19, the experimental data are represented by open circles. The initial and final points of the dynamic stage of combustion, **i** and **f**, are identified there by large open circles and large open squares, respectively, according to their identification in step 4.

Shown in Figures 3.20—3.23 are the life functions of the dynamic stage of com-

Table 3.5: Life function parameters

	1	2	3	4
Θ_i	355	347	355	360
Θ_f	381	379	379	399
α	28.8583	33.476	24.4691	16.5622
χ	3.16596	6.13036	2.50746	2.22327

bustion with their first derivatives. The second derivatives are shown in Figures 3.24—3.27 (step 7).

In Figures 3.28—3.31, the analytical pressure traces (solid lines) obtained from the polytropic compression process and life function of dynamic stage of combustion are shown. Compared with the measured pressure data (open circles), it is shown that the life function of the dynamic stage of combustion is a good method to characterize the combustion process in an IC engine.

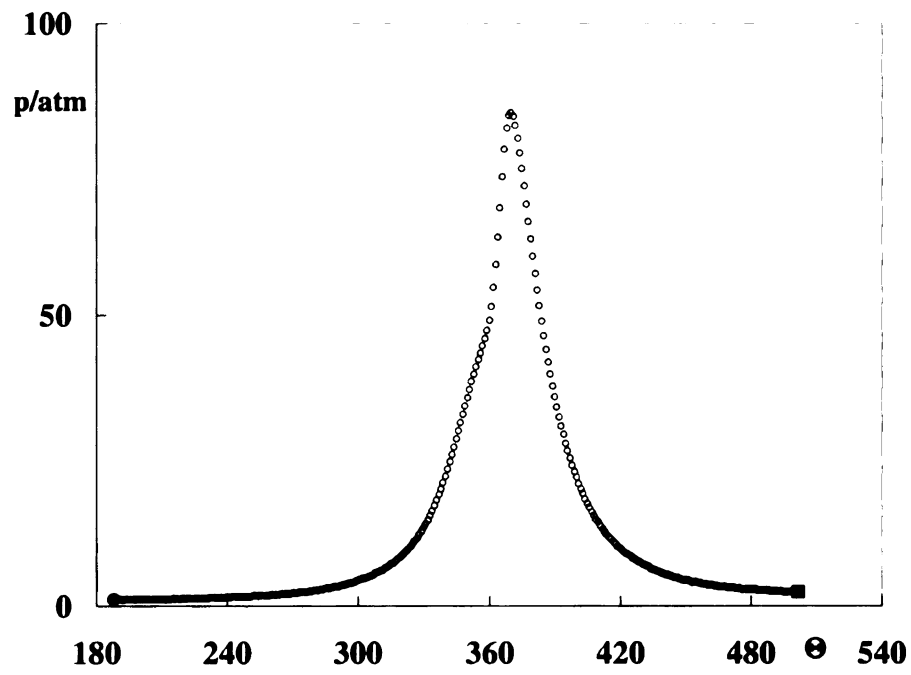


Figure 3.8: Pressure trace of case 1

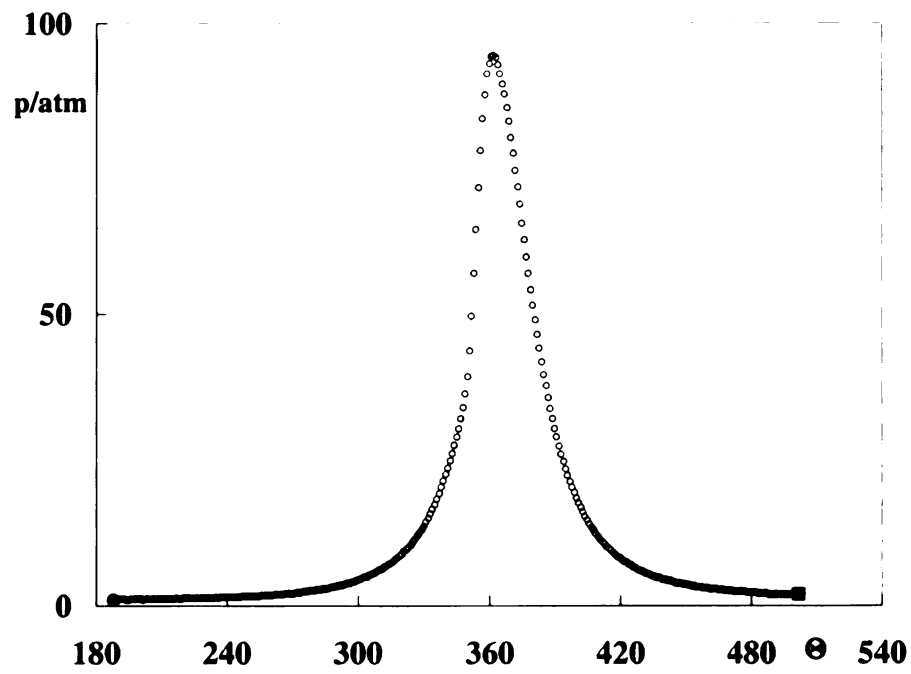


Figure 3.9: Pressure trace of case 2

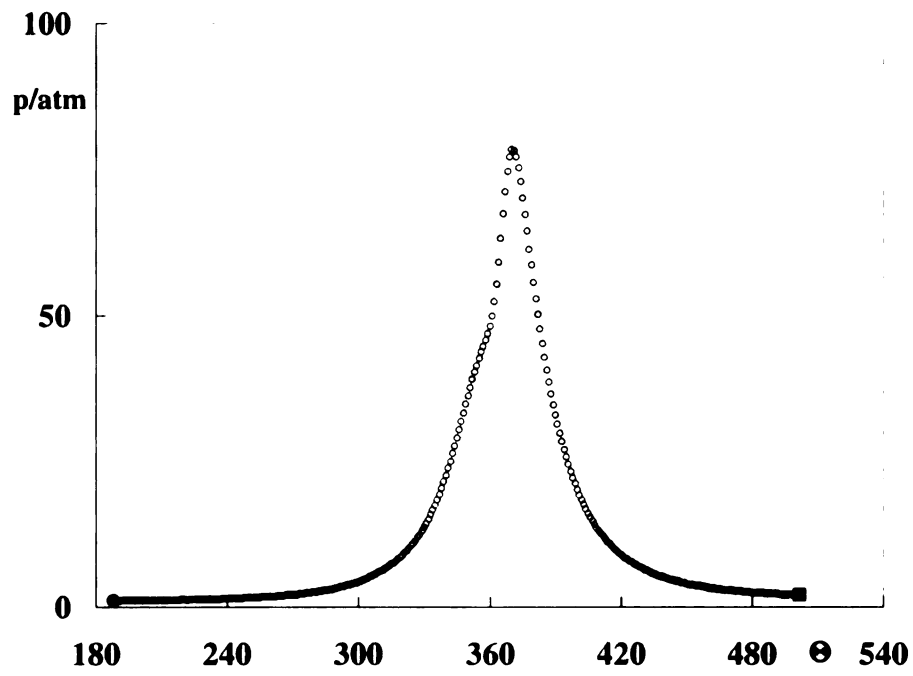


Figure 3.10: Pressure trace of case 3

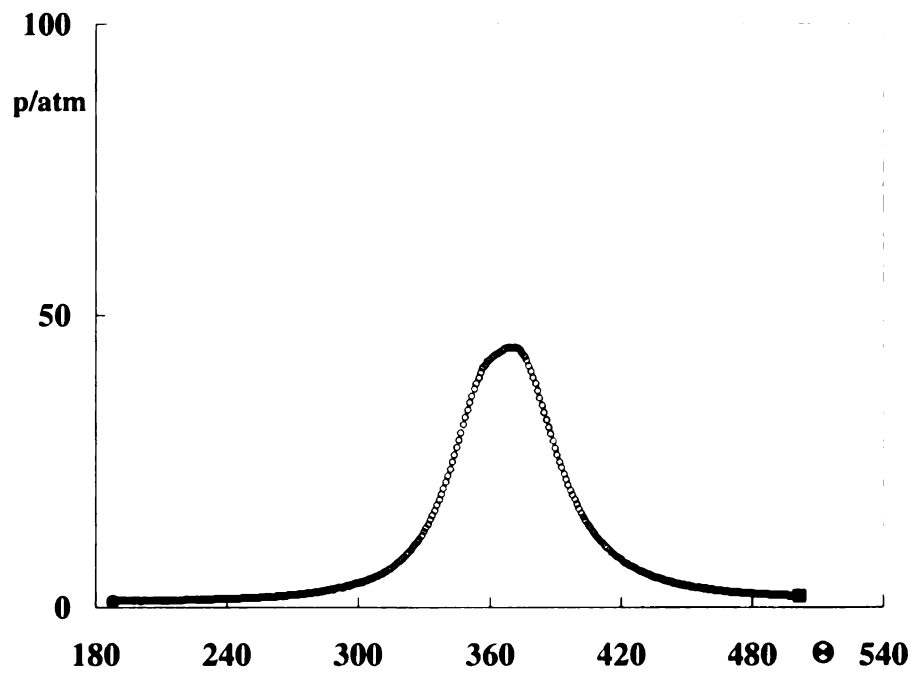


Figure 3.11: Pressure trace of case 4

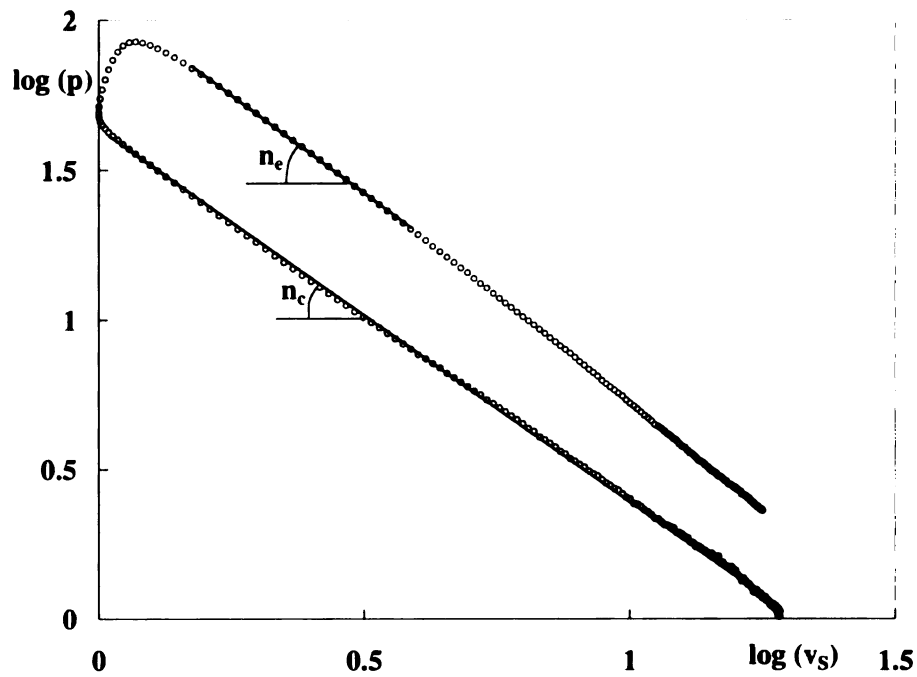


Figure 3.12: Logarithmic indicator of the pressure trace of case 1

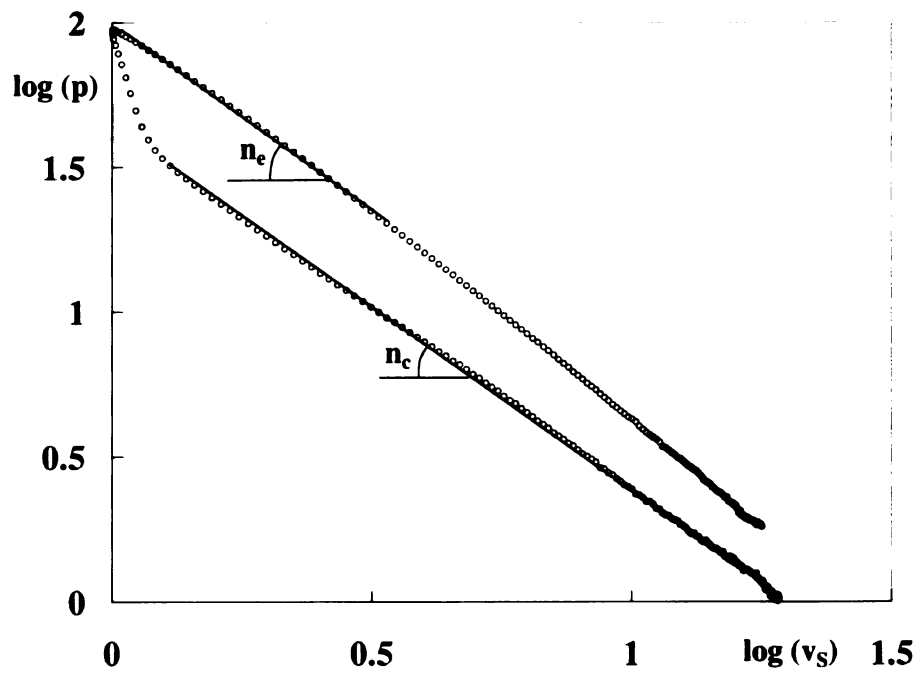


Figure 3.13: Logarithmic indicator of the pressure trace of case 2

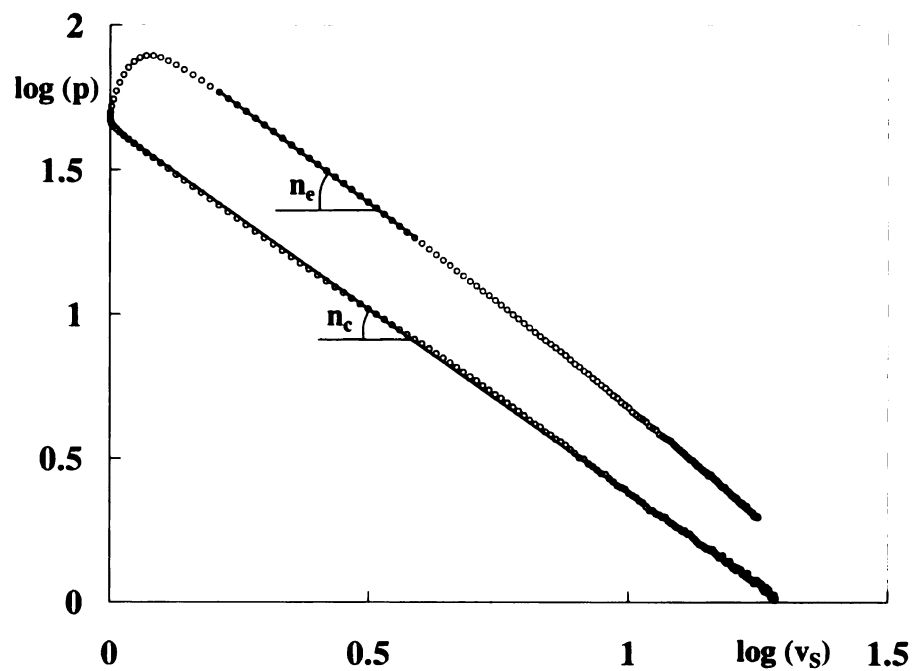


Figure 3.14: Logarithmic indicator of the pressure trace of case 3

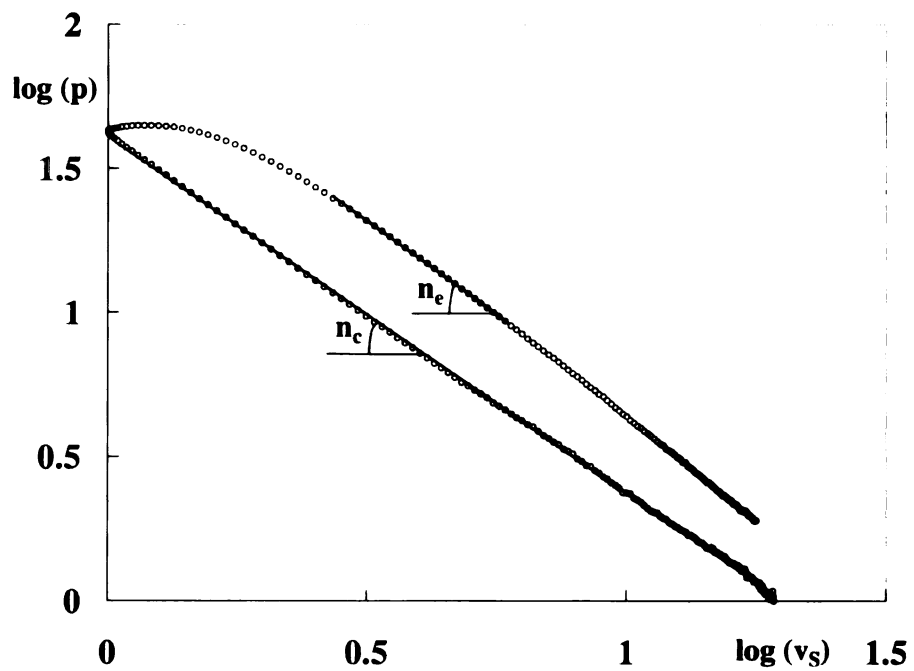


Figure 3.15: Logarithmic indicator of the pressure trace of case 4

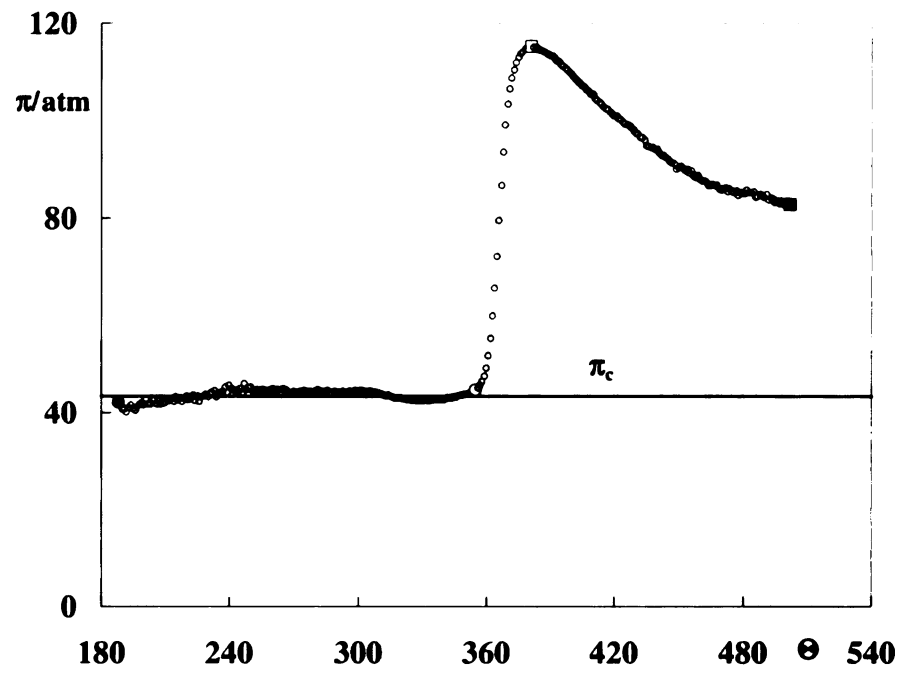


Figure 3.16: Polytopic pressure model of case 1

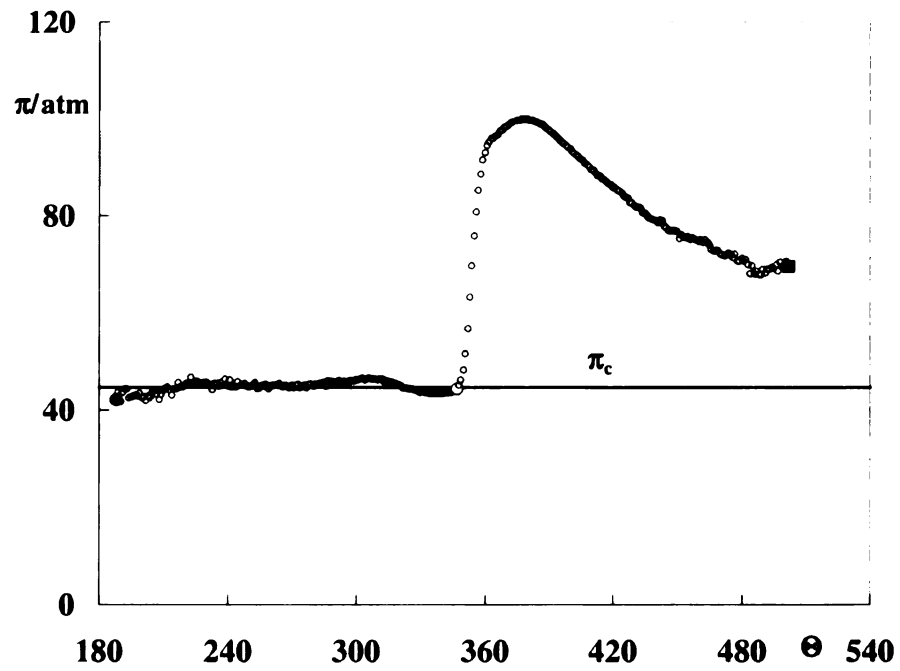


Figure 3.17: Polytopic pressure model of case 2

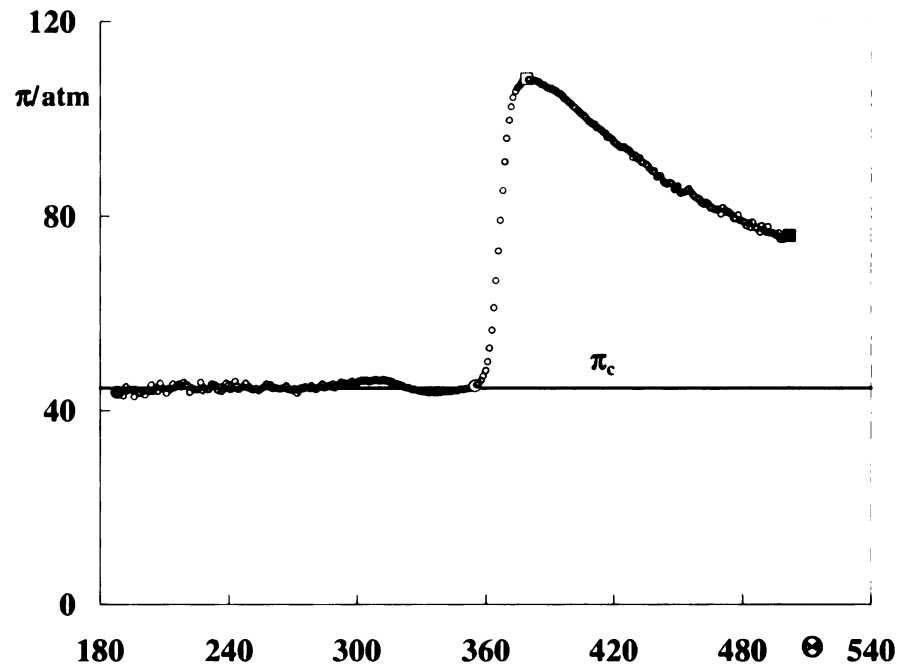


Figure 3.18: Polytopic pressure model of case 3

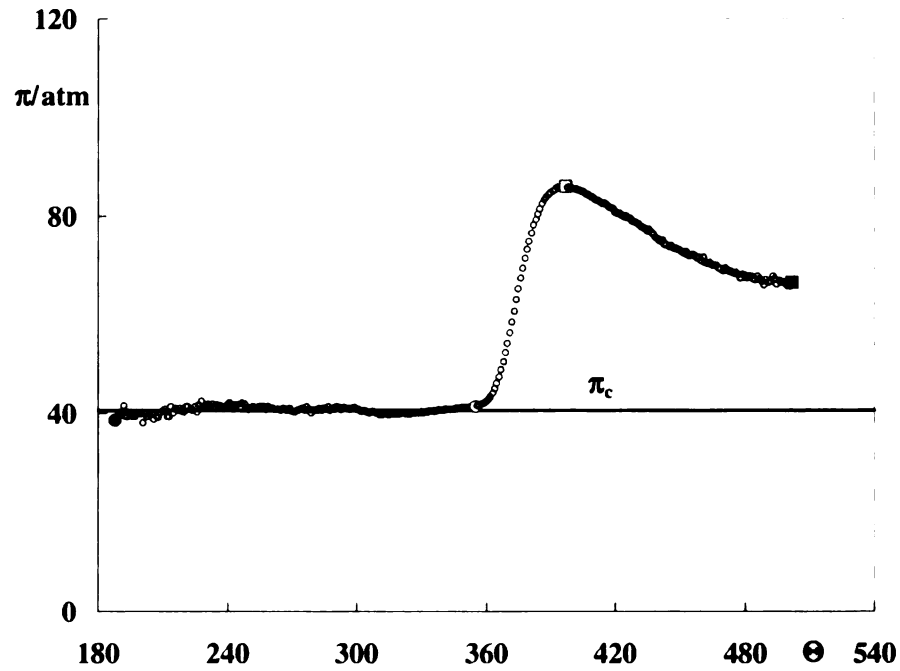


Figure 3.19: Polytopic pressure model of case 4

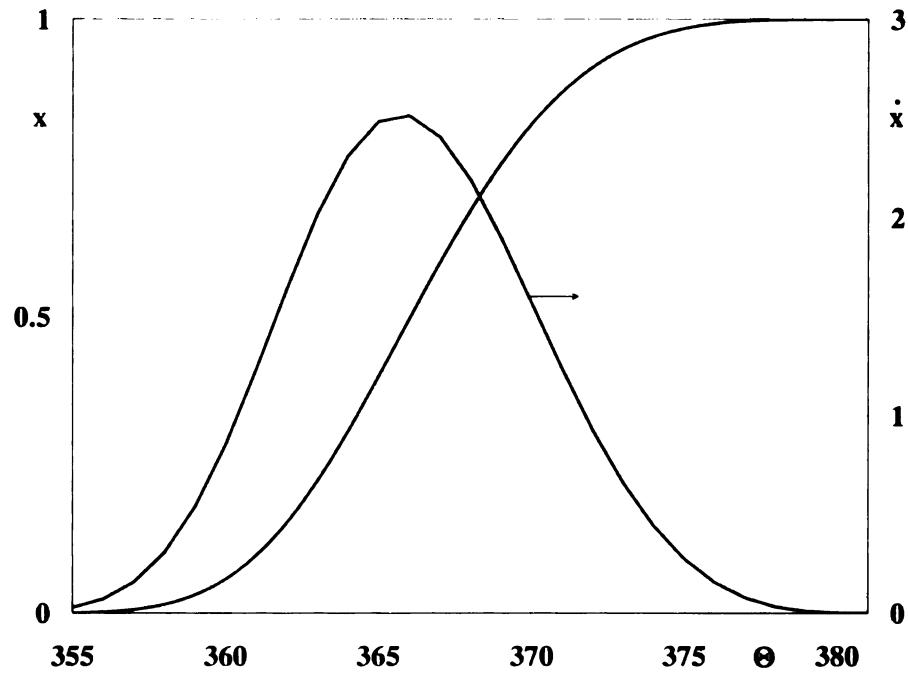


Figure 3.20: Life function of DSC and its first derivative of case 1

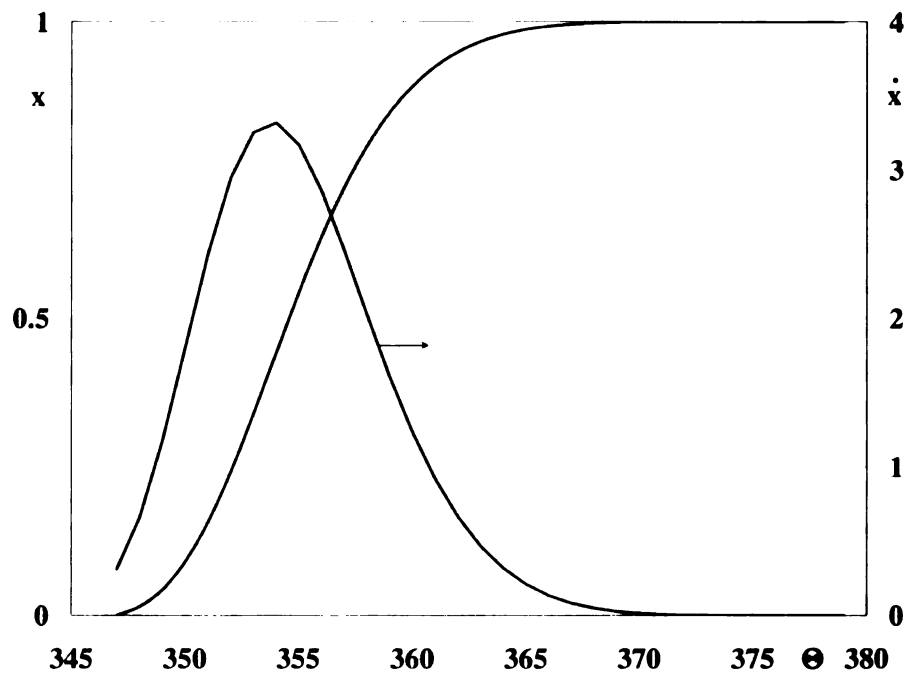


Figure 3.21: Life function of DSC and its first derivative of case 2

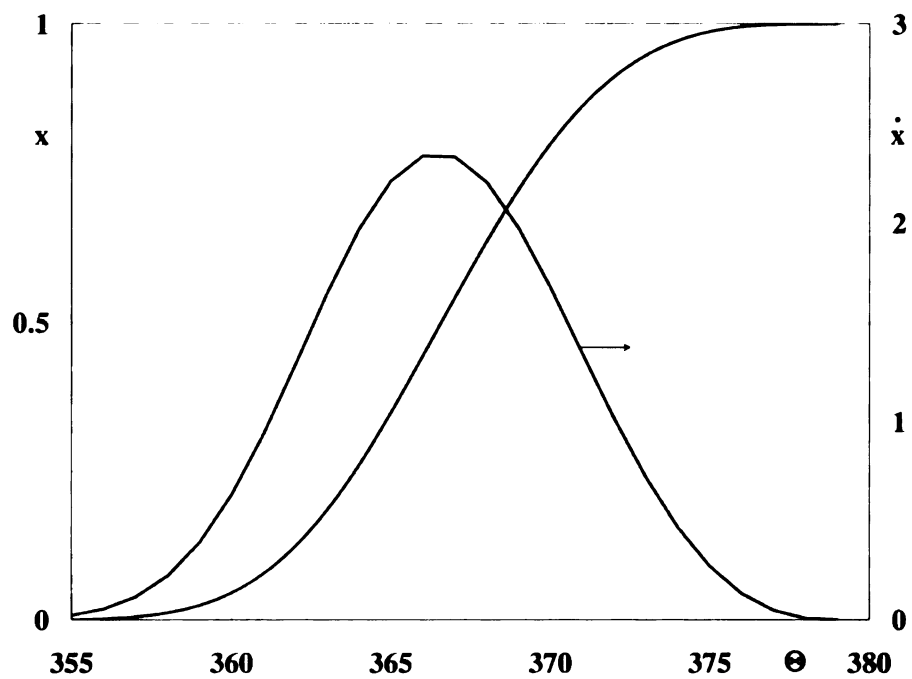


Figure 3.22: Life function of DSC and its first derivative of case 3

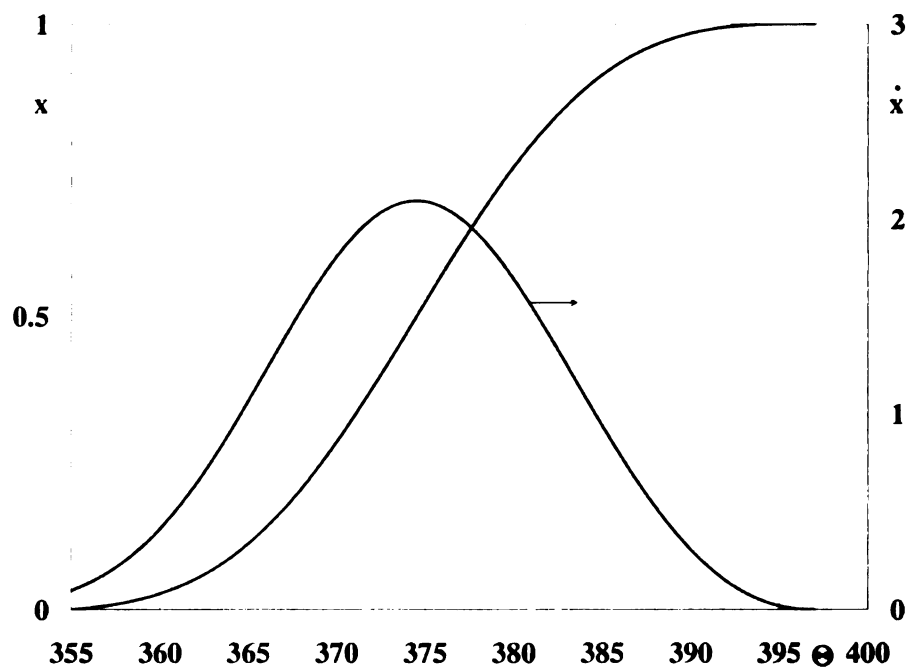


Figure 3.23: Life function of DSC and its first derivative of case 4

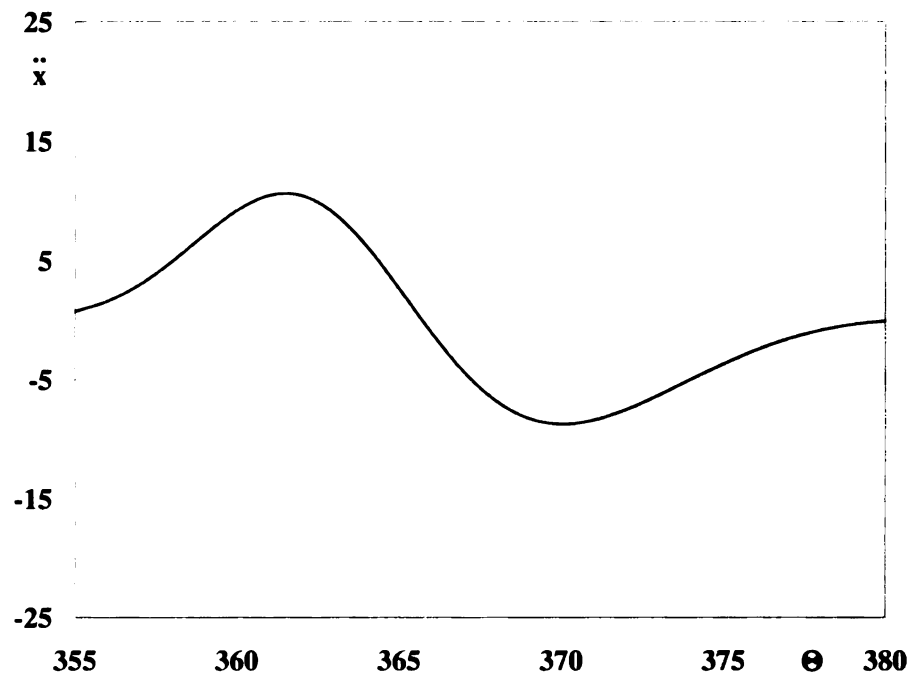


Figure 3.24: Second derivative of life function of DSC of case 1

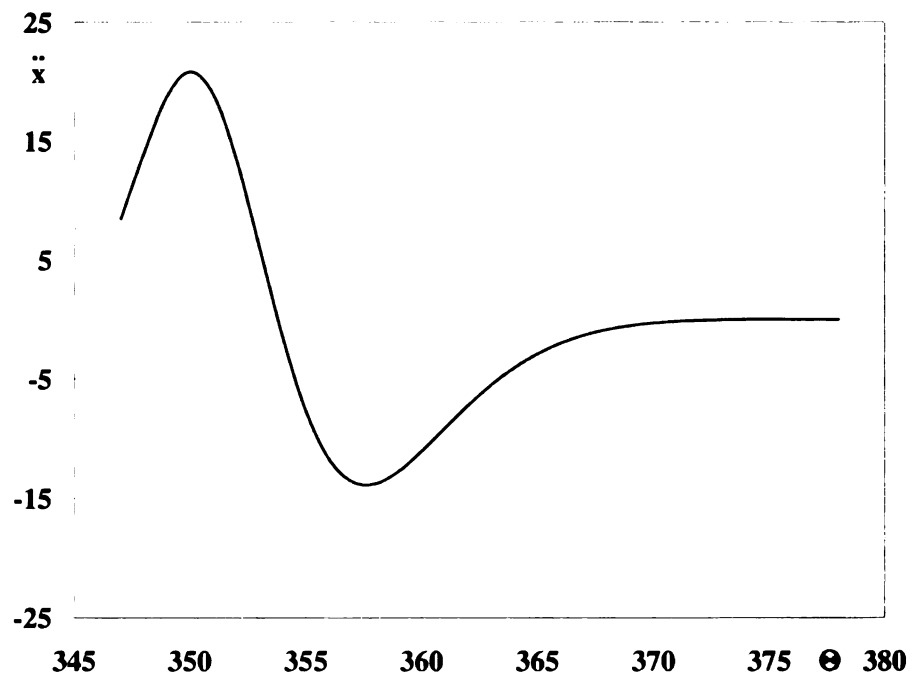


Figure 3.25: Second derivative of life function of DSC of case 2

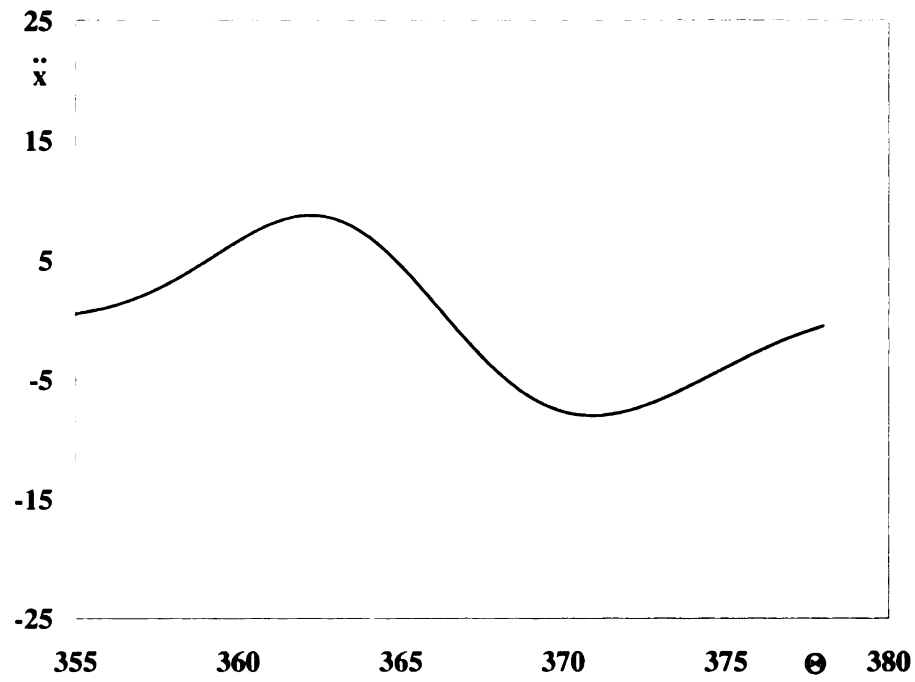


Figure 3.26: Second derivative of life function of DSC of case 3

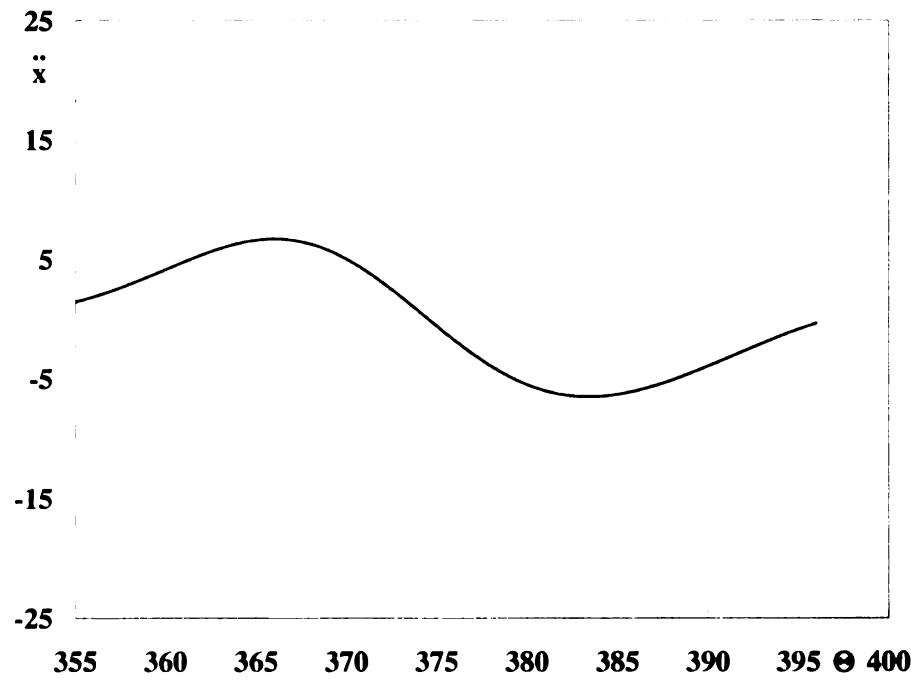


Figure 3.27: Second derivative of life function of DSC of case 4

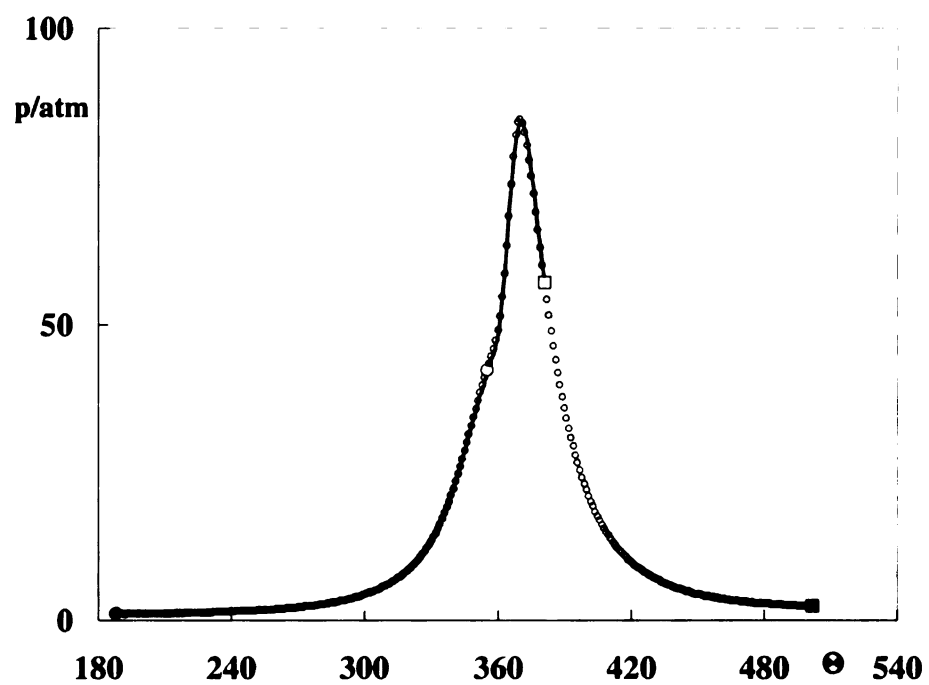


Figure 3.28: Analytical and measured cylinder pressure of case 1

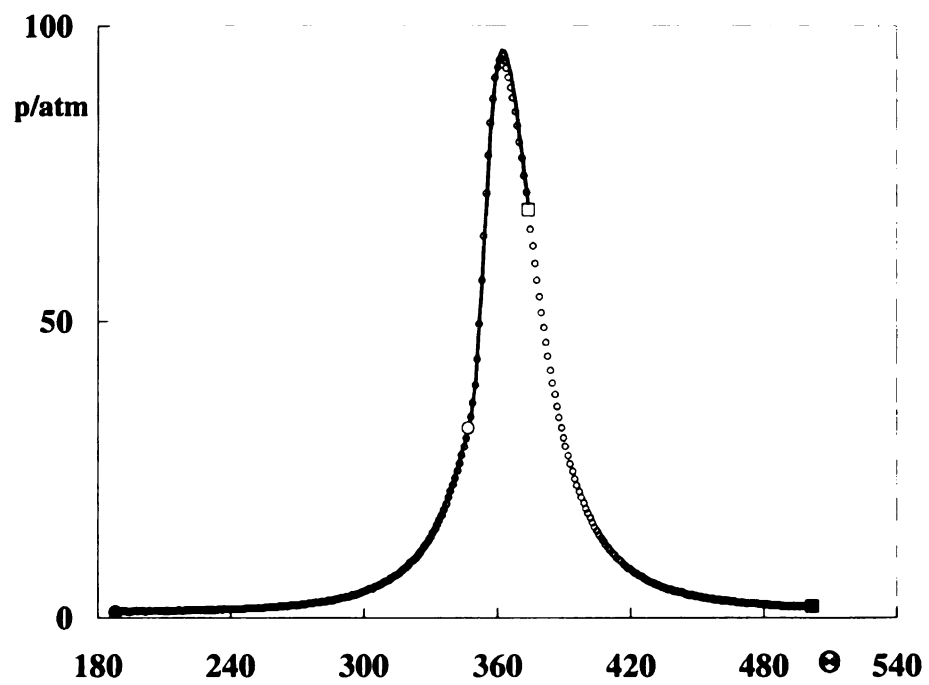


Figure 3.29: Analytical and measured cylinder pressure of case 2

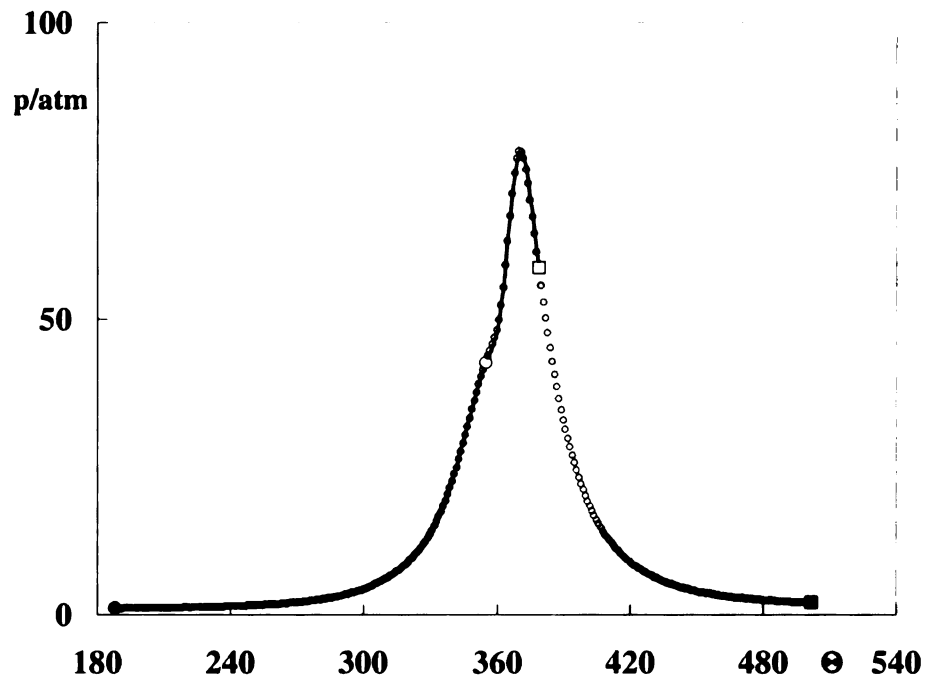


Figure 3.30: Analytical and measured cylinder pressure of case 3

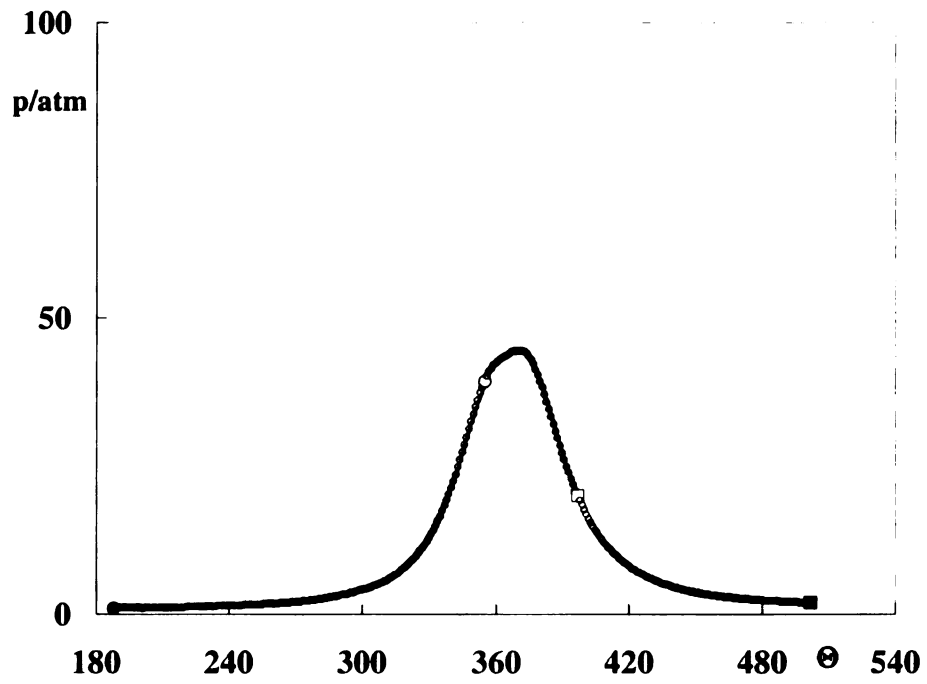


Figure 3.31: Analytical and measured cylinder pressure of case 4

Chapter 4

Exothermic stage of combustion in an IC engine

4.1 Introduction

In chapter 3, the dynamic stage of combustion is introduced to characterize the combustion process in an IC engine and the analytical life function of its evolution is derived, which paves the way for controlling the combustion in the engine. The objectives of combustion control in an IC engine are high output with high efficiency and low pollution as well as reducing cycle-to-cycle variations. In order to achieve the goals, the understanding of the combustion process in an IC engine is necessary.

In an internal combustion engine, the exothermic process of combustion is executed by an oxidation reaction between a hydrocarbon fuel, **F**, and air, **A**, upon their mixing to form a molecular aggregate. During the exothermic process of combustion, the mixture of reactants (fuel and air) is transformed to the products. At the end of the exothermic process, all reactants are transformed to the products. In this chapter, the exothermic process of combustion in an IC engine is defined as the exothermic stage of combustion, then a thermodynamic study on the exothermic stage of combustion is presented and the effectiveness of combustion is quantified.

4.2 State space

A combustion system can be viewed as a set of thermodynamically identified components forming a substance enclosed within an impermeable boundary. The identification of the system is specified by two vector sets: the vectors of component fractions and the vectors of component states. Then, any process of mixing and/or chemical reaction is expressed by an inner product of a selected intersection between the two sets.

4.2.1 Component fractions

Changes in the composition of a system, taking place in the course of its exothermic stage of combustion, are illustrated by a diagram of components, Figure 4.1. It represents an example of a fuel-lean system that consists initially of fuel, **F**, and air, **A**, forming the reactants, **R**. The diagram displays a transformation of their mass fractions, Y_F and Y_A , into products, **P**, so that $Y_F + Y_A = Y_R = Y_P$. The rest of the system's mass, $Y_B = 1 - Y_P$, is taken up by the fraction of cylinder charge that does not participate in this transformation and remains, therefore, invariant throughout the exothermic stage of combustion.

The variation of the component mass fractions, y_K ($K = \mathbf{F}, \mathbf{A}, \mathbf{P}$), taking place in the course of the exothermic stage of combustion, is expressed in terms of the product generation progress parameter (equal to total mass fraction of products), x_P , the degree of transformation from the initial state, **i**, to the terminal state, **t**. While the progress parameter of the dynamic stage of combustion is x_{Π} , the degree of transformation from the initial state, **i**, to the final state, **f**.

According to the definition of the dynamic stage and exothermic stage of combustion, the terminal state, **t**, can only be located at or after the final state, **f**. It can not be located before the final state.

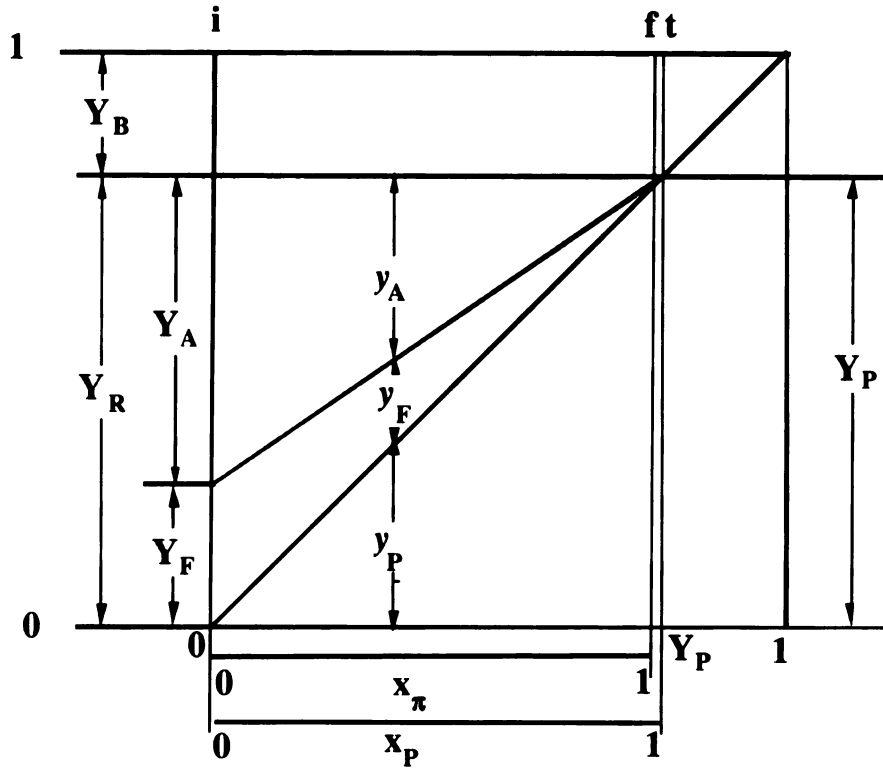


Figure 4.1: Diagram of component fractions

During the exothermic stage of combustion, the variable mass fraction of the generated products is

$$y_P = Y_P x_P \quad (4.1)$$

while for the air or fuel ($K = \mathbf{A}, \mathbf{F}$)

$$y_K = Y_K(1 - x_P) \quad (4.2)$$

4.2.2 Component states

The thermodynamic state of a component is fixed by three parameters in a three-dimensional state space. Adopted usually for this purpose are pressure, p , specific volume, v , and temperature, T . However, this is not a complete specification, because the knowledge of specific heats is required to evaluate the internal energy, e . If

the internal energy is adopted as one of the parameters of state, a point in such a coordinate system provides a complete specification of the state. It is, in fact, the significance of internal energy in this respect, that was brought up by Gibbs [66].

In accordance with this principle, the internal energy, e , is adopted here as a primary parameter of state to form, together with the mechanical parameter, $w = h - e = pv = p/\rho$, and pressure, p , the coordinate system of a three-dimensional state space. The temperature, T , is thus relegated to the secondary role of a dependent variable. This concept is by no means new, having been recognized *de facto* by most classical equations of state, as illustrated by Table 4.1. Of particular significance in this respect is the fact that the mechanical energy, w , as well as the internal energy, e , are readily obtainable from thermodynamic tables, such as JANAF [67], and calculable by the use of computational programs, such as STANJAN [68] and CEA [69][70].

Table 4.1: Equations of state

Van der Walls	$w = \frac{R}{M}T \frac{v}{v-b} - \frac{a}{v}$
Dietrich	$w = \frac{R}{M}T \frac{v}{v-b} e^{-a/vRT}$
Beattie-Bridgeman	$w = \frac{R}{M}T + \frac{\beta}{v} + \frac{\gamma}{v^2} + \frac{\delta}{v^3}$
Becker-Kistakowsky-Wilson (BKW)	$w = \frac{R_u}{M}T[1 + xe^{\beta x}] \quad x = \frac{k}{v(T+\nu)^\alpha}$
Jones-Wilkins-Lee (JWL)	$w = A[1 - \frac{v}{c_{v1}v_c}]ve^{-R_1v/v_c}$ $+ B[1 - \frac{v}{c_{v2}v_c}]ve^{-R_2v/v_c} + \frac{R}{c_v}e$

Principal components of a conventional combustion system are a hydrocarbon fuel and air. They are first combined into a molecular aggregate, and then transformed by an exothermic reaction to form products \mathbf{P} — a process referred to conventionally as “heat release.” In an enclosure, the transformation is observed as a measurable pressure rise manifesting the essential outcome of the exothermic stage of combustion.

For implementation of these principles, the thermodynamic state of a system or of any of its components is expressed in terms of a polar state vector, $\mathbf{z}_K(w, e, p)$, or $\mathbf{z}_K(w, h, p)$, where $K = \mathbf{A}, \mathbf{F}, \mathbf{R}, \mathbf{P}, \mathbf{S}$ respectively for air, fuel, reactants, products and system, in a three-dimensional state (or phase) space, portrayed as a diagram of component states in Figure 4.2. A polar vector is one stemming from the origin of the coordinate system. The locus of states for a component is then *de facto* a vector hodograph, which can be referred to as a state polar — a surface in the three-dimensional state space. The intersection of such a surface with a plane of constant pressure, or a projection of its polar on this plane, is identified by its Cartesian coordinates $z_K = w_K, e_K$, or $z_K = w_K, h_K$.

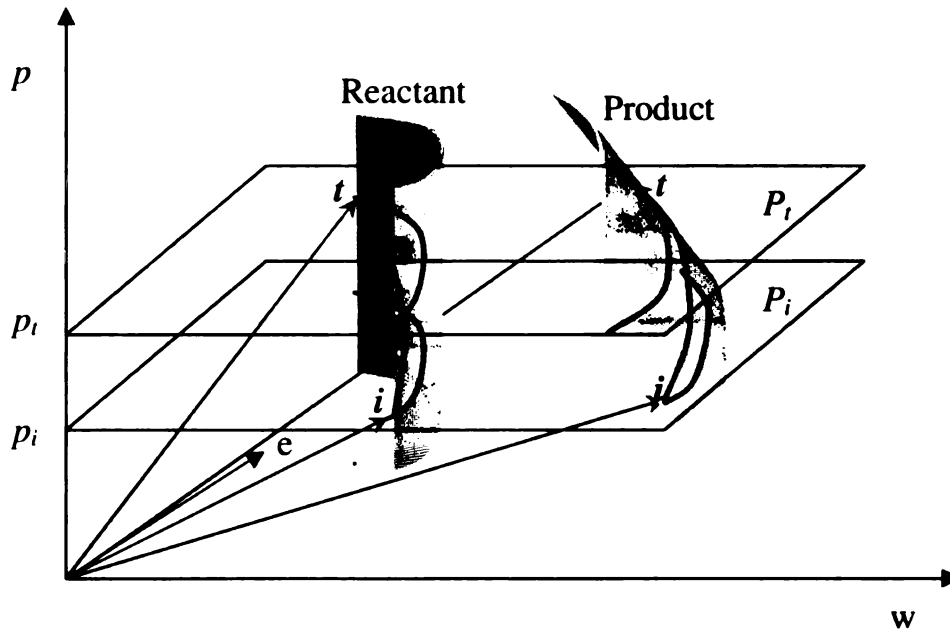


Figure 4.2: 3-D illustration of the state space

The state diagram of Figure 4.3 can be, therefore, visualized as the projection of state vectors on a pressure platform at $p = p_i$, introducing thereby distortions to the shape of the locus of states specified at the initial pressure. This feature is of particular significance for the products \mathbf{P} since, in order to comply with the condition of thermodynamic equilibrium, their composition and, hence, molar masses are variable along the locus of states. The reactants \mathbf{R} , on the other hand, are usually

treated as a perfect gas, because their components, **A** and **F**, are assumed to behave as perfect gases, as they are according to JANAF tables [67], while its composition is fixed by their definition.

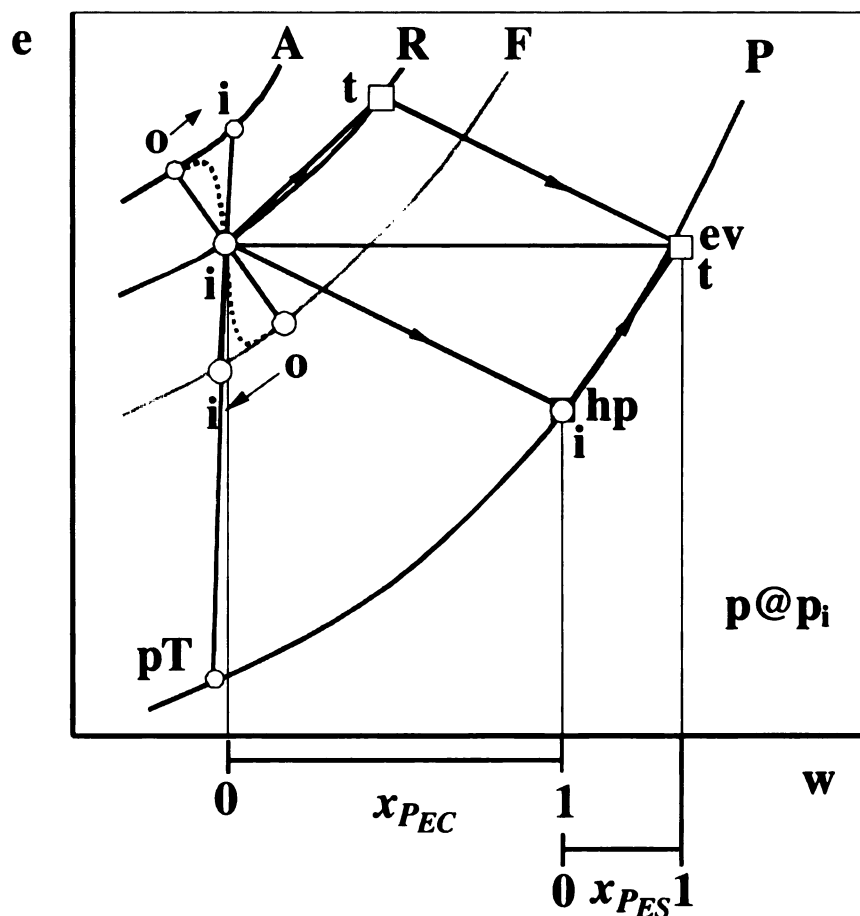


Figure 4.3: Diagram of component states with an illustration of the processes of mixing and adiabatic exothermic center, EC, and exothermic system, ES.

In the case of a perfect gas, the surface of the loci of states is the same at all pressure levels, and is represented by a curved wall parallel to the pressure axis, while that for a perfect gas with constant specific heats the wall is plane. On the diagram of component states, the projection of the latter at any pressure level is, therefore, a straight line. An exothermic process is then a transformation from state **i** to state **t**, expressed by a vector difference between two polar vectors, represented by the vector of transformation, z_{a-z} ($a-z = \mathbf{R}-\mathbf{P}, \mathbf{i}-\mathbf{f}$). Such vectors delineating the four changes of

state taking place at the bounds of an exothermic stage of combustion are as follows:

1. From **i** on **R** to **i** on **P**, both at p_i , representing the process of exothermic reaction from $x_{EC} = 0$ to $x_{EC} = 1$ where $x_{ES} = 0$, subscript EC denoting an exothermic center, while ES the exothermic system.
2. From **i** on **R** to **t** on **R**, representing the compression of reactants as pressure increases from p_i to p_t .
3. From **t** on **R** to **t** on **P**, both at $p_t > p_i$, representing the exothermic reaction at $x_{ES} = 1$.
4. From **i** on **P** at p_i to **t** at p_t , representing the compression of products as pressure increases from p_i to p_t , while the progress parameter changes from $x_{ES} = 0$ to $x_{ES} = 1$.

The coordinates of reactants **R** are evaluated on the basis of their composition specified in the formulation of the problem, while the coordinates of their products **P** are determined by the condition of thermodynamic equilibrium that, according to the Gibbs phase rule, is specified in terms of two parameters of state. For a given initial state, of particular interest states are: (1) **pT** for constant pressure and temperature, (2) **hp** for constant enthalpy and pressure, and (3) **ev** for constant internal energy and specific volume. The latter lies beyond the locus of states, **P**@ p_i , as demonstrated in Figure 4.3, being of interest only when the whole field is composed of a single exothermic center. In fact, the segment from **hp** to **ev** on **P** and that from **i** to **t** on **R**, represent the ideal case of an isochoric and adiabatic system, which consumes all the charge to execute the exothermic process of combustion.

4.3 Combustion processes

4.3.1 Mixing

For a chemical reaction to take place, components in the system must be first mixed to form a molecular aggregate. If, initially, the thermodynamic coordinates of fuel and air are different, they have to be brought to the same state \mathbf{i} on \mathbf{R} — a task accomplished physically by transport processes of molecular mass diffusion and thermal conduction, assisted by viscosity. In Figure 4.3, the concomitant changes of state taking place in the course of molecular mixing are expressed by shifts along the state polars of \mathbf{A} and \mathbf{F} from their original state points, \mathbf{o} , to points \mathbf{i} , of the same pressure and temperature.

The direction of this shift is indicated by arrows between these points. Thus, the effect of mixing is manifested by vector rotation around point \mathbf{i} on \mathbf{R} . Irrespective of the influence of molecular diffusion, which, as a rule, must be involved in forming the reacting aggregate, its outcome is identified right from the outset by the intersection of the straight line between points \mathbf{o} on \mathbf{A} and \mathbf{F} with \mathbf{R} .

4.3.2 Exothermic center

An exothermic center is a site of the exothermic reaction — the source of the exothermic stage of combustion. In combustion literature, exothermic centers have been known for a long time, more or less vaguely, as "hot spots." Their non-steady behavior under the influence of diffusion phenomena has been studied extensively as a site of ignition [71]. Their diffusion-dominated steady state behavior is, in effect, that of a laminar flame. Their non-steady version in a turbulent field is referred to as a "flamelet model" [72].

The fluid mechanical features of exothermic centers have been investigated experimentally and theoretically for their relevance to detonation and explosion phenomena,

leading, among others, to the identification of mild and strong ignition centers [60][74].

As pointed out above in the section on component states, the coordinates of states for the system at any pressure level, $z_S = w_S, e_S$, or $z_S = w_S, h_S$, are given by the scalar product of the vector of components and the vector of states. Thus, with reference to Figure 4.1 and 4.3,

$$z_S = \vec{y} \cdot \vec{z} = y_F z_F + y_A z_A + y_P z_P + y_B z_B \quad (4.3)$$

whence, in view of Equation (4.1) and (4.2)

$$z_S = Y_F z_F + Y_A z_A + Y_B z_B + (Y_P z_P - Y_F z_F - Y_A z_A) x_P \quad (4.4)$$

For the charge, whose composition is fixed by its initial conditions, the state parameters are

$$z_C \equiv Y_F z_F + Y_A z_A + Y_B z_B \quad (4.5)$$

The first two parts of Equation (4.5) identify the state parameters of the reactants, z_R , i.e.,

$$Y_F z_F + Y_A z_A \equiv (Y_F + Y_A) z_R \quad (4.6)$$

then,

$$z_R = \frac{Y_F z_F + Y_A z_A}{Y_F + Y_A} = \frac{z_F + \sigma_R z_A}{1 + \sigma_R} \quad (4.7)$$

where the state coordinates of **F** and **A** are prescribed by their initial chemical specification and σ_R is the air-fuel ratio defined as $\sigma_R = Y_A/Y_F$.

Thus, by virtue of Equation (4.5) and (4.7), Equation (4.4) yields

$$z_S - z_C = Y_P (z_P - z_R) x_P \quad (4.8)$$

A change of state taking place in the course of an adiabatic exothermic reaction

proceeds along a constant enthalpy path — a diagonal on the e - w plane, expressed by $e = h_i - w$, or just a change of the reference parameter, Δw , on the h - w plane, as depicted in Figure 4.4. Displayed there also is the conventional way of identifying the coordinates of a state vector $z = w, e$, or $z = w, h$. It utilizes variable specific heats associated with the drop of internal energy at a reference temperature, referred to as the heat of reaction or “heat release.” As reflected in the geometry of the diagram, the slope $D_K = C_K + 1$. If the reactants are considered as perfect gases, $C_K = c_v/R$, while $D_K = c_p/R$, where $c_{v,p}$ express specific heats at constant volume or constant pressure, while R is the gas constant.

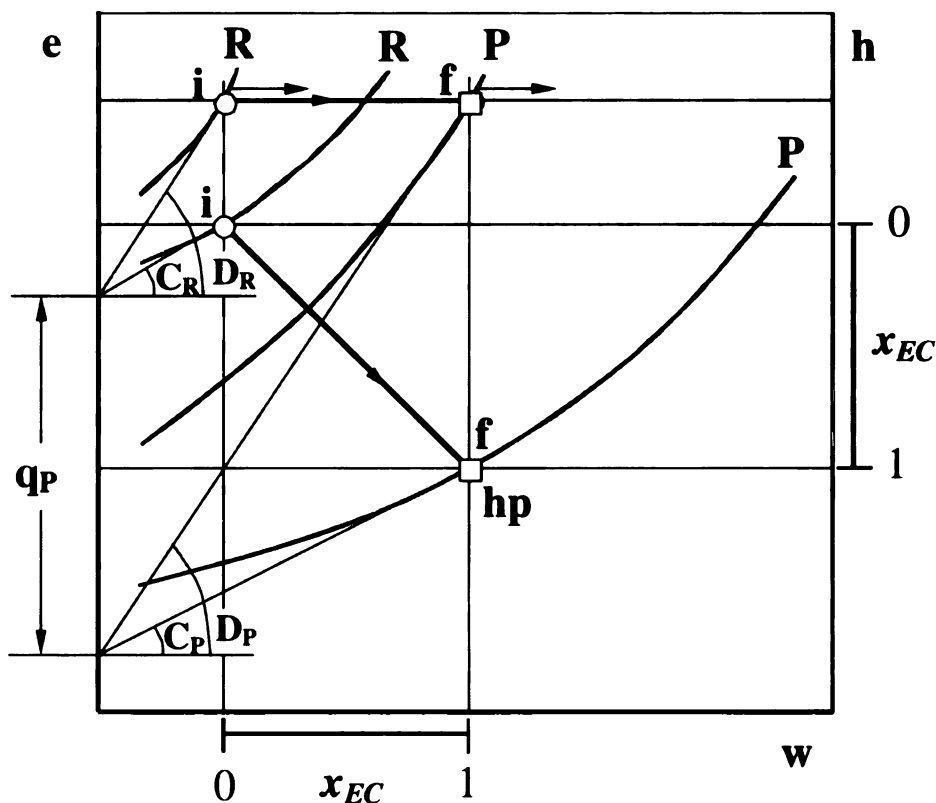


Figure 4.4: Diagram of component states for an adiabatic exothermic center in $w - e$ and $w - h$ space.

Exothermic centers are, in effect, kernels of exothermic fields. Since they take place at discrete sites, for a gasdynamic interpretation disregarding the effects of molecular diffusion, i.e. at the Peclet numbers $Pe = \infty$, they form singularities.

Each of them is then, in effect, a constant pressure deflagration point, rather than front in the classical version of this term. In the field, it acts as a point discontinuity, across which a finite change of state takes place, corresponding to a jump from **i**, where $x_P = 0$ and $z_C = z_{Si}$, to **t**, where $x_P = 1$. Its amplitude is then, according to Equation (4.8)

$$z_{St} - z_{Si} = Y_P(z_P - z_R) \quad (4.9)$$

4.4 Exothermic system

4.4.1 Balances

By definition, a thermodynamic system is confined within an impermeable boundary. The effects of the exothermic reaction it undergoes are expressed by Equation (4.8), while the corresponding change of state is depicted in Figure 4.5.

As evident there, the process progresses along the loci of states on **R** and **P**, rather than across them as in the case of an exothermic center. Hence, the progress parameter, x_P , for the system is different from that for the center, as is apparent from Figure 4.5, in contrast to Figure 4.4. The state transformations associated with the exothermic stage of combustion in a closed system are determined by the balances of volume and energy.

The volume balance is obtained from Equation (4.8) for $z = w$, whence

$$w_S - w_C = Y_P(w_P - w_R)x_P \quad (4.10)$$

Concomitantly, the energy balance is derived from Equation (4.8) for $z = e$

$$e_S - e_C = Y_P(e_P - e_R)x_P \quad (4.11)$$

Upon taking into account the energy expenditure, e_e , the internal energy of the

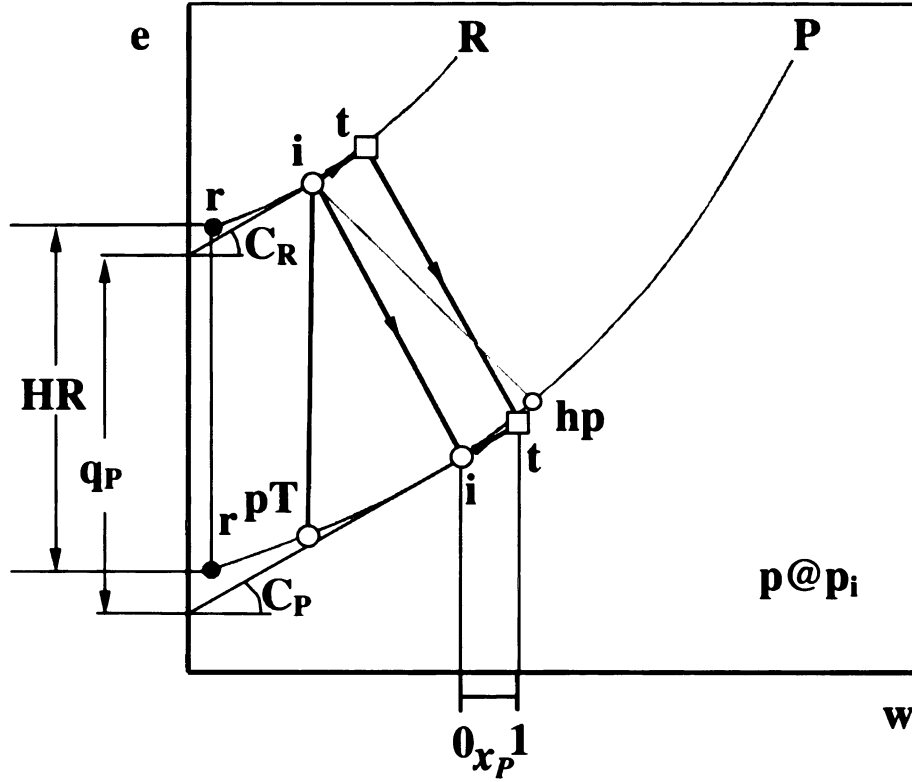


Figure 4.5: Diagram of component states for a non-adiabatic exothermic system in $w - e$ space.

system is

$$e_S = e_{Si} - e_e \quad (4.12)$$

then, Equation (4.11) is rewritten as

$$Y_P(e_P - e_R)x_P = e_{Si} - e_C - e_e \quad (4.13)$$

4.4.2 Coordinates

In Figure 4.5, the coordinates of the four pivotal points, **i** and **t** on **R** and their equivalents on **P**, are identified as follows. First, their directions are expressed in terms of the slopes, $C_K = (e_t - e_i)_K / (w_t - w_i)_K$ ($K = \mathbf{R}, \mathbf{P}$), and, secondly, the separation between them is established by the difference between intersections of their linear

extensions with the e axis, $q_P = e_{R0} - e_{P0}$. The latter furnishes a rational geometric entity that replaces the conventional concept of “heat release” (HR). The awkward role of this concept is displayed in Figure 4.5, let alone the confusion associated with its “apparent” version, as well as with the related notions of higher and lower “heating value”, “heat of reaction”, or “heat of combustion.”

Then, according to the diagram of Figure 4.5,

$$e_R = C_R w_R \quad (4.14)$$

while

$$e_P = C_P w_P - q_P \quad (4.15)$$

Since the initial state of the system is *de facto* the initial state of the charge,

$$e_C - e_{Si} = C_C (w_C - w_{Si}) \quad (4.16)$$

whereas

$$e_R - e_P = C_R w_R - C_P w_P + q_P \quad (4.17)$$

4.4.3 Progress parameter

With Equations (4.14) (4.17) taken into account, the energy balance of Equation (4.13) becomes

$$(C_R w_R - C_P w_P + q_P) Y_P x_P = C_C (w_C - w_{Si}) + e_e \quad (4.18)$$

which, upon eliminating w_P by using the volume balance of Equation (4.11), yields

$$x_P = \frac{1}{Y_P} \frac{C_P (w_S - w_C) + C_C (w_C - w_{Si}) + e_e}{q_P - (C_P - C_R) w_R} \quad (4.19)$$

It is an expression relating the total mass fraction of products x_P with time t via the prescribed functional relationships of $w_S(t)$ and $e_e(t)$, furnishing thus a fundamental relationship for the inverse problem of an exothermic process — pressure diagnostics.

4.4.4 Combustion in a piston engine

For a closed system, such as the cylinder of an internal combustion engine or an explosion test vessel, Equation (4.19) provides the basis for pressure diagnostics: the deduction of information on the evolution of the exothermic stage of combustion from the measured pressure transducer record. In this case, the energy expenditure is

$$e_e \equiv w_w + e_I \quad (4.20)$$

In terms of v_S denoting the ratio of cylinder to clearance volume v_C , the work performed by the system is

$$w_w \equiv v_C \int_{v_{S1}}^{v_S} (p - p_b) dv \quad (4.21)$$

where p_b is the back pressure on the outer side of the piston. The second term, e_I , expresses the energy unmanifested by the measured pressure profile. It is made up primarily of the energy loss incurred by heat transfer to the walls and secondarily of energy associated with mass lost by leakage.

For a piston engine, the process of compression is represented by a polytrope, according to which

$$\frac{w_K}{w_{S1}} = P^{m_C} \quad (K = \mathbf{R}, \mathbf{C}) \quad (4.22)$$

where $P = p/p_i$ and $m_C = 1 - n_C^{-1}$, with n_C denoting the polytropic index of the process of compression. If the process is isentropic, then $n_C = 1 + C_C^{-1}$ and $m_C = (1 + C_C)^{-1}$.

Upon combining Equation (4.19) and (4.20) and normalizing the equation with respect to the initial state of exothermic stage of combustion, Equation (4.19) becomes

$$x_P = \frac{C_P(PV - 1) + (C_P - C_C)(P^{m_C} - 1) + W_k + \Omega_I}{Y_P[\Omega_P - (C_P - C_R)P^{m_R}]} \quad (4.23)$$

where $V = v_S/v_{Si}$, $w_S/w_{Si} = PV$, $w_w/w_{Si} = W_k$, $\Omega_P = q_P/w_{Si}$, and $\Omega_I = e_I/w_{Si}$.

The mass fraction of products, actual and/or total, is considered, in accord with the meaning of e_I , as a sum of two components, so that

$$x_P = x_E + x_I \quad (4.24)$$

where subscript E denotes its effective part, manifested by the effects of the generated pressure, while I marks its ineffective part. Then, Equation (4.23) is divided into

$$x_E = \frac{C_P(PV - 1) + (C_P - C_C)(P^{m_C} - 1) + W_k}{Y_P[\Omega_P - (C_P - C_R)P^{m_R}]} \quad (4.25)$$

and

$$x_I = \frac{\Omega_I}{Y_P[\Omega_P - (C_P - C_R)P^{m_R}]} \quad (4.26)$$

In Equation (4.23), Y_P is not known unless the composition of products is identified from the exhaust gas. Thus, x_P cannot be calculated directly from the equation. However, upon the combination of Equation (4.1) and (4.23), the mass fraction of products during the combustion is obtained as

$$y_P = \frac{C_P(PV - 1) + (C_P - C_C)(P^{m_C} - 1) + W_k + \Omega_I}{\Omega_P - (C_P - C_R)P^{m_R}} \quad (4.27)$$

Similarly,

$$y_E = \frac{C_P(PV - 1) + (C_P - C_C)(P^{m_C} - 1) + W_k}{\Omega_P - (C_P - C_R)P^{m_R}} \quad (4.28)$$

$$y_I = \frac{\Omega_I}{\Omega_P - (C_P - C_R)P^{m_R}} \quad (4.29)$$

4.4.5 Correlation

The heat transfer to the wall, e_I , is not determined. Thus the mass fraction of products, y_P , as well as its ineffective component, y_I , cannot be calculated from Equation (4.27) and (4.29), respectively.

Thermodynamic properties of the system during its exothermic stage of combustion have been established by a study of heat transfer from combustion in a vessel of constant volume, equipped with transfer gauges and pressure transducers [56][74]. In this case, $n_e = 0$, so that $\Pi_e = p$, while the independent variable, Θ , is expressed by time, t . The program of experimental investigations covered a broad range of turbulent conditions. It was found then that the following conditions should be satisfied, whether combustion was propagated in a laminar or turbulent manner.

1. At $y_P = 0$: $y_E/y_{Emax} = 0$, while $dy_E/dy_P = \beta$, i.e., $d(y_E/y_{Emax})/dy_P = \beta/y_{Emax}$;
2. at $y_P = 1$: $y_E/y_{Emax} = 1$, while $dy_E/dy_P = 0$, i.e., $d(y_E/y_{Emax})/dy_P = 0$.

The above conditions are satisfied by a simple power function

$$y_E/y_{Emax} = 1 - (1 - y_P)^{\beta/y_{Emax}} \quad (4.30)$$

which is plotted in Figure 4.6.

It was then established, moreover, that $\beta = y_{Emax}^{1/2}$. In view of this, the correlation function for evaluating the mass fraction of generated products, $y_P(\Theta)$, from its effective part, $y_E(\Theta)$, is obtained by the inverse of Equation (4.30), yielding

$$y_P = 1 - (1 - y_E/y_{Emax})^{y_{Emax}^{1/2}} \quad (4.31)$$

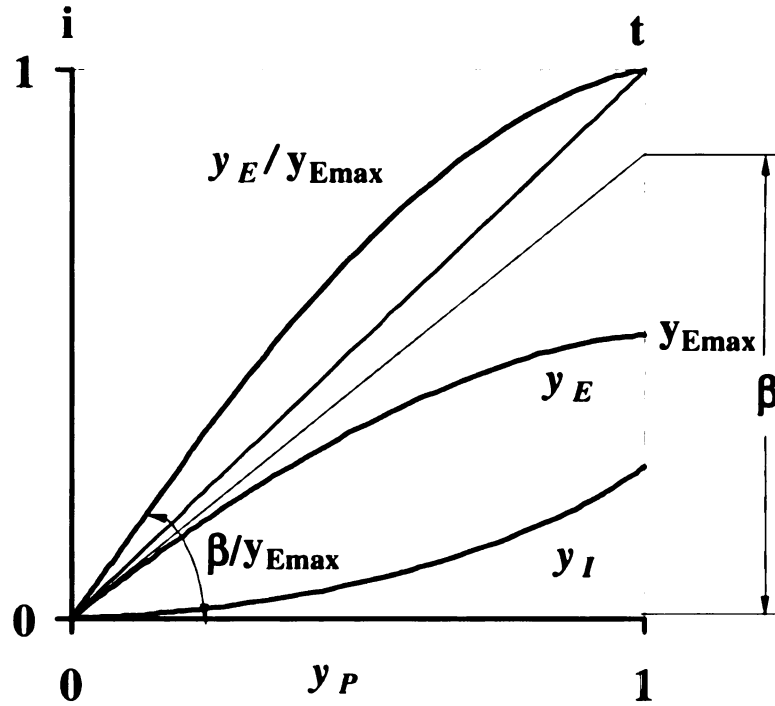


Figure 4.6: Correlation between mass fractions of products.

Application of Equation (4.31) to the enclosure of a variable cylinder volume during the exothermic stage of combustion is based on the postulate that the piston movement does not significantly affect the relationship between the mass fraction of generated products, $y_P(\theta)$, and its effective component, $y_E(\theta)$.

4.5 Closed system

4.5.1 Thermodynamic relationship

Upon the recognition that the mixture in the cylinder can be considered as a closed system during the period starting from the intake valve close (IVC, denoted by **a**) and ending at the exhaust valve open (EVO, denoted by **z**), the method extended to analyze the exothermic stage of combustion can be used to analyze such a closed system.

Because of the change of the analysis system. Equations (4.27). (4.28) and (4.29)

should be changed accordingly for the analysis of such closed system. The system is changed from the cylinder mixture during the exothermic stage of combustion to that in the closed system (from IVC to EVO), the normalization base in Equation (4.27), (4.28) and (4.29) should be changed from the initial state, **i**, to the IVC, **a**. Thus, the mass fraction of products in the closed system is

$$y_P = \frac{C_P(PV - 1) + (C_P - C_C)(P^{m_C} - 1) + W_k + \Omega_I}{\Omega_P - (C_P - C_R)P^{m_R}} \quad (4.32)$$

where $P = p/p_a$, $P_i = p_i/p_a$, $V = v_S/v_{Sa}$, $V_i = v_{Si}/v_{Sa}$, $w_w/w_{Sa} = W_k$, $w_w = v_C \int_{v_{Sa}}^{v_S} (p - p_b)dv$, $\Omega_P = q_P/w_{Sa}$, $\Omega_I = e_I/w_{Sa}$ and $m_C = 1 - n_C^{-1}$, with n_C denoting the polytropic index of the process of compression.

Similarly,

$$y_E = \frac{C_P(PV - 1) + (C_P - C_C)(P^{m_C} - 1) + W_k}{\Omega_P - (C_P - C_R)P^{m_R}} \quad (4.33)$$

$$y_I = \frac{\Omega_I}{\Omega_P - (C_P - C_R)P^{m_R}} \quad (4.34)$$

By observing effective part of the mass fraction of products, it is found the y_E consists of the contribution to the change in internal energy of the system and to the production of piston work, i.e.,

$$y_E = y_\epsilon + y_\omega \quad (4.35)$$

where

$$y_\epsilon = \frac{C_P(PV - 1) + (C_P - C_C)(P^{m_C} - 1)}{\Omega_P - (C_P - C_R)P^{m_R}} \quad (4.36)$$

$$y_\omega = \frac{W_k}{\Omega_P - (C_P - C_R)P^{m_R}} \quad (4.37)$$

From Equation (4.11), the fundamental thermodynamic reference parameter of products, the mechanical energy, is

$$w_P = R_P T_P = w_R + \frac{w_S - w_C}{y_P} \quad (4.38)$$

In terms of the normalized variables and the polytropic relationship formulated by Equation (4.22), the normalized mechanical energy of products is

$$W_P = W_R + \frac{W_S - W_C}{y_P} = P^{m_C} + \frac{PV - P^{m_C}}{y_P} \quad (4.39)$$

All these relations apply well to the process of expansion where $y_P = 1$ and to the exothermic stage of combustion where $0 < y_P < 1$. However, for the process of compression, where $y_P = 0$ and $w_S = w_C$, Equation (4.32) becomes

$$y_P = \frac{C_C(P^{m_C} - 1) + W_k + \Omega_I}{\Omega_P - (C_P - C_R)P^{m_R}} \quad (4.40)$$

Accordingly, Equation (4.33) and (4.36) become

$$y_E = \frac{C_C(P^{m_C} - 1) + W_k}{\Omega_P - (C_P - C_R)P^{m_R}} \quad (4.41)$$

$$y_\epsilon = \frac{C_C(P^{m_C} - 1)}{\Omega_P - (C_P - C_R)P^{m_R}} \quad (4.42)$$

4.5.2 Thermodynamic properties

For the reactants, which composed of air and fuel, its composition is almost fixed, thus the reactants behave as the ideal gas. The temperature of the reactants can be obtained from the equation of state and Equation (4.22).

$$T_R = \frac{pv_R}{p_a v_{Ra}} T_a = \frac{w_R}{w_{Ra}} T_a = P^{m_C} \quad (4.43)$$

The specific volume of the reactants is

$$v_R = \frac{w_R}{w_{Ra}} \frac{p_a}{p} v_{Ra} = P^{m_C} \frac{p_a}{p} v_{Ra} \quad (4.44)$$

where the specific volume of reactants at IVC, v_{Ra} , is obtained by STANJAN.

As a matter of principle, the products do not behave as an ideal gas, since its composition and molar masses are variable in order to comply with the condition of thermodynamic equilibrium. However, if the gas constant of products is assumed to change linearly during the exothermic stage of combustion, it is reasonable to calculate the temperature and specific volume of the products from the equation of state and Equation (4.39), i.e.

$$T_P = \frac{pv_P}{p_i v_{Pi}} \frac{R_P}{R_{Pi}} T_i = \frac{w_P}{w_{Pi}} \frac{R_P}{R_{Pi}} T_i = (P^{mc} + \frac{PV - P^{mc}}{y_P}) \frac{R_P}{R_{Pi}} T_i \quad (4.45)$$

where the gas constant of products $R_P = R_{Pi} + (R_{Pf} - R_{Pi})(\Theta - \Theta_i)/(\Theta_t - \Theta_i)$. The specific volume of the reactants is

$$v_P = \frac{w_P}{w_{Pi}} \frac{p_i}{p} v_{Pi} = (P^{mc} + \frac{PV - P^{mc}}{y_P}) \frac{p_i}{p} v_{Pi} \quad (4.46)$$

where the specific volume of products at the initial state, v_{Pi} , is obtained by STANJAN.

For the system, which is the mixture in the closed system, its temperature and specific volume are the same as those of the reactants during the compression process ($y_P = 0$). During the expansion process ($y_P = 1$), they are the same as those of products. During the exothermic stage of combustion ($0 < y_P < 1$), the temperature and specific volume of the system can be reasonably evaluated from the equation of state with the assumption that the gas constant of the mixture changes linearly. Thus, the temperature of the system is

$$T_S = \frac{pv_S}{p_i v_{Si}} \frac{R_S}{R_{Si}} T_i = \frac{p}{p_i} \frac{v_S}{v_C} \frac{v_C}{v_{Si}} \frac{R_S}{R_{Si}} T_i \quad (4.47)$$

where the gas constant of system $R_S = R_{Si} + (R_{Sf} - R_{Si})(\Theta - \Theta_i)/(\Theta_t - \Theta_i)$ and the volume ratio $v_S/v_C = 1 + 1/2(r_c - 1)[R + 1 - \cos \theta - (R^2 - \sin^2)^{1/2}]$ [1].

The specific volume of the system is

$$v_S = \frac{v_S}{v_{Si}} v_{Si} = \frac{v_S}{v_C} \frac{v_C}{v_{Si}} v_{Si} \quad (4.48)$$

where the specific volume of the system at the initial state, v_{Si} , is obtained by STANJAN.

4.6 Procedure

The procedure for analyzing the exothermic stage of combustion and the closed system is as follows.

1. Identify the initial state **i** and final state **f** of the dynamic state of combustion analyzed in Chapter 2.
2. Use STANJAN to evaluate the internal energy e and mechanical parameter, $w = pv$, of the reactants at the initial state **i** and final state **f** respectively.
3. Plot point **i** and point **f** of reactants in the $e - w$ plane of the state space to evaluate the slope of the state change of reactants, C_R .
4. Since the initial state, **i**, is a singular point for the products, it is impossible to evaluate the internal energy and mechanical parameter of products at the initial state. Therefore one more state is required to evaluate the slope of the state change of products, C_P . As mentioned in Section 4.2.2, point **hp** (constant enthalpy and constant pressure) can be used to evaluate C_P . Therefore, use STANJAN to evaluate the internal energy e and mechanical energy w of the products at point **hp** and point **f**, respectively.
5. Plot point **hp** and point **f** of products in the $e - w$ plane of the state space to evaluate the slope of the state change of products, C_P .

6. Evaluate the heat release, q_P , from the plot in the $e - w$ plane of the state space.
7. Use Equations (4.28) and (4.31) to evaluate the effective component of the mass fraction of products and mass fraction of products itself during the exothermic stage of combustion, respectively. Use Equation (4.24) to evaluate the ineffective component of the mass fraction of products.
8. Identify the terminal state of the exothermic stage of combustion, \mathbf{t} , which is the maximum of the effective component of mass fraction of products.
9. For the closed system, evaluate the mass fraction of products and its components by Equations (4.33), (4.36), (4.37), (4.31) and (4.24).
10. Determine the temperature and specific volume of the reactants, products, and system by Equations (4.43) — (4.48).

4.7 Implementation

4.7.1 Engine

The technique of pressure diagnostics to reveal the performance of a exothermic stage of combustion and a closed system was carried out for the same engine mentioned in section 3.8.1. The engine operation conditions are shown in Table 3.3.

4.7.2 Exothermic stage of combustion

State diagrams of the exothermic stage of combustion for four cases are shown in Figures 4.7–4.10. From these diagrams, the slopes of state changes of reactants and products as well as the heat release during the combustion are evaluated and shown in Table 4.2.

Shown in Figures 4.11--4.14 are the mass fractions of the products and their effective parts during the exothermic stage of combustion. When the effective component of the mass fraction of products reaches its maximum, the terminal state of the exothermic stage of combustion is reached and the combustion is ended. The crank angles of initial state and terminal state of the exothermic stage of combustion for four cases are shown in Table 4.2.

Table 4.2: Parameters to evaluate the mass fraction of products

	1	2	3	4
Θ_i	355	347	355	360
Θ_t	383	380	380	400
C_R	3.0568	3.3242	3.0479	2.8439
C_P	3.6224	3.5834	3.5258	3.5032
q_R (KJ/g)	2.1137	2.0498	1.8351	1.8647

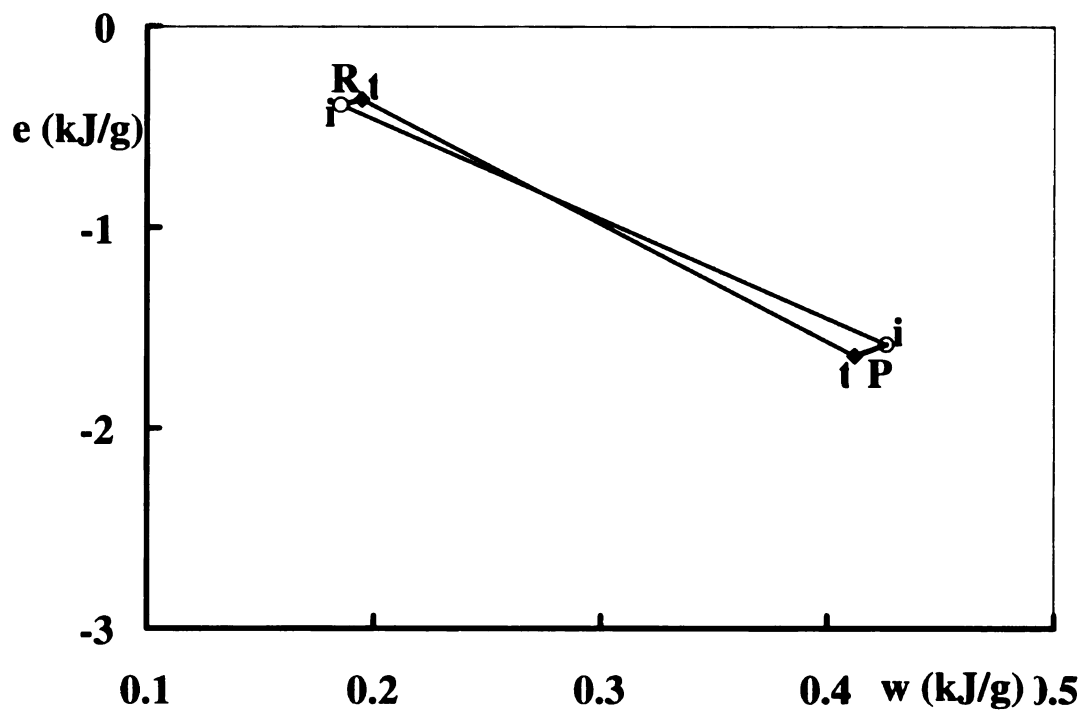


Figure 4.7: State diagram of the exothermic stage of combustion for case 1

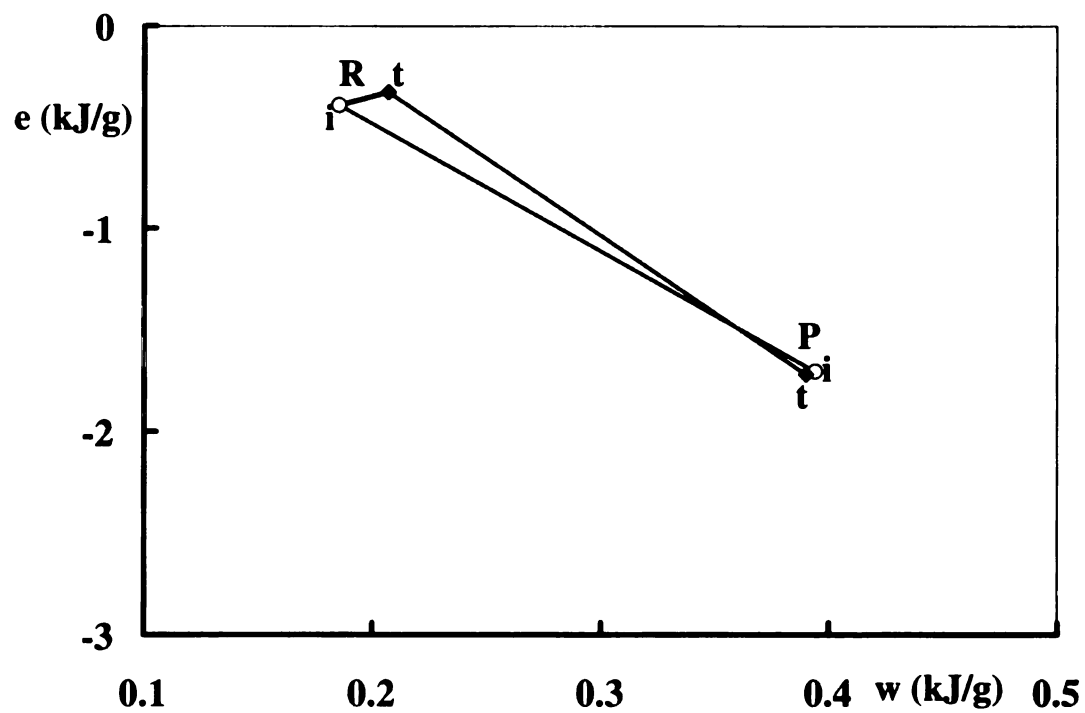


Figure 4.8: State diagram of the exothermic stage of combustion for case 2

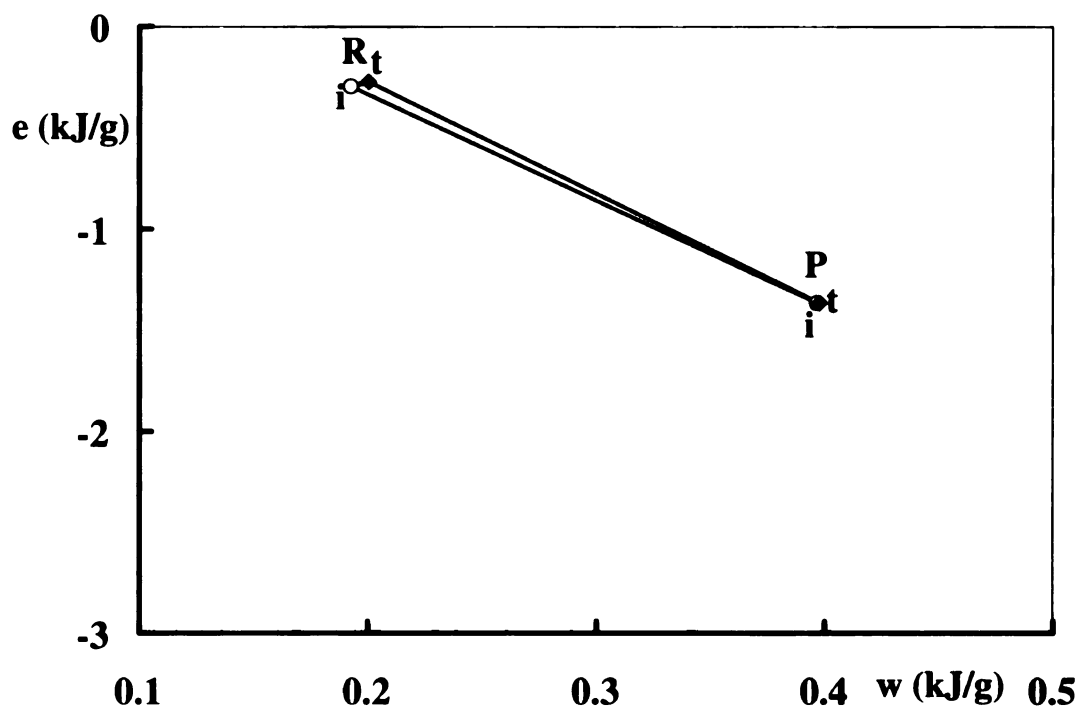


Figure 4.9: State diagram of the exothermic stage of combustion for case 3

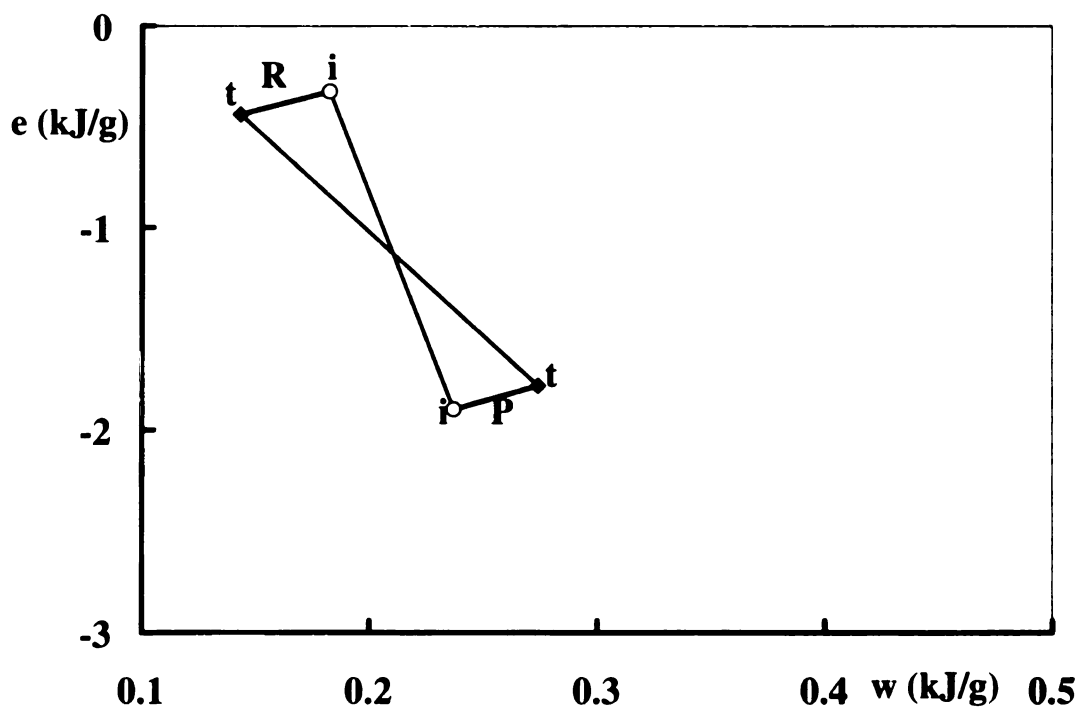


Figure 4.10: State diagram of the exothermic stage of combustion for case 4

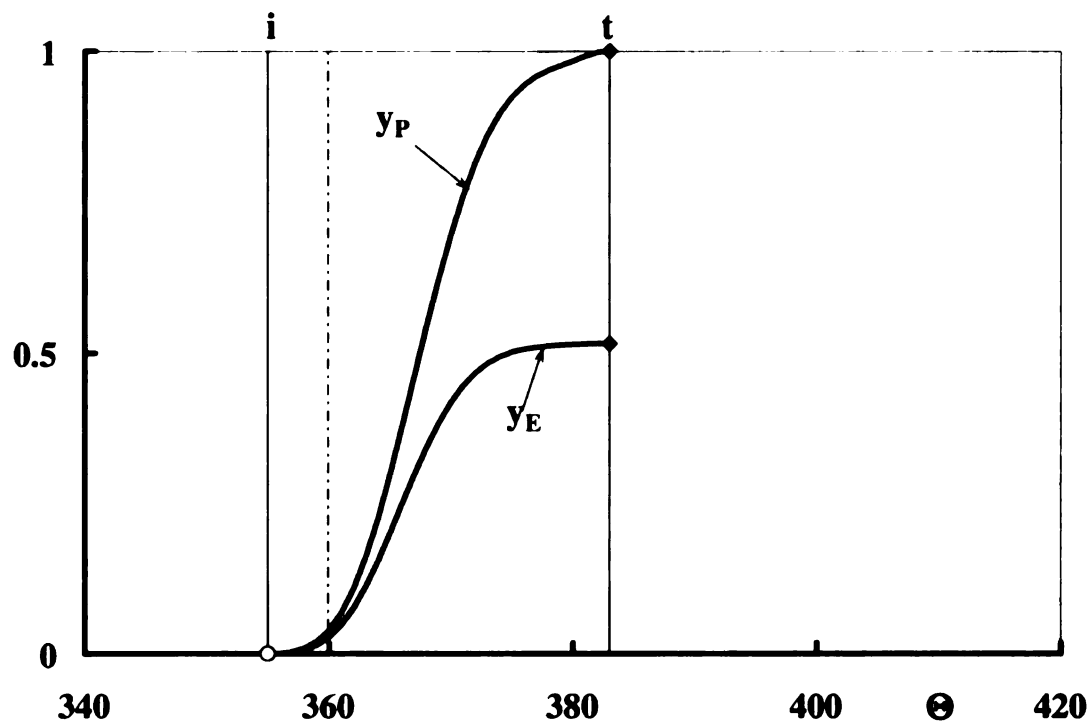


Figure 4.11: Profiles of the mass fraction of products and its effective component of case 1

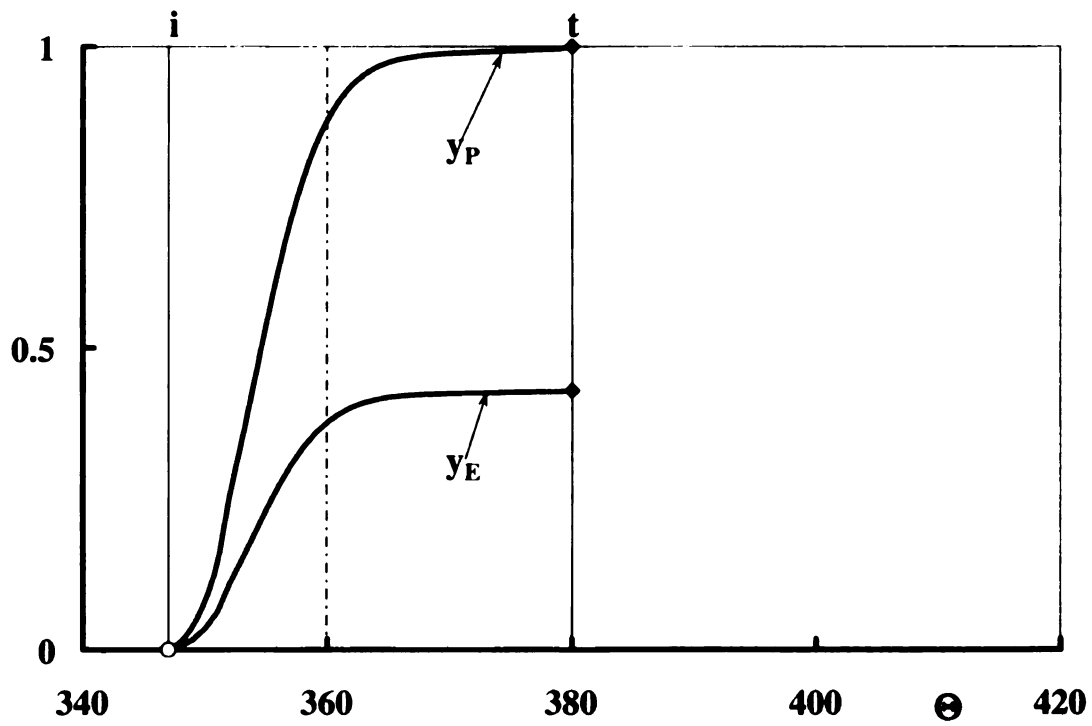


Figure 4.12: Profiles of the mass fraction of products and its effective component of case 2

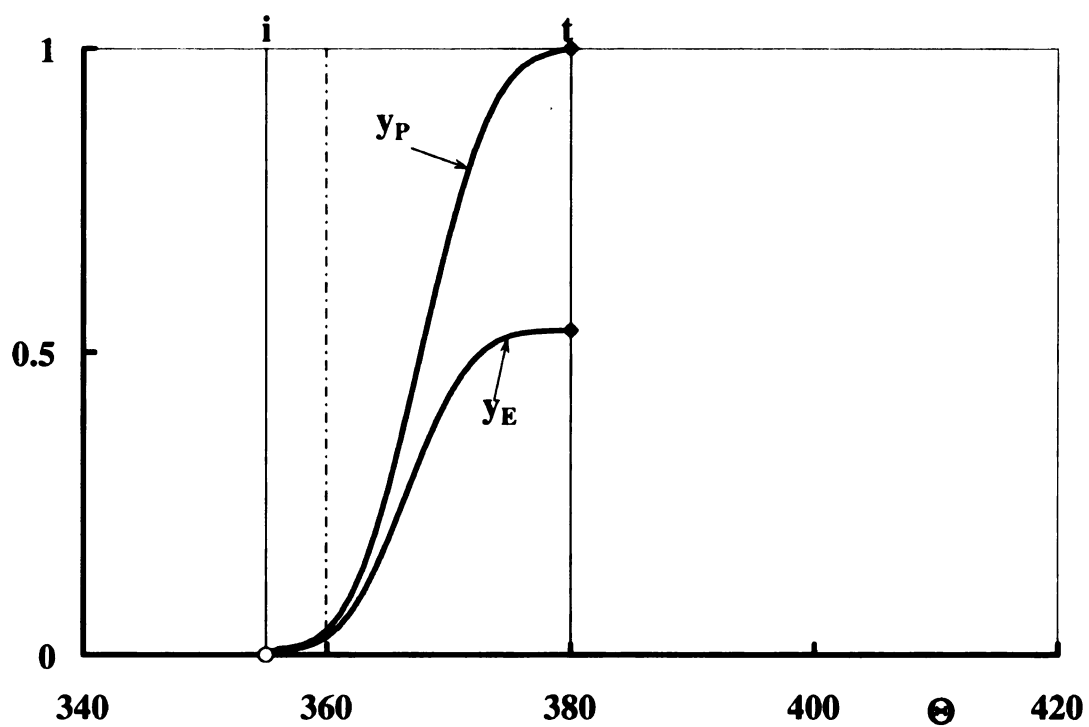


Figure 4.13: Profiles of the mass fraction of products and its effective component of case 3

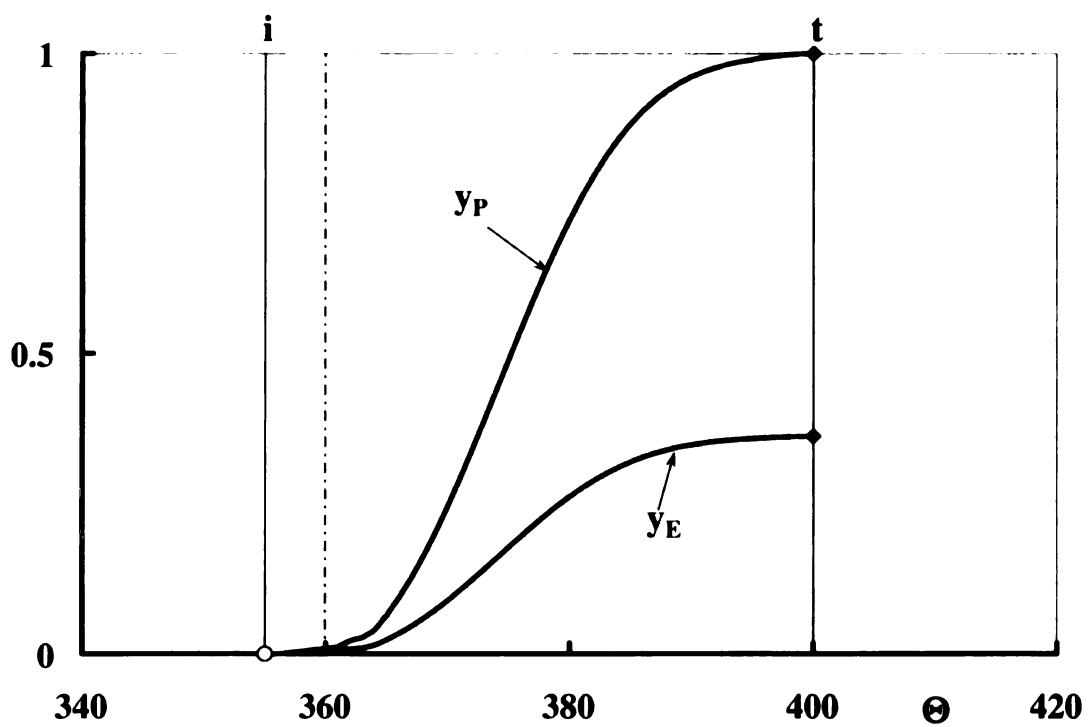


Figure 4.14: Profiles of the mass fraction of products and its effective component of case 4

4.7.3 Closed system

For the closed system, the state diagrams are shown in Figures 4.15—4.18. In figures, the states of system at the crank angle of intake valve close and exhaust valve open are included and denoted by point **a** and **z**.

The mass fraction of products and its components are shown in Figure 4.19 — 4.22. In figures, point **Ij** indicates the crank angle at which the fuel is injected and point **Ig** indicates the crank angle at which the spark discharges for ignition. Upon the observation of y_ϵ and y_ω , respectively reflecting the change of internal energy and work in the closed system, the fuel consumption in the engine cylinder is well understood. The energy is stored in the system by the piston work in the course of compression, with more energy added during the exothermic stage of combustion. The energy is released during the expansion process to produce piston work. Thus, it is a two-step, laser-like, sequence, in which a short process of charging is followed by a long process of discharging.

Shown in Figures 4.23—4.26 are the temperature profiles of reactants, products, and the system. The specific volumes of reactants, products, and the system are shown in Figures 4.27—4.30.

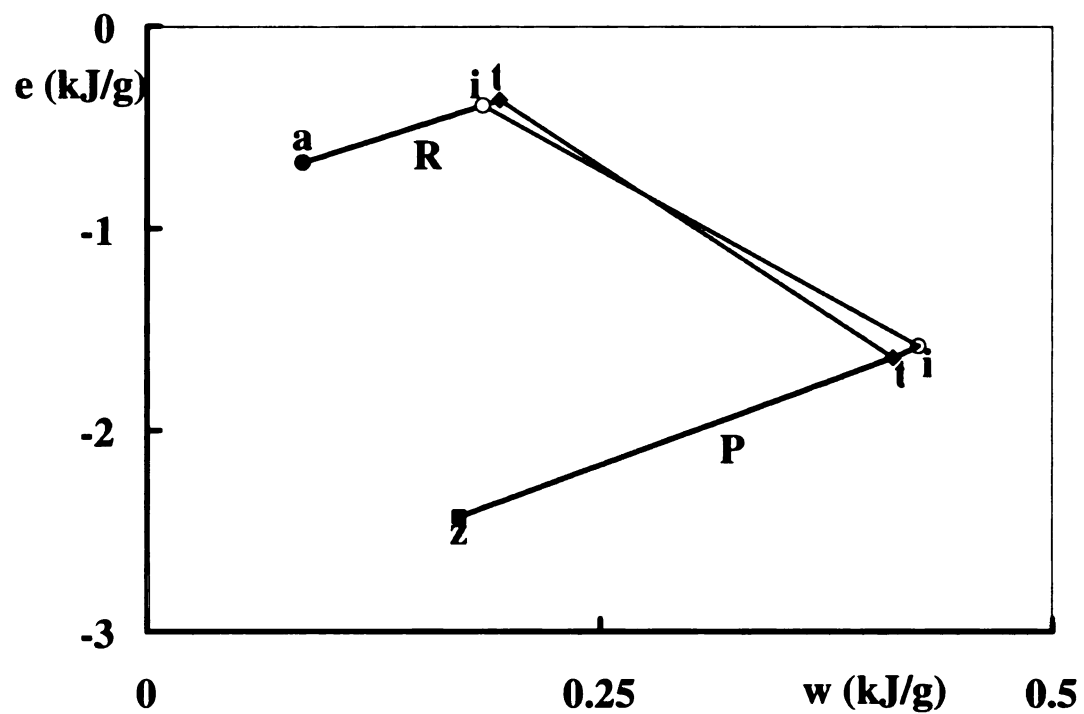


Figure 4.15: State diagram of a closed system for case 1

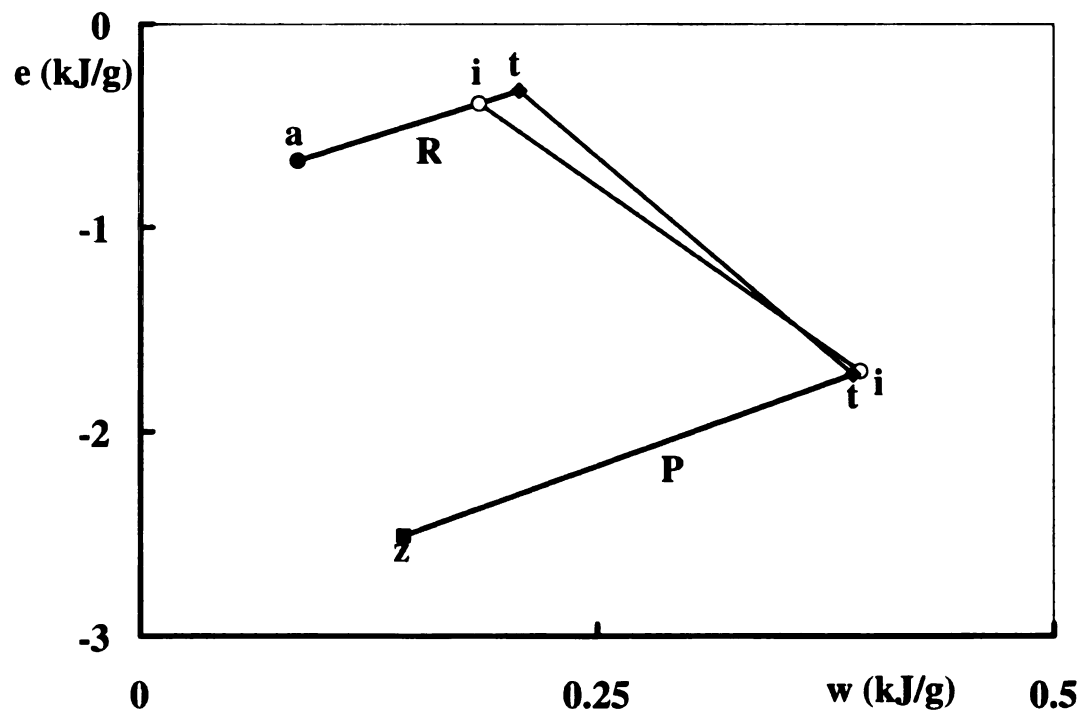


Figure 4.16: State diagram of a closed system for case 2

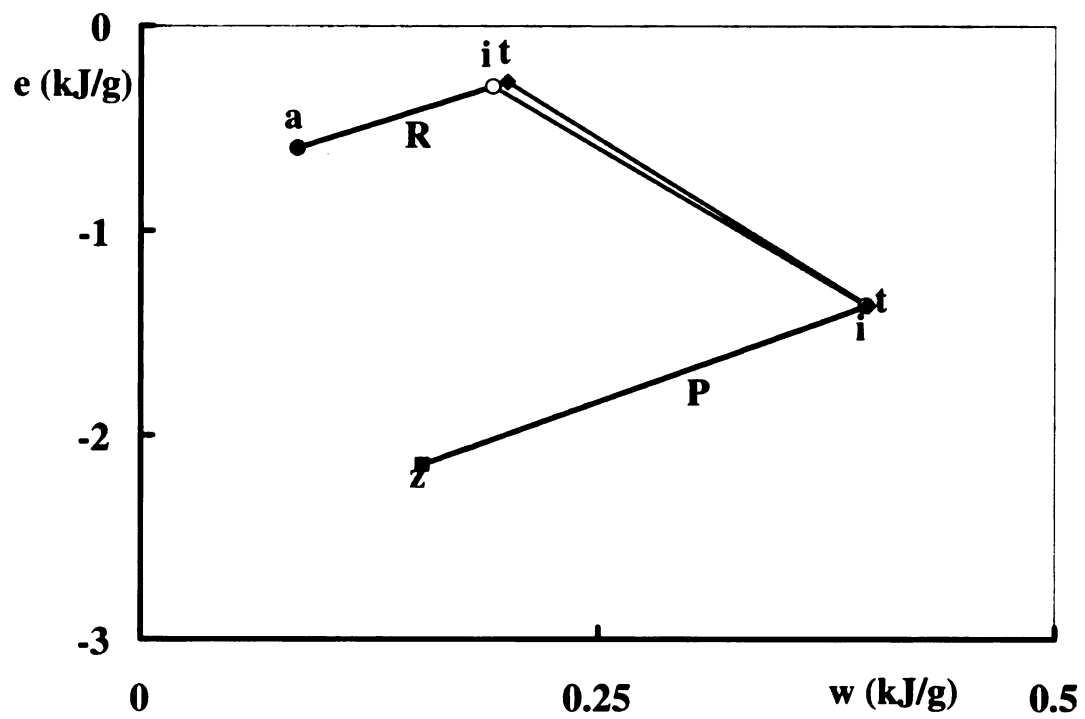


Figure 4.17: State diagram of a closed system for case 3

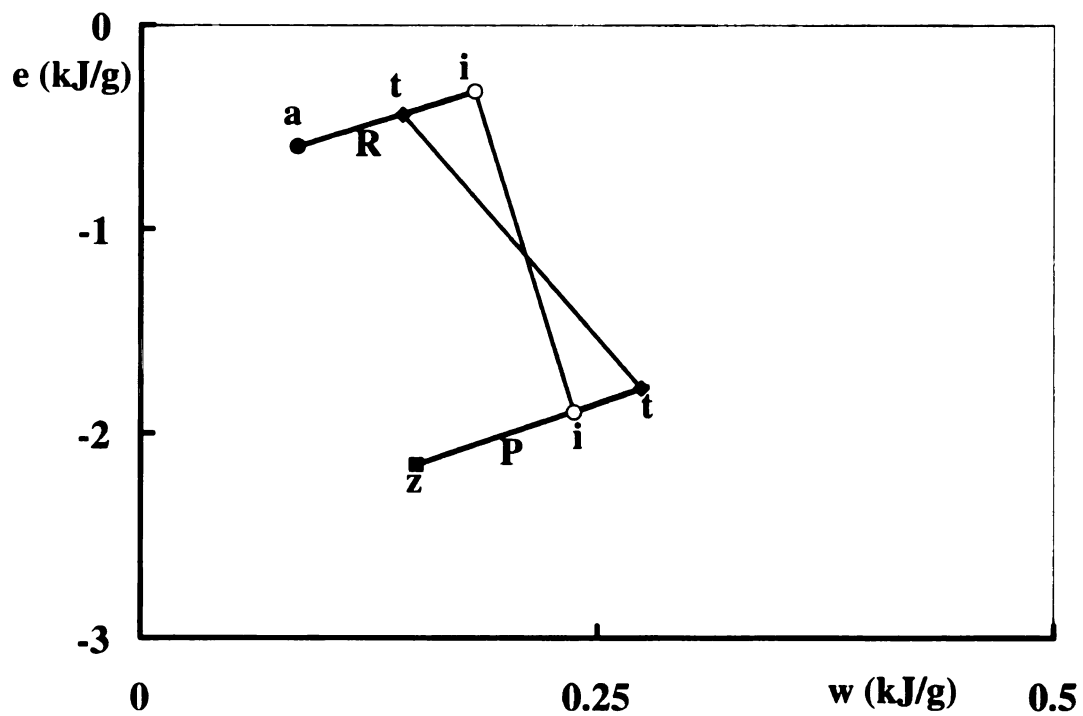


Figure 4.18: State diagram of a closed system for case 4

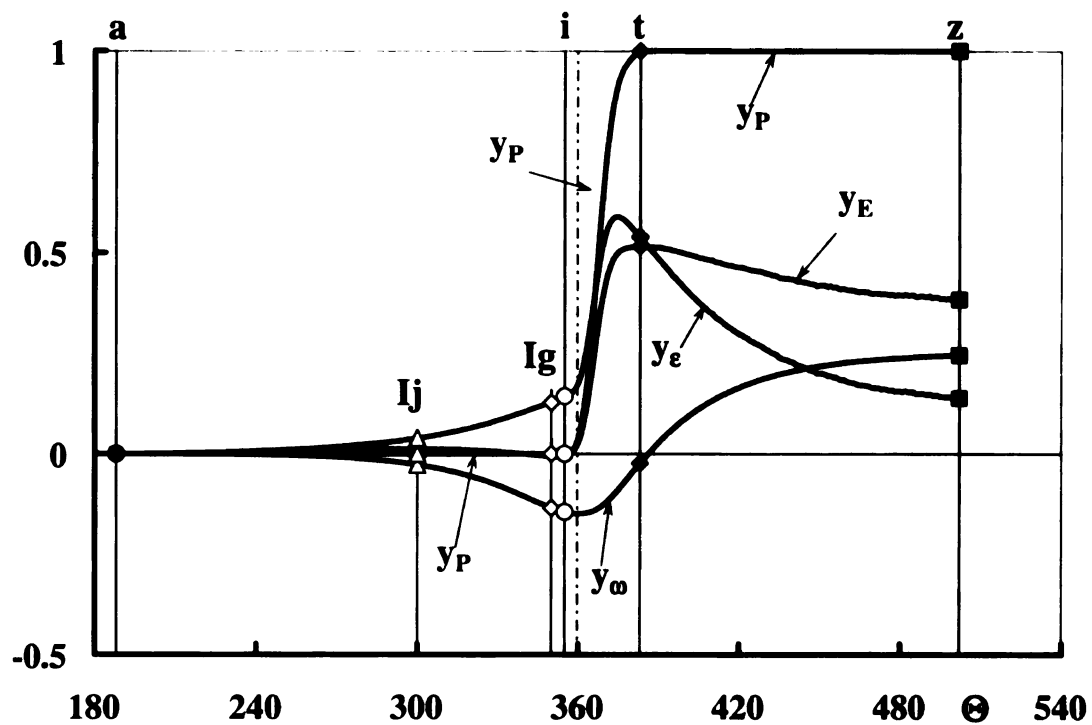


Figure 4.19: Profiles of the mass fraction of products and its components in the closed system of case 1

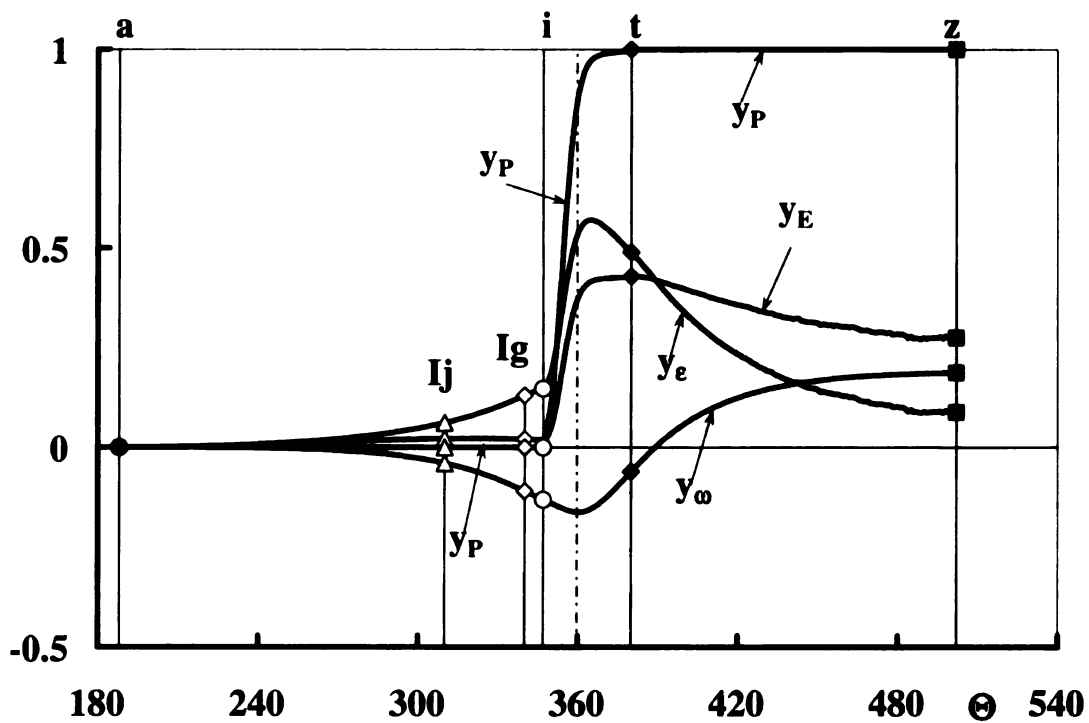


Figure 4.20: Profiles of the mass fraction of products and its components in the closed system of case 2

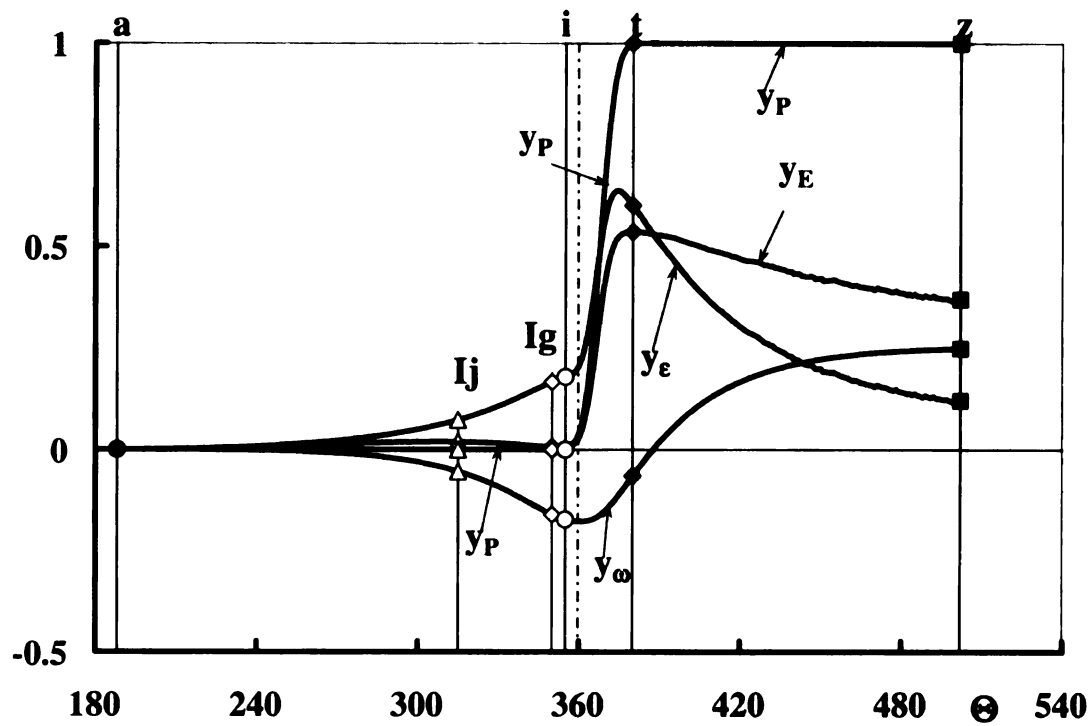


Figure 4.21: Profiles of the mass fraction of products and its components in the closed system of case 3

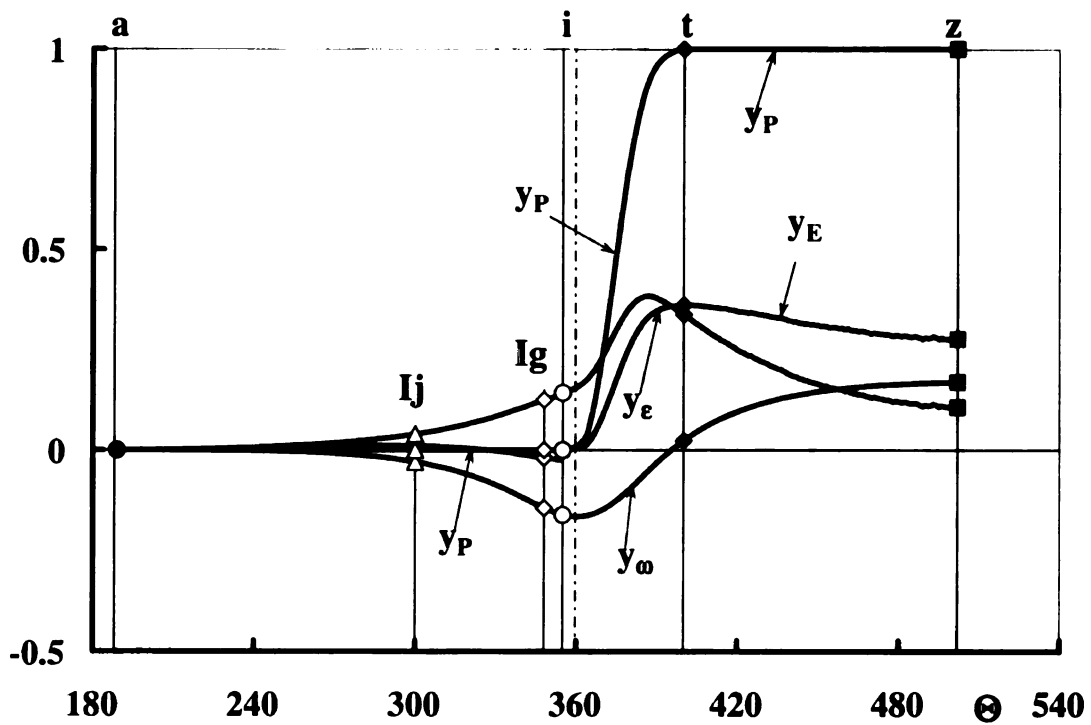


Figure 4.22: Profiles of the mass fraction of products and its components in the closed system of case 4

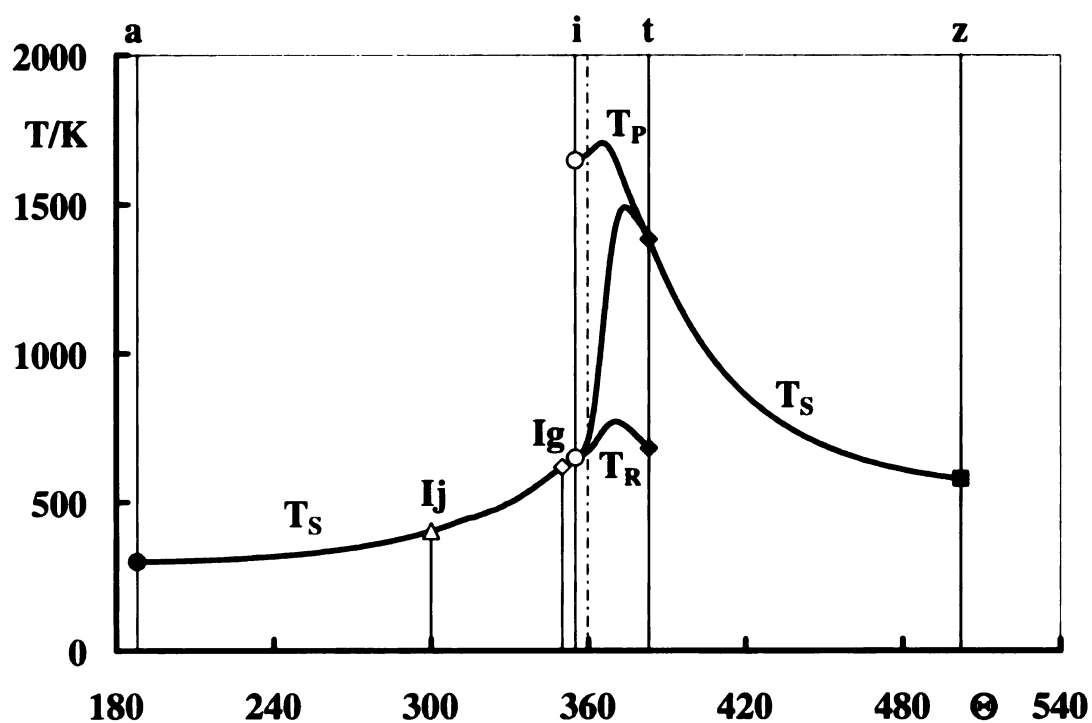


Figure 4.23: Profiles of the temperature of reactants, products, and system of case 1

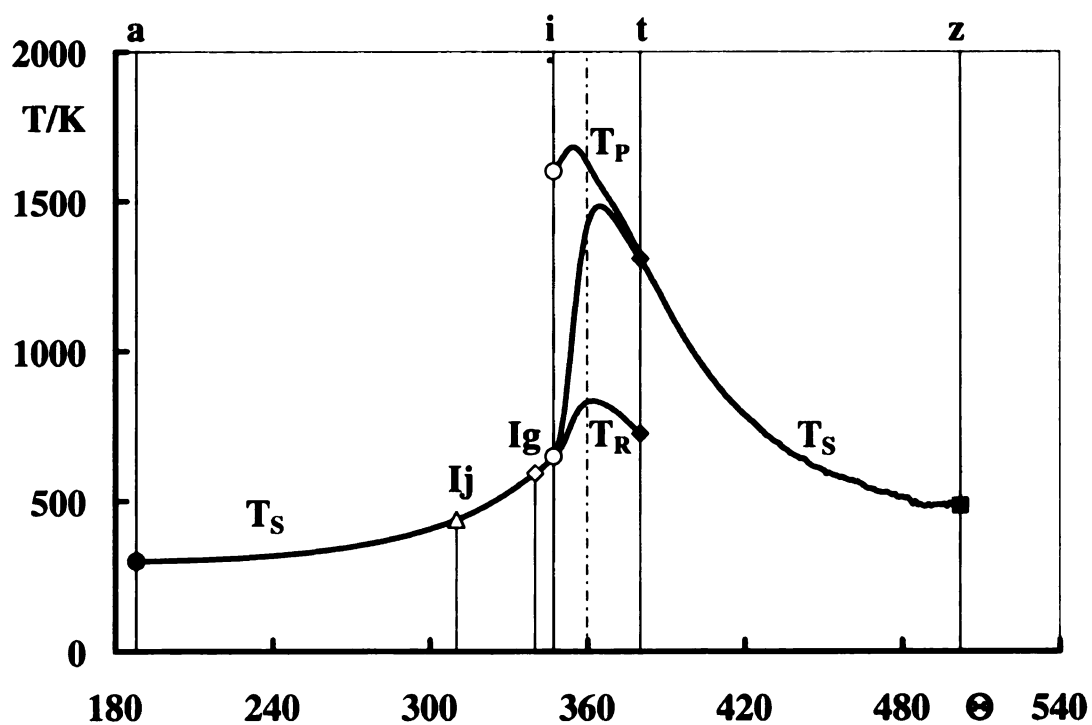


Figure 4.24: Profiles of the temperature of reactants, products, and system of case 2

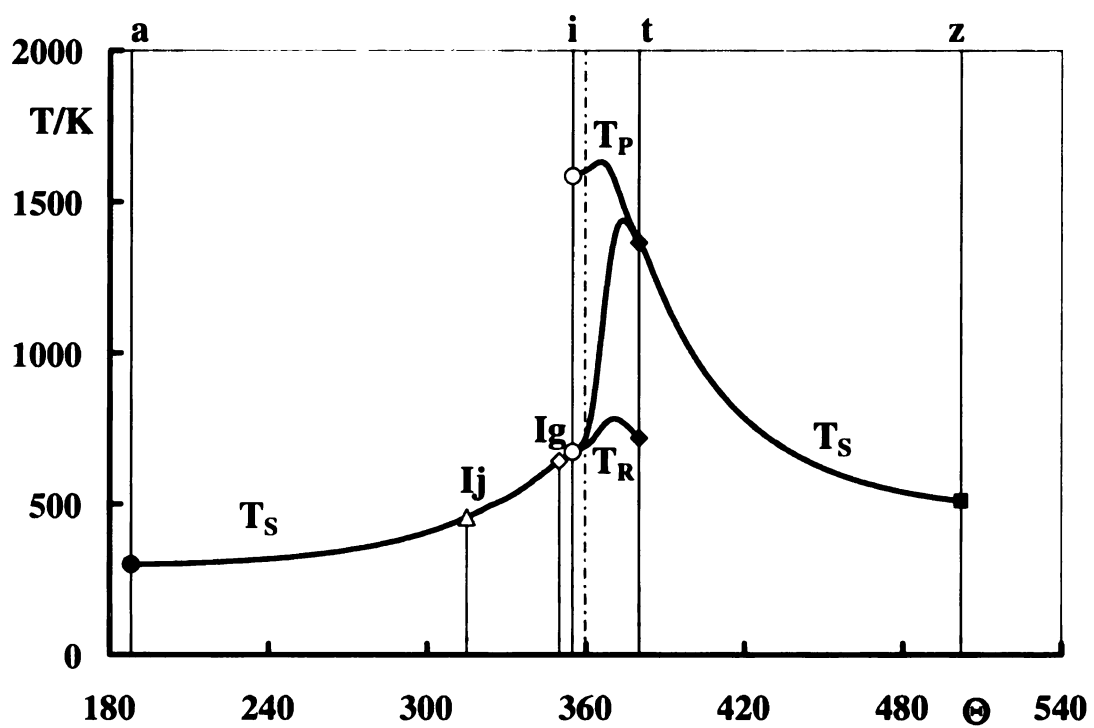


Figure 4.25: Profiles of the temperature of reactants, products, and system of case 3

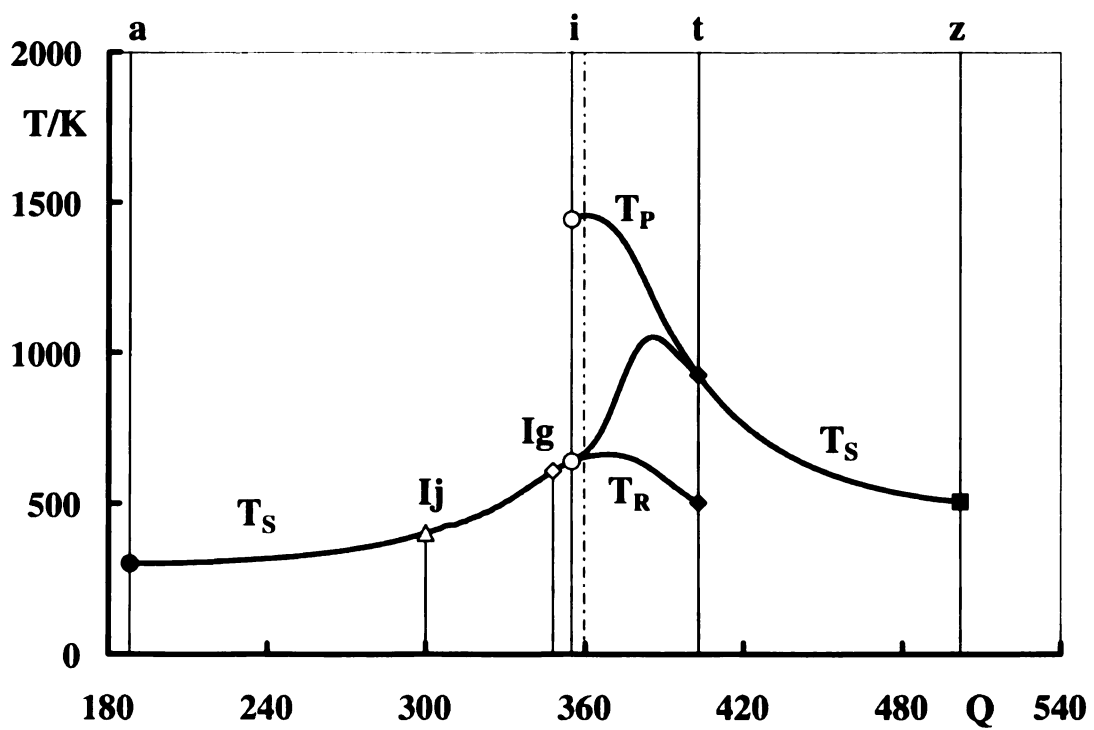


Figure 4.26: Profiles of the temperature of reactants, products, and system of case 4

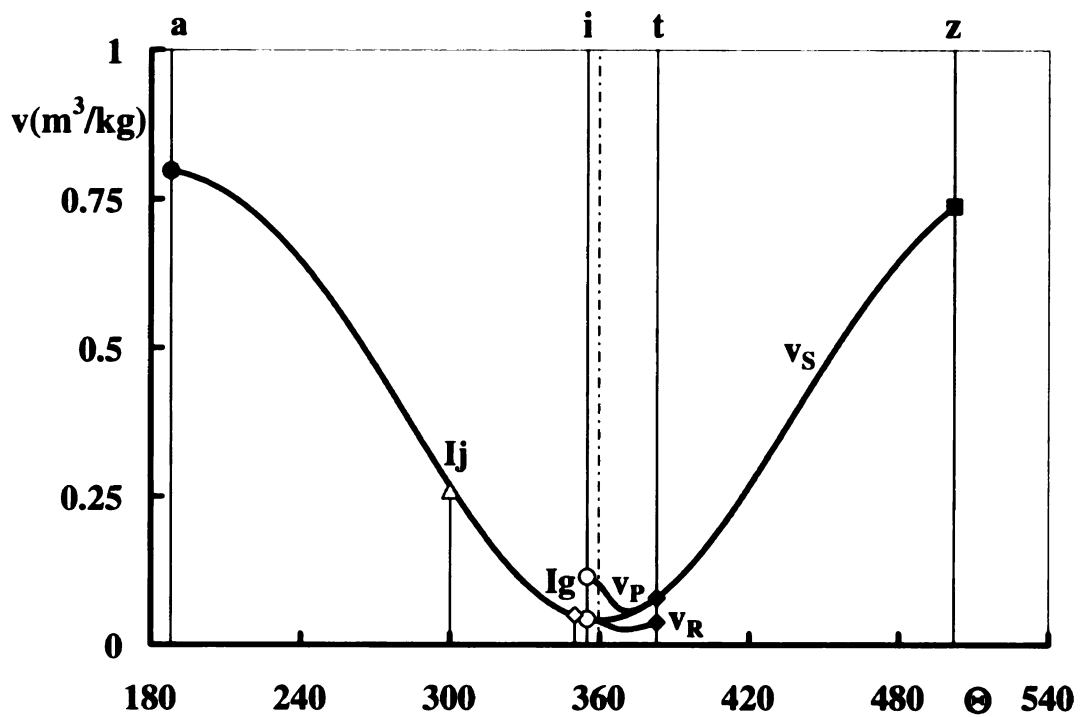


Figure 4.27: Profiles of the specific volume of reactants, products, and system of case 1

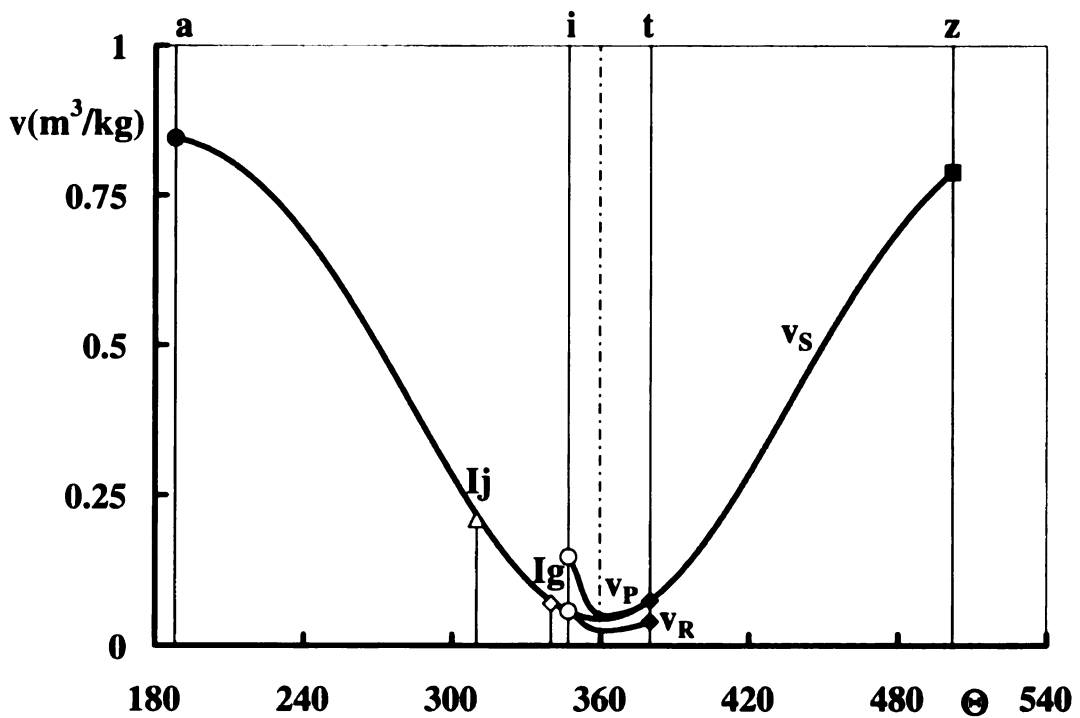


Figure 4.28: Profiles of the specific volume of reactants, products, and system of case 2

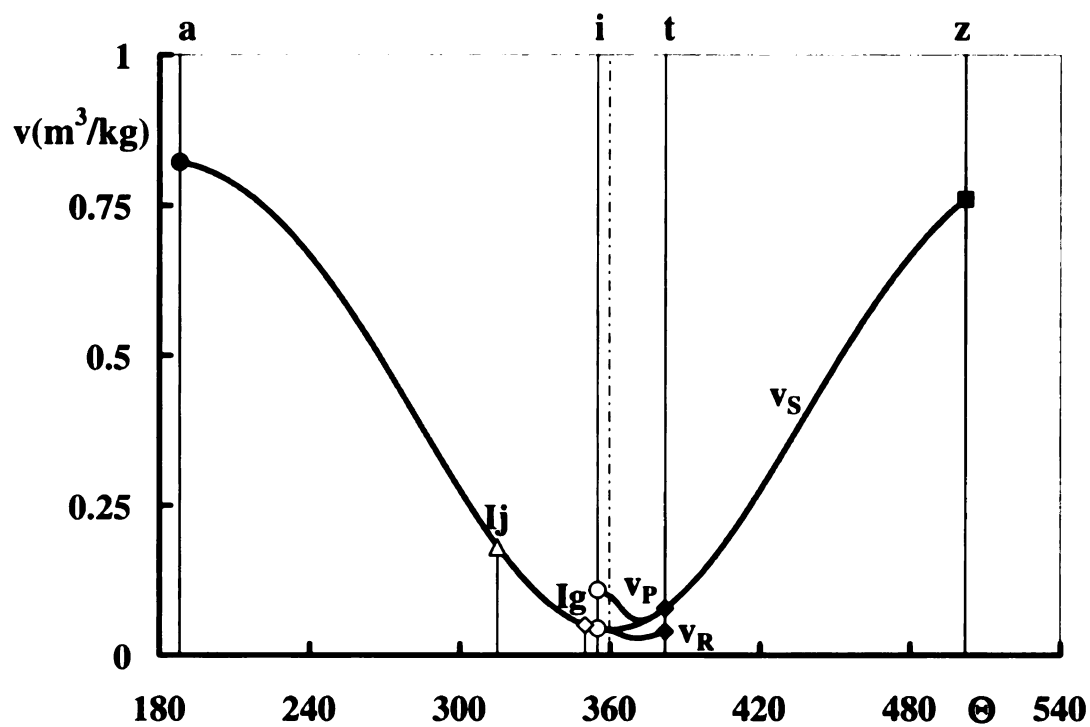


Figure 4.29: Profiles of the specific volume of reactants, products, and system of case 3

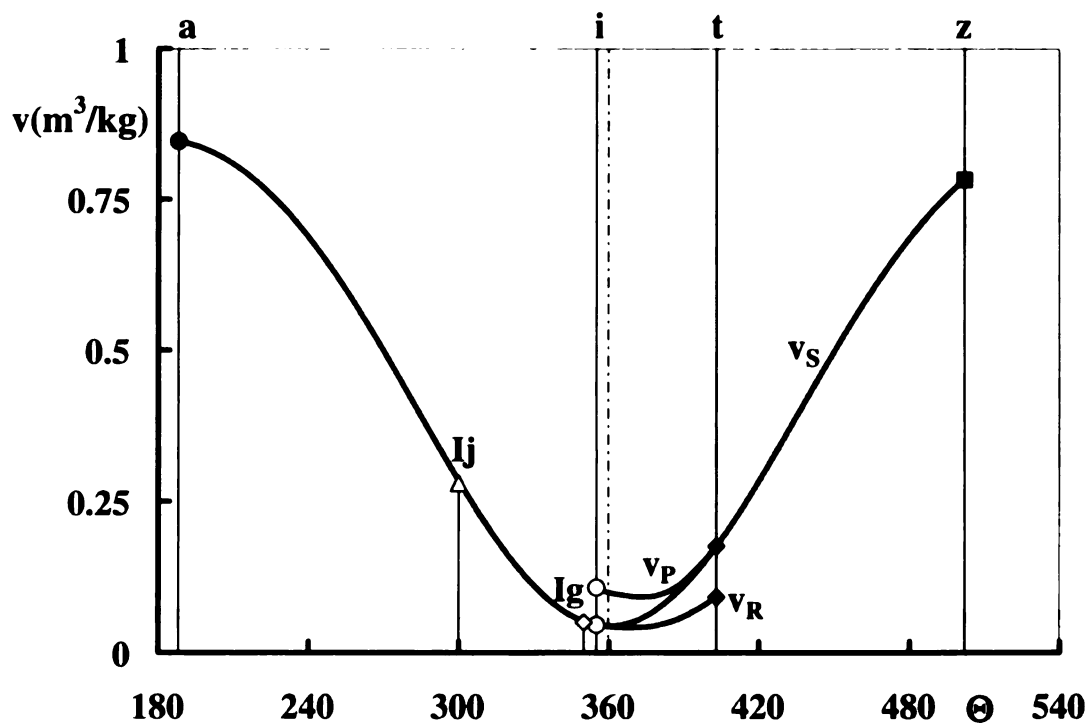


Figure 4.30: Profiles of the specific volume of reactants, products, and system of case 4

Chapter 5

Thermodynamic analysis in an IC engine

5.1 Introduction

In chapter 4, the exothermic stage of combustion is analyzed to understand the combustion process in an IC engine and the effectiveness of combustion is calculated. In the analysis, several assumptions were made in deducing the mass fraction of products and its effective components, which are shown as following:

1. The state changes of reactants and products from initial state, **i**, to terminal state, **t**, are linear as shown in Figure 4.5.
2. The heat release evaluated from the state diagram is a reasonable approximation.
3. The final state of dynamic stage of combustion, **f**, is employed to approximate the terminal state of exothermic state of combustion, **t**, for the evaluating the slope of state change of products.
4. In the state diagram, point **hp** of products falls on the straight line connecting point **i** and point **t** of products.
5. During the exothermic stage of combustion, the process of compression for the reactants is polytropic and the polytropic exponent is the same as that during

the compression process.

Because of these approximations, the mass fraction of products and its effective component may be artificial results. It is necessary to study their credibility for the well understanding of the combustion process. In this chapter, a simple thermodynamic model is proposed to calculate the cylinder pressure from the heat release function. The calculated cylinder pressure is then compared with the measured pressure and the effectiveness of analysis on the exothermic stage of combustion is studied.

5.2 Thermodynamic analysis

Thermodynamic analysis for the mixture in the cylinder has been carried out extensively [1][75][76]. By taking different assumptions for the heat addition (combustion) to the system in the cylinder, different models have been proposed. In this chapter, a model based on heat release function is present, which is proposed by Ferguson [77] and improved by the author.

A thermodynamic analysis is applied to the control volume enclosed by the dashed line shown in Figure 5.1. In this thermodynamic analysis, the mixture inside the cylinder is assumed to be the ideal gas. Then the relationship among the pressure (P), specific volume (v), and temperature (T) can be expressed by the equation of state

$$pv = RT \quad (5.1)$$

$$\ln p + \ln v = \ln R + \ln T \quad (5.2)$$

During the combustion process, the intake valve and exhaust valve are both closed, therefore the mass of the mixture, m , is constant. By assuming the gas constant R is not changing with temperature during the combustion, Equation (5.3) is obtained

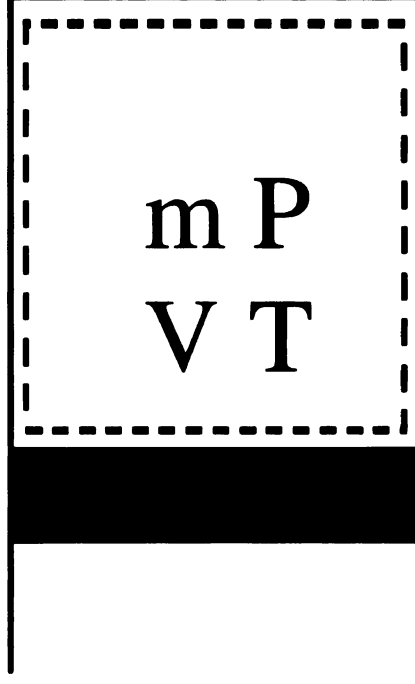


Figure 5.1: Schematic of the mixture in a cylinder of a four-stroke IC engine.

by differentiating Equation (5.2).

$$\frac{dp}{p} + \frac{dv}{v} = \frac{dT}{T} \quad (5.3)$$

According to the first law of thermodynamics, the differential form of the energy conservation in the control volume shown in Figure 5.1 can be expressed as

$$du = dq - dw \quad (5.4)$$

Since $du = c_v dT$ and $dw = p dv$, then

$$c_v dT = dq - p dv \quad (5.5)$$

It is assumed that the mixture in the cylinder is the ideal gas, then the relation-

ships among constants of ideal gas are shown in Equation (5.6) and (5.7).

$$R = c_p - c_v \quad (5.6)$$

$$\gamma = \frac{c_p}{c_v} \quad (5.7)$$

Dividing Equation (5.5) by Equation (5.1) and combining Equation (5.6) and (5.7), the first law of thermodynamics is transformed to

$$\frac{dT}{(\gamma - 1)T} = \frac{dq}{pv} - \frac{dv}{v} \quad (5.8)$$

By differentiating Equation (5.8) with respect to the crank angle degree or CAD, Θ , an ordinary differential equation (ODE) is obtained.

$$\frac{1}{(\gamma - 1)T} \frac{dT}{d\Theta} = \frac{1}{pv} \frac{dq}{d\Theta} - \frac{1}{v} \frac{dv}{d\Theta} \quad (5.9)$$

Similarly, differentiating Equation (5.3) with respect to the CAD Θ , the differential form of the equation of state is obtained.

$$\frac{1}{p} \frac{dp}{d\Theta} + \frac{1}{v} \frac{dv}{d\Theta} = \frac{1}{T} \frac{dT}{d\Theta} \quad (5.10)$$

Upon the combination of Equations (5.9) and (5.10), the change of pressure with respect to the change of the crank angle is shown as follows:

$$\frac{dp}{d\Theta} = \frac{\gamma - 1}{v} \frac{dq}{d\Theta} - \frac{\gamma p}{v} \frac{dv}{d\Theta} \quad (5.11)$$

To evaluate Equation (5.11), the heat release Q during the combustion should be known. Physically, heat release in an IC engine is a function of the CAD, i.e., $Q = Q(\Theta)$. Therefore, heat release, Q , can be expressed as $q = q_{in}x(\Theta)$ and $Q = \int_i^t q d\Theta$, where $x(\Theta)$ is the heat release function shown in Figure 5.2.

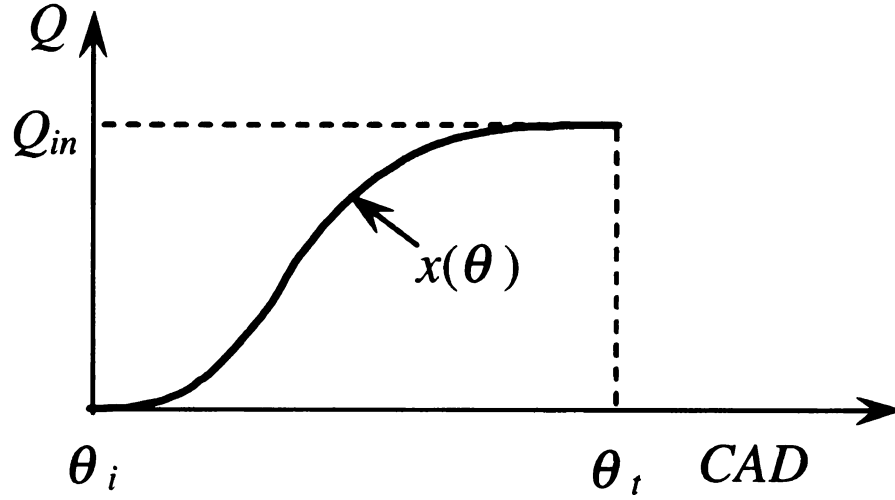


Figure 5.2: Heat release function.

Then,

$$\frac{dp}{d\Theta} = \frac{(\gamma - 1)q_{in}}{v} \frac{dx}{d\Theta} - \frac{\gamma p}{v} \frac{dv}{d\Theta} \quad (5.12)$$

It is known that at the initial state of the exothermic stage of combustion, the cylinder pressure is p_i and the cylinder volume is V_i . Then, a normalized ordinary differential equation of pressure change is

$$\frac{dP}{d\Theta} = \frac{(\gamma - 1)q_{in}}{p_i v_i V} \frac{dx}{d\Theta} - \frac{\gamma P}{V} \frac{dV}{d\Theta} \quad (5.13)$$

where $P = p/p_i$ and $V = v/v_i$. Then,

$$\frac{dP}{d\Theta} = \frac{K}{V} \frac{dx}{d\Theta} - \frac{\gamma P}{V} \frac{dV}{d\Theta} \quad (5.14)$$

where $K = (\gamma - 1)q_{in}(p_i v_i)$.

Equation (5.14) can be simplified in the form

$$\frac{dP}{d\Theta} + \alpha(\Theta)P = \beta(\Theta) \quad (5.15)$$

where $\alpha(\Theta) = (\gamma/V)dV/d\Theta$ and $\beta(\Theta) = V^{-1}Kdx/d\Theta$.

The solution to Equation (5.15) is

$$P = \left[C + \int_{\Theta_i}^{\Theta_t} \beta(\phi) \exp \left(\int^{\phi} \alpha(\omega) d\omega \right) d\phi \right] \exp \left(- \int^{\phi} \alpha(\omega) d\omega \right) \quad (5.16)$$

since

$$\int^{\phi} \alpha(\omega) d\omega = \gamma \int^{\Theta} \frac{1}{V} \frac{dV}{d\omega} d\omega = \gamma \ln V(\Theta) = \ln V(\Theta)^\gamma \quad (5.17)$$

then

$$P = \frac{C}{V^\gamma} + \frac{1}{V^\gamma} \int_{\Theta_i}^{\Theta_t} \beta(\phi) V(\phi)^\gamma d\phi \quad (5.18)$$

By imposing the boundary condition that $p = p_i$ and $v = v_i$ at the initial state of the exothermic stage of combustion, the normalized pressure is

$$P = \frac{p_i}{V_i^\gamma} + \frac{K}{V_i^\gamma} \int_{\Theta_i}^{\Theta_t} \frac{dx}{d\phi} V(\phi)^\gamma d\phi \quad (5.19)$$

The complete solution is obtained by specifying the heat release function, $x(\Theta)$. Then the integral can be numerically integrated and the cylinder pressure is obtained by

$$p = Pp_i \quad (5.20)$$

5.3 Heat release function

In Chapter 4, the mass fraction of products during the exothermic stage of combustion is introduced. At the initial state **i**, there is no product, thus the mass fraction of products $y_P = 0$. At the terminal state **t**, no more product is generated, thus the mass fraction of products $y_P = 1$. With the assumption that there is no inert components in the mixture, i.e., $Y_P = 1$, the progress parameter is equal to the mass fraction of products, $x_P(\Theta) = y_P(\Theta)$. Therefore, the initial state and terminal state of the

exothermic stage of combustion mark the start and end of the combustion respectively, and the progress parameter of the exothermic stage of combustion, x_P , is the heat release function of combustion.

By using the heat release function and the effectiveness of combustion obtained in Chapter 3, the analytical cylinder pressure can be obtained by Equations (5.19) and (5.20).

5.4 Results

The engine studied here is the same as that in Chapter 3 and Chapter 4. Engine geometry and operating conditions are shown in and Table 3.2 and Table 3.3. In studies, the engine is fuelled with methanol, and the heat release during the exothermic stage of combustion is obtained from STANJAN and shown in Table 4.2.

Shown in Figures 5.3 — 5.6 are comparisons of the measured cylinder pressure and analytical cylinder pressure obtained from the simple thermodynamic model. It is shown that the simple thermodynamic analysis gives good qualitative results. Both the measured pressure and analytical pressure in the cylinder increase after the ignition, rising to the maximum, then decreasing. Quantitatively, the relative errors of the simple thermodynamic analyses are 8.3%, 21.0%, 12.8%, and 23.7% respectively for the four cases. The errors exist because of the following:

1. Several approximations were made to obtain the mass fraction of products and some of them are rough ones.
2. In the thermodynamic analysis, it is assumed that there is no inert components in the mixture. However, because of the existence of the residual gas in the cylinder, the inert components are inevitable.
3. Leakage, blowby and friction are ignored in the thermodynamic analysis.

4. In the analysis of the exothermic stage of combustion and the thermodynamic model, the mixture in the cylinder is assumed to be perfect gas. The gas constant and specific heat are assumed constant. However, the mixture in the cylinder is high-pressure, high-temperature gas, whose composition is determined by chemical equilibrium, the gas constant and specific heat are changing with temperature.

Noting that the model used in thermodynamic analysis is simple, it is admitted that the discrepancies between the analytical and measured cylinder pressure are acceptable, though they are over 20% in case 2 and case 4. Thus, assumptions made to calculate mass fraction of products and its components are reasonable.

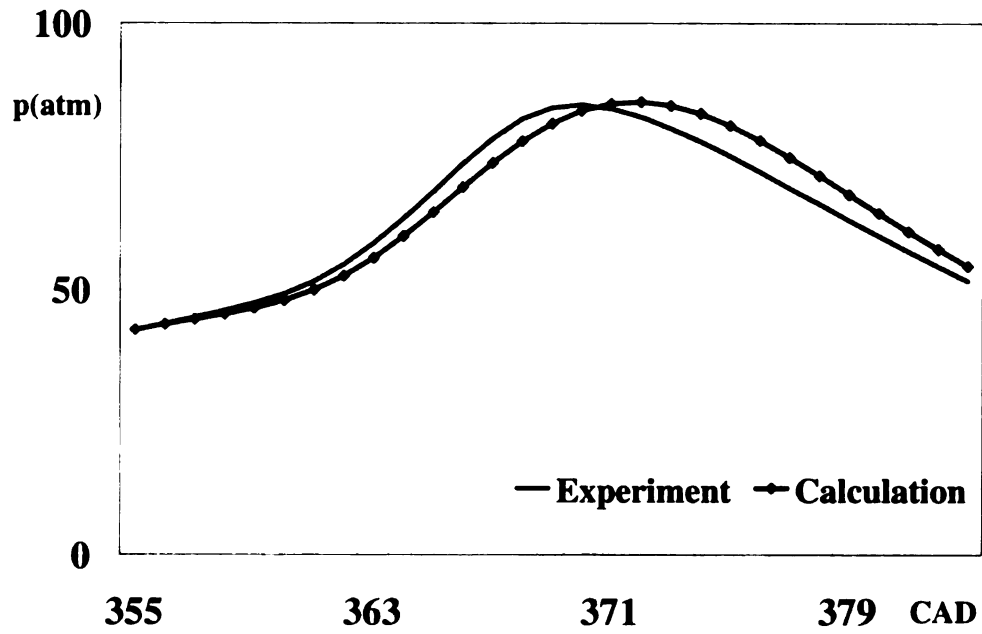


Figure 5.3: Comparison of measured cylinder pressure and analytical cylinder pressure for case 1

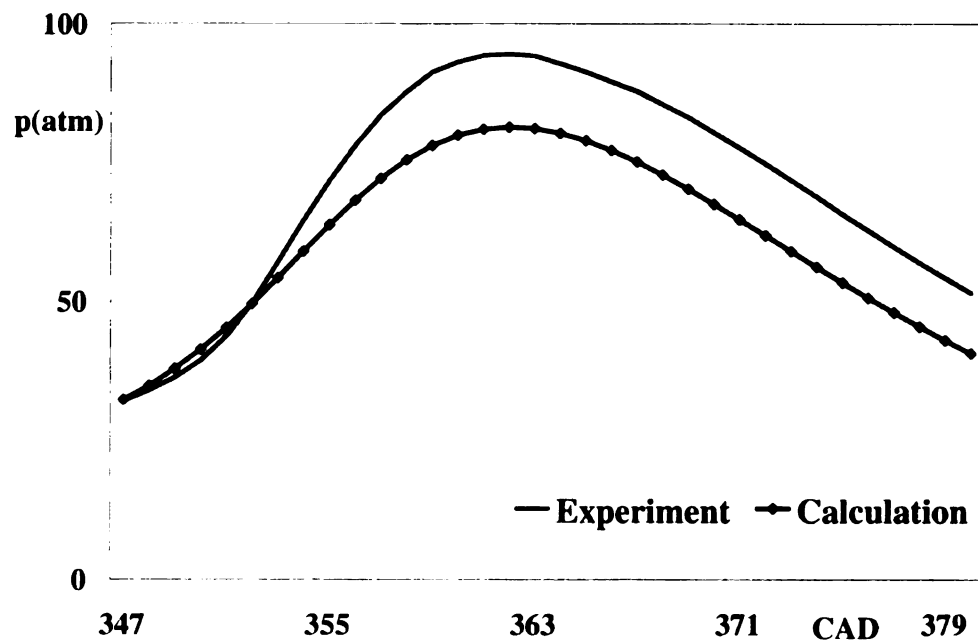


Figure 5.4: Comparison of measured cylinder pressure and analytical cylinder pressure for case 2

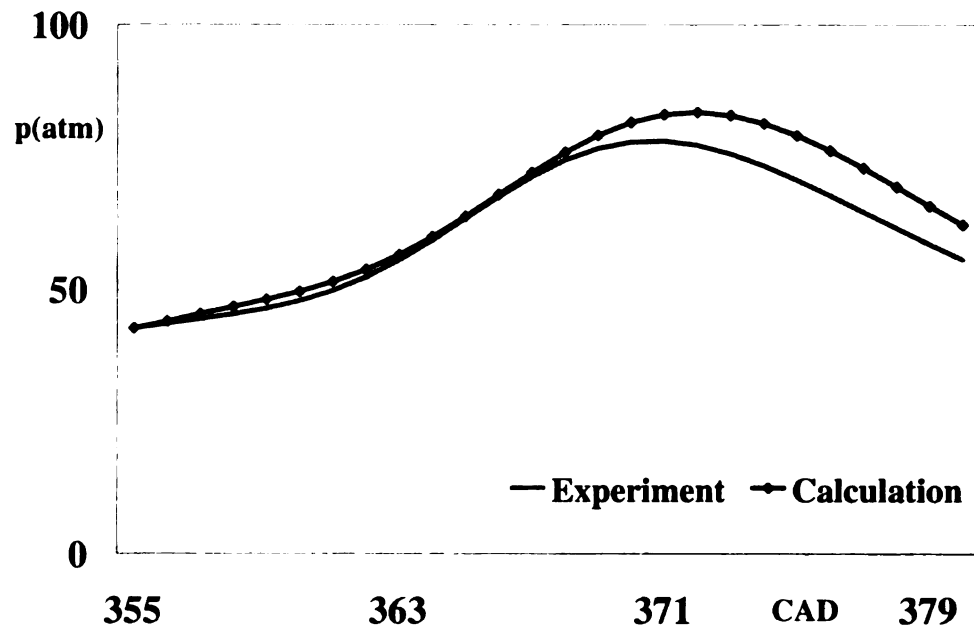


Figure 5.5: Comparison of measured cylinder pressure and analytical cylinder pressure for case 3

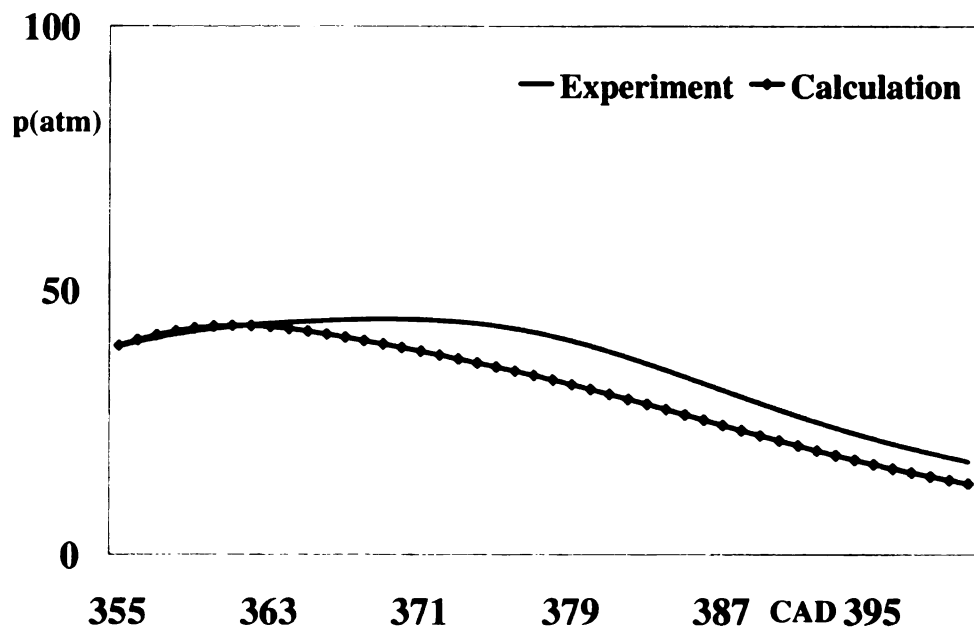


Figure 5.6: Comparison of measured cylinder pressure and analytical cylinder pressure for case 4

Chapter 6

Conclusions and recommendations

6.1 Conclusions

In this dissertation, cycle-to-cycle variations in internal combustion (IC) engines were quantified and strategies to control the cyclic variability were proposed. According to the operation sequence of a four-stroke IC engine, the studies were divided into two phases: pre-combustion phase and combustion phase.

For studies on the pre-combustion phase, a statistical method was employed to study cycle-to-cycle variations of the pre-combustion flow. By generating the probability density function of the normalized circulation of the flow on the tumble or swirl plane, the rotational motion and cycle-to-cycle variations of the flow were quantified. The influences of different port blockers on the rotational motion and cycle-to-cycle variations of the flow in a DaimlerChrysler four-stroke engine were investigated. It was determined that the rotational motion and cyclic variability of the pre-combustion flow can be controlled by changing the shape of the port blocker.

For controlling the cycle-to-cycle variations during the combustion phase, a method of pressure diagnostics for an internal combustion engine and its application to a direct injection methanol engine was presented. In an internal combustion engine, the compression and expansion are polytropic processes, between which is the combustion process. By introducing a polytropic pressure model, $\pi_k = pv^{n_k}$, the end of the polytropic compression and the beginning of polytropic expansion were identified, which

are two bounds of dynamic stage of combustion (DSC). Three boundary conditions were set for the dynamic stage of combustion and an ordinary differential equation satisfying the boundary conditions was solved to obtain an analytical life function of the dynamic stage of combustion. Since the life function is analytical and continuous, its first and second derivatives were obtained. Similar to using the speed and acceleration to control the distance, the first and second derivatives of the life function of DSC can be used to control the progress of the dynamic stage of combustion.

Controlling the progress of dynamic stage of combustion is only a method to control the combustion process, it is not a control goal. For an internal combustion engine, the stability and effectiveness of combustion are desired. To achieve this, the exothermic stage of combustion was investigated. In this study, the product of cylinder pressure and specific volume of the system in the cylinder, $w = pv$, expressing the mechanical properties of force and displacement, was adopted as a principal thermodynamic reference parameter. Together with the mechanical parameter, w , the internal energy, e , was adopted as another thermodynamic parameter to construct the state space. With STANJAN, a computational program for chemical equilibrium analysis, the state transformations of reactants and products during the exothermic stage of combustion were evaluated and two relationships between the mechanical parameter and internal energy were obtained. Combining these two relationships with the volume balance and energy balance equations, the effectiveness of combustion was calculated. Upon evaluating the effectiveness of combustion, a control strategy was reached for a controlled combustion engine, which is to maximize the effectiveness of combustion by controlling the progress of dynamic stage of combustion.

The thermodynamic analysis for the exothermic stage of combustion was extended to investigate the closed system in the cylinder, from the moment when the intake valve is closed to that when the exhaust valve is opened. By analyzing the change of internal energy and work of the system, the manner of engine operation was ther-

modynamically well understood. Upon deposition of a relatively minor amount of internal energy into the working substance by piston compression, the major amount of internal energy was acquired by the substance during the exothermic stage of combustion. And this is followed by the process of expansion, when piston work is derived entirely by expenditure of the previously acquired internal energy. Therefore, it is a two-step, laser-like, sequence of events: a short process of charging succeeded by a long process of discharging.

When using the exothermic stage of combustion to study the effectiveness of combustion, several assumptions were made to simplify the analysis. In the dissertation, a simple thermodynamic model was proposed to calculate the cylinder pressure from the heat release function. The calculated cylinder pressure was then compared with the measured pressure and it was found that the calculated cylinder pressure trace matches the measured cylinder pressure, indicating the assumptions made for pressure diagnostics are reasonable.

6.2 Recommendations

In this dissertation, the quantification and control of cycle-to-cycle variations during the pre-combustion phase and combustion phase were studied separately. It is believed that the identification of the interaction between these two phases would be of help to improve the control strategy for reducing cyclic variability of the engine.

For the study of cycle-to-cycle variations during the combustion phase, a new method of pressure diagnostics was introduced and applied to a direct injection spark ignition engine fuelled with methanol. In principle, the combustion mechanism in a spark ignition engine is quite different from that in a diesel engine or a homogeneous charge compression ignition (HCCI) engine. Thus, a study of the applicability of the new pressure diagnostics to a diesel or HCCI engine is necessary.

For the quantification of the effectiveness of combustion, thermodynamic proper-

ties of air, fuel, reactants, and products at the initial and terminal state of exothermic stage of combustion were evaluated with STANJAN. However, STANJAN is not capable of evaluating thermodynamic properties and concentrations of intermediate species during the combustion. The author believes that the evaluation of thermodynamic properties and concentrations of intermediate species will give a better understanding of the combustion process in an internal combustion engine and suggests employing CHEMKIN for this task.

APPENDIX

Appendix A

Evaluation of state transformations of reactants and products with STANJAN

A.1 Introduction

The state space has been introduced in Chapter 3. In the state space, the thermodynamic state transformations of reactants and products during the exothermic stage of combustion are well illustrated. Figure A.1 shows a general state space illustrating four thermodynamic state transformations during the exothermic state of combustion, which are i) from **i** on **R** to **i** on **P**, ii) from **i** on **R** to **t** on **R**, iii) from **t** on **R** to **t** on **P**, and iv) from **i** on **P** at p_i to **t** at p_t . Also shown in Figure A.1 are the air/fuel mixing process and three states of products under special combustion conditions.

In Figure A.1, the slopes of state change of reactants and products from the initial state **i** to the terminal state **t** of the exothermic state of combustion are important to the evaluation of the effectiveness of combustion. Therefore, the determination of thermodynamic states of reactants and products at the initial and terminal states is critical.

The combustion process is a chemical reaction during which the thermodynamic properties of reactants and products can be obtained from thermodynamic tables such as JANAF [67] or calculated by the computational program, such as STANJAN [68] and CEA [69][70]. In this analysis, STANJAN is used to evaluate the thermodynamic

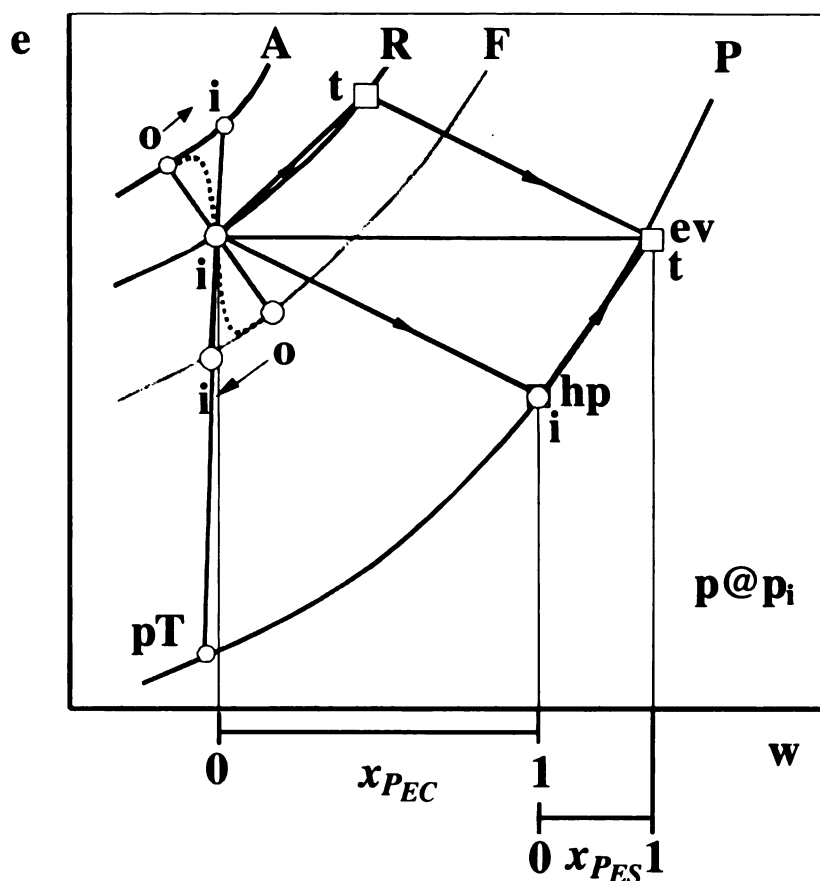


Figure A.1: Diagram of component states with an illustration of the processes of mixing and adiabatic exothermic center, EC, and exothermic system, ES.

properties of air, fuel, reactants, and products at the states of interest.

A.2 Procedure

STANJAN is a powerful and easy-to-use program for analysis of chemical equilibrium in single- or multi-phase systems based on the method of element potentials and JANAF tables [78]. To evaluate thermodynamic properties of the system with STANJAN, two thermodynamic parameters of the system are required. In this analysis, two sets of thermodynamic parameters are used:

1. temperature and pressure;

2. enthalpy and pressure same as last run.

Two stages of combustion, sharing the same initial state, were defined in Chapter 3 and 4, respectively. The dynamic stage of combustion (DSC) starts from the initial state and ends at the final state, which is the maximum of the polytropic pressure model. The exothermic stage of combustion (ESC) starts from the initial state and ends at the terminal state, which is the maximum of effectiveness of combustion.

The determination of terminal state of ESC requires prior knowledge of the thermodynamic properties of reactants/products at the terminal state of ESC. However, the evaluation of thermodynamic properties at the terminal state of ESC cannot be implemented without determining the terminal state of ESC. According to studies [79][80], the terminal state of ESC is located after the final state of DSC, but they are close to each other. Therefore, the final state of DSC can be utilized to approximate the terminal state of ESC. After employing thermodynamic properties of reactants/products at final state of DSC to determine the location of the terminal state of ESC, the thermodynamic properties of reactants/products at the terminal state of ESC were evaluated. By comparing thermodynamic properties of reactants/products at the final state of DSC to those at the terminal state of ESC, it was concluded that the final state of DSC is a good approximation to the terminal state of ESC when evaluating thermodynamic properties.

The flowchart of evaluating thermodynamic states of reactants and products is shown in Figure A.2. By assuming that the mixture in the cylinder the ideal gas, the temperature of reactants and products can be calculated from the ideal gas equation. At the initial state of ESC, the temperature of the system, which contains only reactants, can be calculated with knowledge of inlet temperature. Then the thermodynamic state of reactants at initial state of ESC can be obtained from STANJAN by inputting the temperature and pressure of reactants.

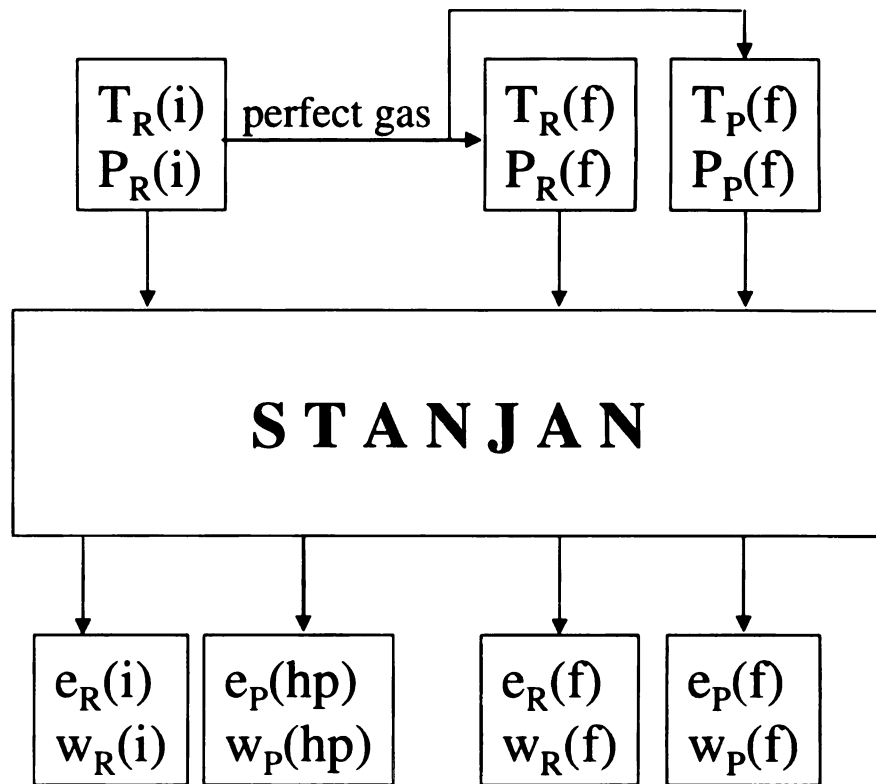


Figure A.2: Flowchart of evaluating thermodynamic states of reactants and products during the exothermic stage of combustion.

As previously discussed in Chapters 3 and 4, it is impossible to obtain the temperature of products from the ideal gas equation, since the initial state of ESC is a singular point. However, it is reasonable to assume that the combustion process at the initial state of ESC is under constant enthalpy and pressure conditions. Thus, the thermodynamic state of products at initial state of ESC can be obtained from STANJAN by specifying that the enthalpy and pressure of products are the same as those of reactants at the initial state of ESC.

After evaluating the temperatures of reactants and products at the final state of DSC with Equations (4.43) and (4.47) respectively, the thermodynamic states of reactants and products at final state of DSC can be obtained from STANJAN by inputting the temperature and pressure of reactants and products.

Steps for evaluating thermodynamic properties of reactants and products with STANJAN are following. Figures illustrating the evaluation of thermodynamic properties of reactants/products in the methanol engine described in Chapters 3 and 4 are shown with each step.

1. Specify the data file including reactants and products species (Figures A.3 and A.4);
2. Enter the mole number of each species in the reactants (Figure A.5);
3. Enter the temperature and pressure of reactants at the initial state of ESC and obtain the thermodynamic properties at this state (Figures A.6 and A.7);
4. Enter the temperature and pressure of reactants at the final state of ESC and obtain the thermodynamic properties at this state (Figures A.8 and A.9);
5. Change to the products analysis and choose all the species in the data file as the components of products (Figure A.10);
6. Enter the pressure and enthalpy of products at the initial state of DSC, which are the same as those of reactants at the initial state of DSC respectively, and obtain the thermodynamic properties of products at this state (Figures A.11 and A.12);
7. Enter the temperature and pressure of products at the final state of DSC and obtain the thermodynamic properties at this state (Figures A.13 and A.14);
8. Return to step 2 to evaluate thermodynamic properties of reactants/products of another case or quit STANJAN (Figure A.15).

```
STANJAN
(c) Stanford University 1981, 1984, 1985, 1986, 1987

Finds the equilibrium state for a system consisting of one or more phases.
The gas phase is treated as a mixture of ideal gases, and condensed phases
are treated as ideal solutions. Specific heats are temperature-dependent.
Also handles constrained equilibrium or frozen composition.

You should be able to run STANJAN by responding to the prompts. Try it!

For more information or for help with difficult cases call the program author:

    Prof. Wm. C. Reynolds
    Department of Mechanical Engineering
    Stanford University
    Stanford, CA 94305-3030 (415)-723-3840

Do you want to be instructed? n

(return) may be used for "no"

Select a species data file or (return) if no file is desired.
Species data file? COMBMETH.SUD
```

Figure A.3: Step 1a — Specify the data file

```
STANJAN
Species data file? COMBMETH.SUD

Getting species data file COMBMETH.SUD                PLEASE WAIT!
C(S)
CH3OH
CH4
CO
CO2
C12H26
C3H8
H
H2O
H2
H2O
H2O(L)
N
NC3H18
NO
NO2
N2
O
O2

Is this the file you wanted? y
```

Figure A.4: Step 1b — The species in the data file COMB.SUD



Figure A.5: Step 2 — Specify the mole number of each species in the reactants



Figure A.6: Step 3a — Specify the temperature and pressure of reactants at the initial state of DSC

```

Select STANJAN

species      mol fraction   mol fraction   mass fraction   mols*
              in the phase   in mixture
phase 1: molal mass = 29.123 kg/kmol T = 649.30 K
CH3OH        .85397E-01    .85397E-01    .93956E-01    1.00000E+00
O2           .19214E+00    .19214E+00    .21112E+00    2.25000E+00
N2           .72246E+00    .72246E+00    .69493E+00    8.46000E+00

Calculations made using frozen composition.

* Species mols for the atom populations in mols.

Mixture properties: molal mass = 29.123 kg/kmol
P = 4.2860E+06 Pa    V = 4.3249E-02 m**3/kg
U = -.3914E+06 J/kg    H = -.2061E+06 J/kg    S = .6802E+04 J/kg-K
WARNING! The thermochemical data for CH3OH are extrapolated above 500 K.

Made 0 (T,P) iterations; 0 equilibrium iterations; v 3.84 IBM-PC

On IBM-PC, use <ctrl-PrtSc> to stop printer (optional).

```

Figure A.7: Step 3b — Thermodynamic properties of reactants at the initial state of DSC

```

Select STANJAN

Do you want to CHANGE the SETUP?

Want to mix reactants from last run?

Enter P (atm): 66.0
Enter T (K): 724.8

The sound speed can be calculated, but then the calculations take longer.

Do you want the SOUND SPEED?

Do you want to SAVE the run OUTPUT in a file?

Do you want to MONITOR the run (probably not)?

Working; PLEASE WAIT!

OUTPUT READY

Use ctrl-s to stop/start the screen display.

Do you want to see the JANNAF data used?

```

Figure A.8: Step 4a — Specify the temperature and pressure of reactants at the final state of DSC

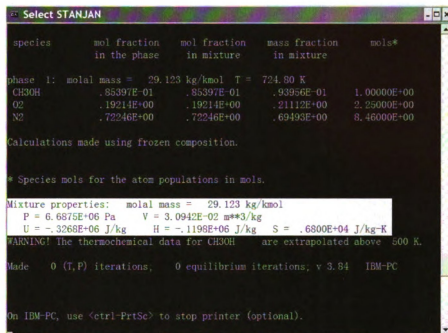


Figure A.9: Step 4b — Thermodynamic properties of reactants at the final state of DSC

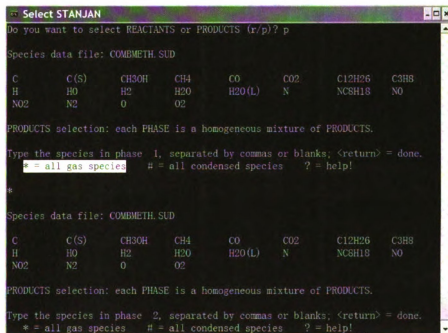


Figure A.10: Step 5 — Specify the species of products

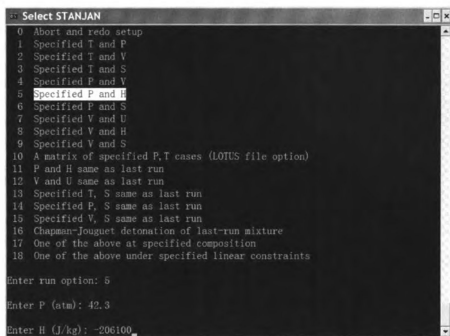


Figure A.11: Step 6a — Specify the pressure and enthalpy of products at the initial state of DSC



Figure A.12: Step 6b — Thermodynamic properties of products at the initial state of DSC

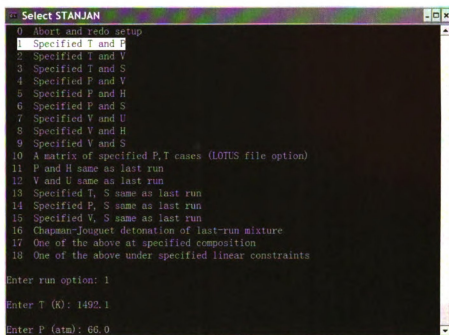


Figure A.13: Step 7a — Specify the temperature and pressure of products at the final state of DSC

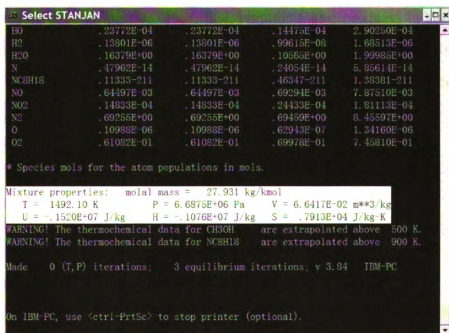


Figure A.14: Step 7b — Thermodynamic properties of products at the final state of DSC



Figure A.15: Step 8 — Quit STANJAN

A.3 Results

The thermodynamic properties of air, fuel, reactants, and products in the methanol engine under 4 operating conditions listed in Table 3.3 are shown in Tables A.1 — A.2. The state transformations of air, fuel, reactants, and products during the ESC are shown in Figures A.16 — A.19.

Table A.1: Thermodynamic properties of air, fuel, reactants, and products in case 1

	States	p(atm)	T(K)	v(m ³ /kg)	u(kJ/g)	h(kJ/g)	w(kJ/g)	M(g/mol)
A	a	1.1	300.0	0.80495	-0.0846	0.0019	0.0865	28.581
	i	42.3	649.3	0.043657	0.1761	0.3630	0.1869	
	f	66.0	724.8	0.031234	0.2359	0.4448	0.2089	
	t	51.5	681.8	0.037653	0.2017	0.3982	0.1965	
F	a	1.1	300.0	0.72478	-6.3580	-6.2800	0.0780	32.042
	i	42.3	649.3	0.039309	-5.8650	-5.6960	0.1690	
	f	66.0	724.8	0.028123	-5.7530	-5.5650	0.1880	
	t	51.5	681.8	0.033903	-5.8160	-5.6400	0.1760	
R	a	1.1	300.0	0.79742	-0.6740	-0.5883	0.0857	29.123
	i	42.3	649.3	0.043249	-0.3914	-0.2061	0.1853	
	f	66.0	724.8	0.030942	-0.3268	-0.1198	0.2070	
	t	51.5	681.8	0.037301	-0.3637	-0.1691	0.1946	
P	hp=i	42.3	2084.9	0.14486	-0.8270	-0.2061	0.6209	27.92
	f	66.0	1492.1	0.066415	-1.5200	-1.0760	0.4440	27.931
	t	51.5	1383.2	0.078907	-1.6390	-1.2270	0.4120	

Table A.2: Thermodynamic properties of air, fuel, reactants, and products in case 2

	States	p(atm)	T(K)	v(m ³ /kg)	u(kJ/g)	h(kJ/g)	w(kJ/g)	M(g/mol)
A	a	1	300.0	0.85325	-0.0846	0.0019	0.0865	28.581
	i	31.9	648.7	0.057837	0.1757	0.3626	0.1869	
	f	91.2	827.0	0.025791	0.3189	0.55728	0.2383	
	t	51.4	724.3	0.04008	0.2355	0.4442	0.2087	
F	a	1	300.0	0.76826	-6.3580	-6.2800	0.0780	32.042
	i	31.9	648.7	0.05208	-5.8660	-5.6970	0.1690	
	f	91.2	827.0	0.02322	-5.6010	-5.3870	0.2140	
	t	51.4	724.3	0.03609	-5.7530	-5.5660	0.1870	
R	a	1	300.0	0.84526	-0.6740	-0.5883	0.0857	29.123
	i	31.9	648.7	0.057296	-0.3919	-0.2067	0.1852	
	f	91.2	827.0	0.025549	-0.2373	-0.0012	0.2361	
	t	51.4	724.3	0.039703	-0.3272	-0.1204	0.2068	
P	hp=i	31.9	2084.0	0.19201	-0.8273	-0.2067	0.6206	27.919
	f	91.2	1628.4	0.052457	-1.3680	-0.8829	0.4851	27.931
	t	51.4	1308.0	0.07476	-1.7200	-1.3300	0.3900	

Table A.3: Thermodynamic properties of air, fuel, reactants, and products in case 3

	States	p(atm)	T(K)	v(m ³ /kg)	u(kJ/g)	h(kJ/g)	w(kJ/g)	M(g/mol)
A	a	1	300.0	0.85325	-0.0846	0.0019	0.0865	28.581
	i	42.6	673.0	0.044932	0.1948	0.3887	0.1939	
	f	58.6	728.1	0.035338	0.2386	0.4484	0.2098	
	t	50.2	700.8	0.039705	0.2168	0.4187	0.2019	
F	a	1	300.0	0.76826	-6.3580	-6.2800	0.0780	32.042
	i	42.6	673.0	0.040457	-5.8300	-5.6550	0.1750	
	f	58.6	728.1	0.031819	-5.7480	-5.5590	0.1890	
	t	50.2	700.8	0.03575	-5.7880	-5.6060	0.1820	
R	a	1	300.0	0.82166	-0.5966	-0.5109	0.0857	29.087
	i	42.6	673.0	0.044567	-0.2970	-0.1046	0.1924	
	f	58.6	728.1	0.035051	-0.2501	-0.0420	0.2081	
	t	50.2	700.8	0.039382	-0.2734	-0.0731	0.2003	
P	hp=i	42.6	1949.7	0.13392	-0.6826	-0.1046	0.5870	28.043
	f	58.6	1400.6	0.069925	-1.2990	-0.8440	0.4150	28.048
	t	50.2	1340.0	0.078091	-1.3640	-0.9663	0.3977	

Table A.4: Thermodynamic properties of air, fuel, reactants, and products in case 4

	States	p(atm)	T(K)	v(m ³ /kg)	u(kJ/g)	h(kJ/g)	w(kJ/g)	M(g/mol)
A	a	1	300.0	0.85325	-0.0846	0.0019	0.0865	28.581
	i	39.3	638.9	0.046237	0.1680	0.3521	0.1841	
	f	21.8	548.0	0.071495	0.0982	0.2561	0.1579	
	t	15.4	500.9	0.092509	0.0628	0.2071	0.1443	
F	a	1	300.0	0.76826	-6.3580	-6.2800	0.0780	32.042
	i	39.3	638.9	0.041632	-5.8800	-5.7140	0.1660	
	f	21.8	548.0	0.064374	-6.0150	-5.8730	0.1420	
	t	15.4	500.9	0.083295	-6.0850	-5.9550	0.1300	
R	a	1	300.0	0.84631	-0.5966	-0.5109	0.0857	29.087
	i	39.3	638.9	0.045861	-0.3257	-0.1431	0.1826	
	f	21.8	548.0	0.070914	-0.4008	-0.2442	0.1566	
	t	15.4	500.9	0.091757	-0.4390	-0.2958	0.1432	
P	hp=i	39.3	1923.6	0.14322	-0.7134	-0.1431	0.5703	28.044
	f	21.8	1017.3	0.136524	-1.6920	-1.3900	0.3020	28.048
	t	15.4	925.1	0.175737	-1.7810	-1.5070	0.2740	

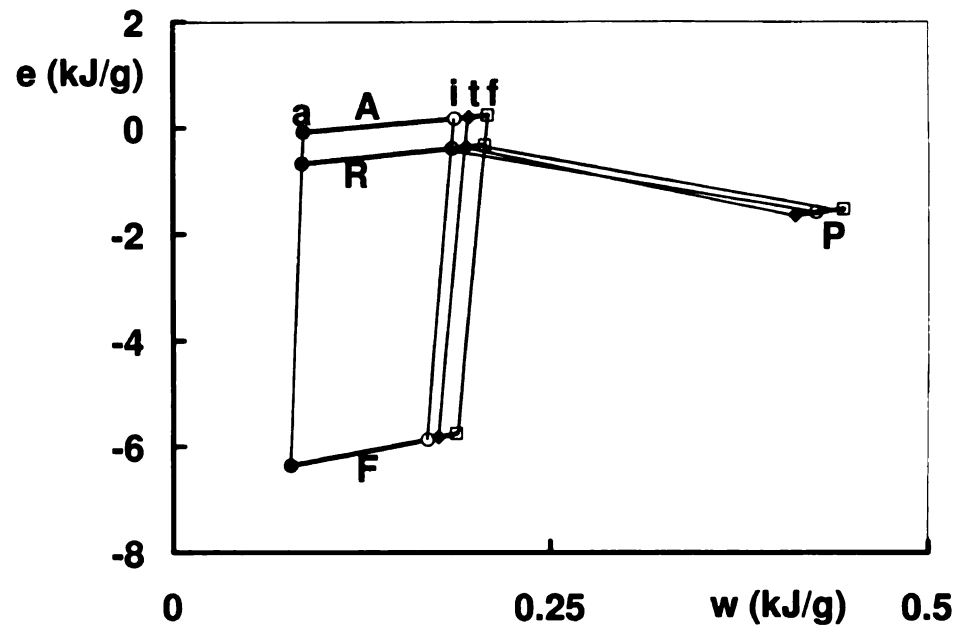


Figure A.16: State transformations of air, fuel, reactants, and products in case 1

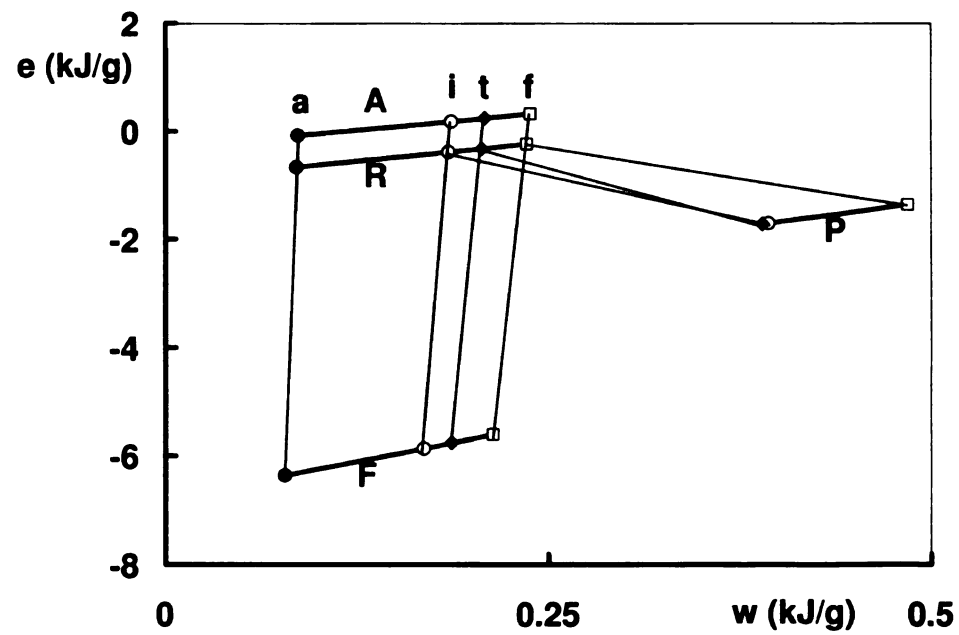


Figure A.17: State transformations of air, fuel, reactants, and products in case 2

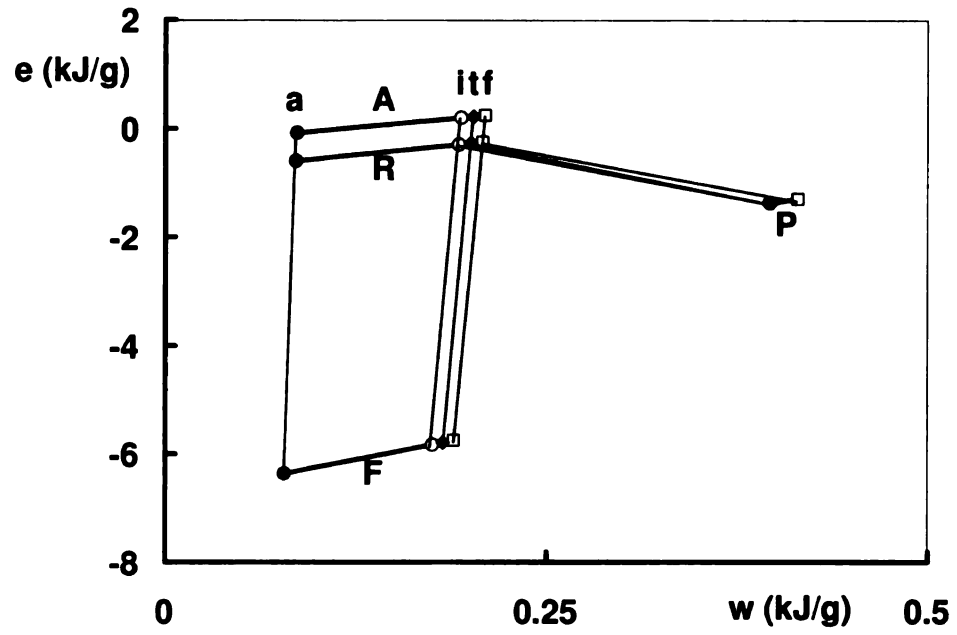


Figure A.18: State transformations of air, fuel, reactants, and products in case 3

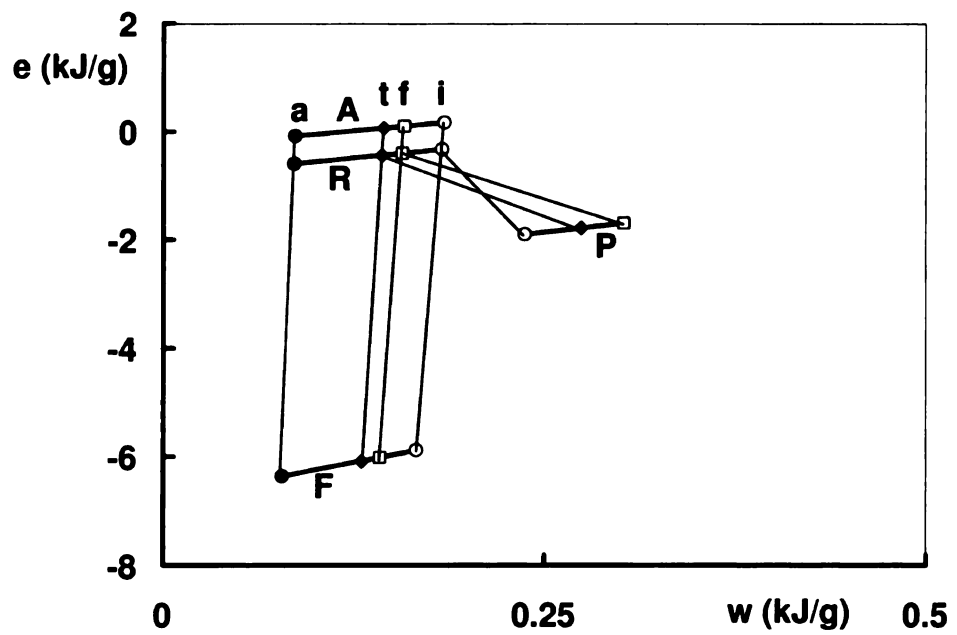


Figure A.19: State transformations of air, fuel, reactants, and products in case 4

BIBLIOGRAPHY

Bibliography

- [1] Heywood, J.B., *Internal Combustion Engine Fundamentals*, McGraw-Hill Publishing Company, 1988.
- [2] Stone, R., *Introduction to Internal Combustion Engines*, SAE International, 2000.
- [3] Dai, W., Trigui, N., and Lu, Y., "Modeling of Cyclic Variations in Spark-Ignition Engines," SAE Paper 2000-01-2036, 2000.
- [4] Letellier, C., Meunier-Guttin-Cluzel, S., et. al., "Use of the Nonlinear Dynamical System Theory to Study Cycle-to-Cycle Variations from Spark Ignition Engine Pressure Data," SAE Paper 971640.
- [5] Ozdor, N., Dulger, M., and Sher, E., "An Experimental Study of the Cyclic Variability in Spark Ignition Engines," SAE Paper 960611, 1996.
- [6] Koochesfahani, M.M., "Molecular Tagging Velocimetry (MTV): Progress and Applications," AIAA Paper AIAA-99-3786, 1999.
- [7] Stier, B. and Koochesfahani, M.M., "Molecular Tagging Velocimetry (MTV) Measurements in Gas Phase Flows," *Experiments in Fluids*, Vol. 26, pp. 297–304, 1999.
- [8] Gendrich, C.P. and Koochesfahani, M.M., "A Spatial Correlation Technique for Estimating Velocity Fields Using Molecular Tagging Velocimetry (MTV)," Vol. 22, pp. 67–77, 1996.
- [9] Trigui, N., Kent, J.C., et al., "Characterization of Intake Generated Fluid Flow Fields in IC Engines Using 3-D Particle Tracking Velocimetry (3-D PTV)," SAE Paper 940279, 1994.
- [10] Choi, W.C. and Guezennec, Y.G., "Measurement of Cycle-to-Cycle Variations and Cycle-Resolved Turbulence in an IC Engine Using a 3-D Particle Tracking Velocimetry," *JSME International Journal, Series B*, Vol. 41, No. 4, pp. 991–1003, 1998, 1998.
- [11] Reuss, D.L., "Cyclic Variability of Large-Scale Turbulent Structures in Directed and Undirected IC Engine Flows," SAE Technical Paper 2000-01-0246, 2000.

- [12] Khalighi, B., "Study of the Intake Tumble Motion by Flow Visualization and Particle Tracking Velocimetry," *Experiments in Fluids*, Vol. 10, pp. 230–236, 1991.
- [13] Zhang, L., Ueda, T., et al., "Cycle-to-Cycle Variation of In-Cylinder Flow in a Motored Engine," *JSME International Journal, Series B*, Vol. 38, No. 3, pp. 426–431, 1995.
- [14] Hascher, H.G., Novak, M., et al., "The 3-D In-Cylinder Charge Motion of a Four-Valve SI Engine under Stroke, Speed, and Load Variation," SAE Technical Paper 2000-01-2789, 2000.
- [15] Lee, K., Yoo, S.C., et al., "An Experimental Study of In-Cylinder Air Flow in a 3.5L Four Valve SI Engine by High Speed Flow Visualization and Two-Component LDV Measurement," SAE Technical Paper 930478, 1993.
- [16] Urushihara, T., Murayama, T, et al., "Turbulence and Cycle-by-cycle Variations of Mean Velocity Generated by Swirl and Tumble Flow and Their Effects on Combustion," SAE paper 950813, 1995.
- [17] Schock, H., Shen, Y., et. al., "The Measurement and Control of Cyclic Variations of Flow in a Piston Cylinder Assembly," SAE Technical Paper 2003-01-1357, 2003.
- [18] Tomonori, U., Taichi, M., et al., "Turbulence and Cycle-by-Cycle Variation of Mean Velocity Generated by Swirl and Tumble Flow and Their Effects on Combustion," SAE Technical Paper 950813, 1995.
- [19] Jaffri, K., Hascher, H.G., et al., "Tumble and Swirl Quantification within a Motored Four-Valve SI Engine Cylinder Based on 3-D LDV Measurements," SAE Technical Paper 970792, 1997.
- [20] Floch, A., Frank, J.V, and Ahmed, A., "Comparison of the Effects of Intake-Generated Swirl and Tumble on Turbulence Characteristics in a 4-Valve Engine," SAE Technical Paper 952457, 1995.
- [21] Munson, B.R., Young, D.F., and Okiishi, T.H., *Fundamentals of Fluid Mechanics*, John Wiley & Sons, Inc., 1998.
- [22] Daw, C.S. and Kahl, W.K., "Interpretation of Engine Cycle-to-cycle Variation by Chaotic Time Series Analysis," SAE Technical Paper 902103, 1990.
- [23] Ludwig, C., Leonhardt, S., et al., "Measurement and Monitoring of Pressure Curves in Diesel Engines," *Proceedings of the American Control Conference*, San Francisco, California, June 1993.
- [24] Roberts, J.B., Peyton Jones, J.C., and Landsborough, K.J., "Cylinder Pressure Variations as a Stochastic Process," SAE Technical Paper 970059, 1997.

- [25] Rassweiler, G.M. and Withrow, L., "Motion Pictures of Engine Flames Correlated with Pressure Cards," SAE Technical Paper 800131, 1980.
- [26] Homsy, S.C. and Atreya, A., "An Experimental Heat Release Rate Analysis of a Diesel Engine Operating Under Steady State Conditions," SAE Technical Paper 970889, 1997.
- [27] Brunt, M.F.J., Rai, H., and Emtage, A.L., "The Calculation of Heat Release Energy from Engine Cylinder Pressure Data," SAE Technical Paper 981052, 1998.
- [28] Urushihara, T., Murayama, T, et al., "Turbulence and Cycle-by-cycle Variations of Mean Velocity Generated by Swirl and Tumble Flow and Their Effects on Combustion," SAE paper 950813, 1995.
- [29] Johansson, B. and Olsson, K., "Combustion Chambers for Natural Gas SI Engines Part I: Fluid Flow and Combustion," SAE Technical Paper 950469, 1995.
- [30] Stevens, S.P., Shayler, P.J., and Ma, T.H., "The Impact of Combustion Phasing on Cycle-by-cycle Performance of a Spark Ignition Engine," SAE Technical Paper 950687, 1995.
- [31] Young, M.B., "Cyclic Dispersion in the Homogeneous-Charge Spark-Ignition Engine — A Literature Survey," SAE Technical Paper 810020, 1980.
- [32] Hill, P.G. and Kapil, A., "The Relationship between Cyclic Variations in Spark-Ignition Engines and the Small Structure of Turbulence," *Combustion and Flame*, Vol. 78, pp. 237–247, 1989.
- [33] Foakes, A.P. and Pollard, D.G., "Investigation of a Chaotic Mechanism for Cycle-to-cycle Variations," *Combustion Science and Technology*, Vol. 90, pp. 281–287, 1993.
- [34] Kantor, J.C., "A Dynamical Instability of Spark-Ignited Engines," *Science*, Vol. 224, pp. 1233–1235, 1984.
- [35] Russ, S., Peet, G., and Stockhausen, W., "Measurements of the Effect of In-Cylinder Motion on Flame Development and Cycle-to-Cycle Variations Using an Ionization Probe Head Gasket," SAE Technical Paper 970507, 1997.
- [36] Ohsuga, M., Yamaguchi, J., et al., "In-Cylinder Air Fuel Ratio and Combustion Control for Spark Ignition Engines," SAE Technical Paper 950076, 1995.
- [37] Johansson, B., Neij, H., et al., "Investigations of the Influence of Mixture Preparation on Cyclic Variations in a SI-Engine, Using Laser Induced Fluorescence," SAE Technical Paper 950108, 1995.
- [38] Daily, J.W., "Cycle-to-Cycle Variations: A Chaotic Process?" *Combustion Science and Technology*, Vol. 57, pp. 149–162, 1988.

- [39] Docquier, N. and Candel, S., "Combustion Control and Sensors: a Review," *Progress in Energy and Combustion Science*, Vol. 28, pp. 107-150, 2002.
- [40] Najt, P.M. and Foster, D.E., "Compression-Ignited Homogeneous Charge Combustion," SAE Technical Paper 830264, 1983.
- [41] Flynn, P., Hunter, G., et al. "Premixed Charge Compression Ignition Engine with Optimal Combustion Control," US Patent 6276334 B1.
- [42] Kamei, E., Namba, H., et al., "Application of Reduced Order Model to Automotive Engine Control System," *Journal of Dynamic Systems, Measurement, and Control, Transaction of the ASME*, Vol. 109, pp. 232-237, 1987.
- [43] Wolanski, P. and Oppenheim, A.K., "Controlled Combustion Engines (CCE)," SAE Technical Paper 1999-01-0324, 1999.
- [44] Oppenheim, A.K., "Prospects for Combustion in Piston Engines," SAE Technical Paper 2002-01-0999, 2002.
- [45] Neumeier, Y. and Zinn, B.T., "Active Control of Combustion Instabilities with Real Time Observation of Unstable Combustor Modes," AIAA-96-0758, *34th Aerospace Sciences Meeting & Exhibit*, Reno, NV, 1996.
- [46] Gavillet, G.G., Maxson, J.A. and Oppenheim, A.K., "Thermodynamic and Thermochemical Aspects of Combustion in Premixed Charge Engines Revisited," SAE Technical Paper 930432, 1993.
- [47] Maxson, J.A., Hensinger, D. M., Hom, K., and Oppenheim, A. K., "Performance of Multiple Stream Pulsed Jet Combustion Systems," SAE Technical Paper 910565, 1991.
- [48] Maxson, J.A. and Oppenheim, A. K., "Pulsed Jet Combustion — Key to a Refinement of the Stratified Charge Concept," *Twenty-Third Symposium (International) on Combustion*, Pittsburgh, The Combustion Institute, pp. 1041-1046, 1991.
- [49] Oppenheim, A.K., "The Knock Syndrome — Its Cures and Its Victims," SAE Technical Paper 841339, 1984.
- [50] Oppenheim, A.K., "The Beauty of Combustion Fields and Their Aero-Thermodynamic Significance," *Dynamics of Reactive Systems Part 1: Flames, Progress in Astronautics and Aerodynamics*, Washington D.C., AIAA pp.251-265, 1985.
- [51] Oppenheim, A.K., "Quest for Controlled Combustion Engines," *SAE Transactions, The Journal of Engines*, Vol. 97(6), pp.1033-1039, 1988.
- [52] Oppenheim, A.K., "Life on Earth at the Point of Inflection & The Future of Combustion in Engines," *Proceedings of the Institution of Mechanical Engineers*, C448/076 & 022, ImechE, pp. 215- 220 & 187-192, 1992.

- [53] Oppenheim, A.K., "Aerodynamic Control of Combustion," *Journal of Fluids Engineering*, Vol. 115(4), pp. 561–567, 1993.
- [54] Oppenheim, A.K., "Turbulent Combustion in Contrast to Flames," *Modern Developments in Energy, Combustion and Spectroscopy*, Oxford, Pergamon Press, pp. 1–13, 1993.
- [55] Oppenheim, A.K. and Maxson, J.A., "Thermodynamics of Combustion in an Enclosure," *Progress in Astronautics and Aeronautics*, American Institute of Aeronautics and Astronautics, New York, pp. 365–382, 1991.
- [56] Oppenheim, A.K. and Maxson, J.A., "A Thermochemical Phase Space for Combustion in Engines," *Twenty-Fifth Symposium (International) on Combustion*, The Combustion Institute, Pittsburgh, Pennsylvania, pp. 157–165, 1994.
- [57] Oppenheim, A.K., Barton, J.E., Kuhl, A.L. and Johnson, W.P., "Refinement of Heat Release Analysis," SAE Technical Paper 970538, 1997.
- [58] Oppenheim, A. K., Beltramo, J. et al., "Combustion by Pulsed Jet Plumes—Key to Controlled Combustion Engines," *SAE Transactions, The Journal of Engines*, Vol. 98, pp. 175–182, 1989.
- [59] Oppenheim A.K., Kuhl A.L., et al., "Model and Control of Heat Release in Engines," *Engine Combustion and Flow Diagnostics*, SP-1157, SAE Technical Paper 960601, pp. 15–23, 1996.
- [60] Oppenheim, A.K., Maxson, J.A., et al., "Fireball Mode of Combustion and Its Adaptive Control," *Twenty-Sixth International Symposium on Automotive Technology and Automation*, Aachen, Germany, 1993.
- [61] Oppenheim, A.K., Maxson, J.A., and Shahed S.M., "Can the Maximization of Fuel Economy be Compatible with the Minimization of Pollutant Emissions?" SAE Technical Paper 940479, 1994.
- [62] Gutowski, J.A., Balles, E.N. et al., "Heat Release Analysis of Engine Pressure Data," SAE Technical Paper 841359, 1984.
- [63] Heywood, J.B., Higgins, J.M., et al. "Development and Use of a Cycle Simulation to Predict SI Engine Efficiency and NO_x Emissions," SAE Technical Paper 790291, 1979.
- [64] Benson, R.A., *The Thermodynamics and Gas Dynamics of Internal-Combustion Engines*, Vol. 1, Clarendon Press, Oxford, 1962.
- [65] George, R.S., Schock, H.J., et al. "Design of a High Compression Direct Injection Spark-Ignition Methanol Fuelled Research Engine with an Integral Injector Ignition Source Insert," SAE Technical Paper 2001-01-3651, 2001.
- [66] Gibbs, J.W., "On the Equilibrium of Heterogeneous Substances," *Transactions of the Connecticut Academy*, III 1875-76: pp. 108-248.

- [67] Stull, D.R. and Prophet H. "JANAF Thermochemical Tables," National Bureau of Standards (currently NIST for National Institute of Standards and Technology), U.S. Department of Commerce, Report NSRDS-NBS 37, 1971.
- [68] Reynolds, W.C., "STANJAN Interactive Computer Programs for Chemical Equilibrium Analysis", Department of Mechanical Engineering, Stanford University, Stanford, California, 1986.
- [69] Gordon, S. and McBride, B.J., "Computer Program for Calculation of Complex Chemical Equilibrium Compositions and Applications, I. Analysis", NASA Reference Publication 1311, 1994.
- [70] McBride, B.J. and Gordon, S., "Computer Program for Calculation of Complex Chemical Equilibrium Compositions and Applications, II. Users Manual and Program Description", NASA Reference Publication 1311, 1996
- [71] Boddington, T., Gray, P. and Harvey, D.L., "Thermal Theory of Spontaneous Ignition: Criticality in Bodies of Arbitrary Shape," *Philosophical Transactions of the Royal Society of London, Series A, Mathematical and Physical Sciences*, Vol. 270, No. 1207, pp. 467-506, 1971.
- [72] Peters, N., *Turbulent Combustion*, Cambridge University Press, 2000.
- [73] Oppenheim, A.K., "Dynamic Features of Combustion," *Philosophical Transactions of the Royal Society of London, Series A, Mathematical and Physical Sciences*, Vol. 315, No. 1534, pp. 471-508, 1985.
- [74] Oppenheim, A.K. and Kuhl, A.L., "Energy Loss from Closed Combustion Systems," *Proceedings of the Combustion Institute*, Vol. 28, 2000.
- [75] Ferguson, C.R. and Kirkpatrick, A.T., *Internal Combustion Engines : Applied Thermosciences*, 2nd Edition, John Wiley & Sons, 2001.
- [76] Van Wylen, G.J. and Sonntag, R.E., *Fundamentals of Classical Thermodynamics*, 3rd Edition, John Wiley & Sons, 1985.
- [77] Ferguson, C.R., *Internal Combustion Engines : Applied Thermosciences*, 1st Edition, John Wiley & Sons, 1986.
- [78] Reynolds, W.C., "The Element Potential Method for Chemical Equilibrium Analysis: Implementation in the Interactive Program STANJAN," Version 3, Department of Mechanical Engineering, Stanford University, Stanford, California, 1986.
- [79] Shen, Y., Schock, H., et al., "Dynamic Stage of Combustion in a Direct Injection Methanol Fueled Engine," SAE Technical Paper 2002-01-0998, 2002.
- [80] Shen, Y., Schock, H. and Oppenheim, A., "Pressure Diagnostics of Closed System in a Direct Injection Spark Ignition Engine," SAE Technical Paper 2003-01-0723, 2003.

- [81] Pope, S.B., *Turbulent Flows*, Cambridge University Press, 2000.
- [82] Hinze, J.O., *Turbulence*, McGraw-Hill Book Company, 1959.

MICHIGAN STATE UNIVERSITY LIBRARIES



3 1293 02504 9838